



TABLE OF CONTENTS

	<u>Page</u>
LIST OF TABLES . . . . .	v
LIST OF FIGURES . . . . .	vii
EXECUTIVE SUMMARY . . . . .	ix
1. INTRODUCTION . . . . .	1
2. THE CENTRALLY-MODERATED FMSR [(CM)FMSR] CONCEPT . . . . .	3
2.1 INTRODUCTION . . . . .	3
2.2 CELL BURNUP CALCULATIONS . . . . .	4
2.3 AIMS OF THE PRESENT STUDY . . . . .	6
2.4 (CM)FMSR DESIGN AND CALCULATIONS . . . . .	8
2.4.1 Reactor Configuration . . . . .	8
2.4.2 Startup Core Calculations . . . . .	10
2.4.3 Fuel Management Strategy . . . . .	14
2.4.4 Results of Burnup Calculations . . . . .	20
2.4.5 Reactivity Coefficients . . . . .	24
2.4.6 Reactor Control During Burnup Cycles . . . . .	29
2.4.7 Thermal-Hydraulic Calculations . . . . .	29
2.5 URANIUM RESOURCE REQUIREMENTS . . . . .	31
3. THE EXTENDED FUEL CYCLE FMSR [(EC)FMSR] CONCEPT-PHYSICS ANALYSIS	33
3.1 INTRODUCTION . . . . .	33
3.2 (EC)FMSR DESIGN CONSIDERATIONS . . . . .	36
3.3 CALCULATIONAL METHODS . . . . .	39
3.3.1 Cross-Section Generation . . . . .	39
3.3.2 Hexagonal and R-Z Models of the (EC)FMSR Core . . . . .	44
3.4 RESULTS OF THE (EC)FMSR PHYSICS ANALYSES . . . . .	49
3.4.1 Reactivity Swing and Plutonium Concentrations During the Fuel Cycle . . . . .	49

TABLE OF CONTENTS (cont'd)

	<u>Page</u>
3.4.2 Power Shape and Power Swing. . . . .	51
3.4.3 Burnup and Fast Fluence Damage . . . . .	55
3.4.4 Reactivity Coefficients. . . . .	55
3.4.5 Radial and Axial Blankets. . . . .	64
3.4.6 Reactivity Control Systems . . . . .	64
4. THERMAL-HYDRAULIC ANALYSIS OF THE (EC)FMSR . . . . .	78
4.1 GENERAL DESIGN CONSIDERATIONS . . . . .	78
4.2 METHOD OF CALCULATION . . . . .	78
4.3 THERMAL-HYDRAULIC PERFORMANCE . . . . .	79
5. (EC)FMSR FUEL CYCLE COST ANALYSIS. . . . .	83
5.1 INTRODUCTION. . . . .	83
5.2 FUEL CYCLE COST MODEL AND THE ECONOMIC ENVIRONMENT. . . . .	83
5.3 RESULTS AND CONCLUSIONS . . . . .	88
6. THE 30-YEAR (EC)FMSR . . . . .	94
6.1 PRELIMINARY RESULTS OF THE 30-YEAR (EC)FMSR . . . . .	94
7. CONCLUSIONS AND RECOMMENDATIONS. . . . .	102
7.1 CONCLUSIONS . . . . .	102
7.2 RECOMMENDATIONS . . . . .	103
REFERENCES . . . . .	105

## LIST OF TABLES

<u>Table</u>		<u>Page</u>
2.1	Equilibrium Cycle Performance, Sodium-Cooled, Centrally-Moderated FMSR . . . . .	5
2.2	Thermohydraulic Parameters, Sodium-Cooled (CM)FMSR and CRBR	11
2.3	Startup Reactor Loading, Centrally-Moderated FMSR. . . . .	15
2.4	Sodium-Cooled (CM)FMSR Results of Burnup Calculations Over Reactor Life . . . . .	21
2.5	Changes in Isotope Inventories During Selected Burnup Cycles [Sodium-Cooled (CM)FMSR] . . . . .	23
2.6	Summary of Reactor Physics Calculations, Sodium-Cooled (CM)FMSR . . . . .	26
2.7	Natural Uranium Resource Requirements of the (CM)FMSR. . . . .	32
3.1	General Core Data. . . . .	40
3.2	Fuel Subassembly Data. . . . .	41
3.3	BNL 20-Group Structure . . . . .	43
3.4	LIB-IV Group Structure . . . . .	45
3.5	Multiplication Factor, Fissile Inventory and Conversion Ratios as a Function of Time . . . . .	50
3.6	Plutonium Isotopic Composition of (EC)FMSR Fuel. . . . .	52
3.7	Zone-Averaged Power Densities (MW <sup>T</sup> /L), R-Z Representation. . . . .	54
3.8	Zone-Averaged Burnup Increments (MWD/kg), R-Z Representation	59
3.9	Zone-Averaged Fast Fluence increments ( $10^{23}$ n/cm <sup>2</sup> > 0.1 MeV), R-Z Representation . . . . .	60
3.10	Doppler Coefficients . . . . .	62
3.11	Sodium Void Reactivity Effect ( $\beta_1 = 0.0041 \Delta K$ ) . . . . .	62
3.12	Control Systems Reactivity Requirements (% $\Delta K$ ) . . . . .	66
3.13	Control Subassembly Design Data. . . . .	68
3.14	Control Rod Assignments. . . . .	68
3.15	Multiplication Factor as a Function of Control Rod Position	71

LIST OF TABLES (cont'd)

<u>Table</u>		<u>Page</u>
3.16	Control Rod Reactivity Worths . . . . .	72
4.1	Summary of Core Fuel Thermal Hydraulics for the (EC)FMSR. .	80
4.2	Thermal-Hydraulic Results for Average Pin at Nominal Conditions in Zone 1 of (EC)FMSR. . . . .	82
4.3	Thermal-Hydraulic Results for the Hot Pin in Zone 1 of the (EC)FMSR. . . . .	84
5.1	Unit Cost and Financial Parameters Used in the Fuel Cycle Cost Calculations . . . . .	86
5.2	Unit Cost of Fissile Plutonium Based on the Recovery Costs from PWR Spent Fuel . . . . .	87
5.3	Cash Flow Associated with Core and Blanket Fuel Assemblies of (EC)FMSR . . . . .	89
5.4	Cash Flow Associated with Core and Blanket Fuel Assemblies of a Homogeneous LMFBR (1200 MW(e)) . . . . .	91
5.5	Cash Flow Associated with Core and Blanket Fuel Assemblies of a Heterogeneous LMFBR (1000 MW(e) Core). . . . .	92
5.6	Comparison Between the Levelized Fuel Cycle Cost of the (EC)FMSR and a Homogeneous and Heterogeneous LMFBR. . . . .	93
6.1	Comparison Between 10- and 30-Year (EC)FMSR Cores . . . . .	95
6.2	30-Year FMSR Performance. . . . .	98
6.3	Cash Flow Associated with Core and Blanket Fuel Assemblies of the 30-Year FMSR . . . . .	99
6.4	Comparison Between the Levelized Fuel Cycle Cost of the 10- and 20-Year FMSR and a Heterogeneous LMFBR. . . . .	100
6.5	Advantages and Disadvantages of the 30-Year FMSR Design . .	100

LIST OF FIGURES

<u>Figure</u>		<u>Page</u>
2.1	Variation of $K_{eff}$ and Breeding Ratio with Peak Cell Burnup . . . . .	7
2.2	Schematic View of the Centrally-Moderated FMSR in the X-Y Plane. . . . .	9
2.3	Reactor Layout in the X-Y Plane for the (CM)FMSR . . . . .	12
2.4	Schematic R-Z Representation of the (CM)FMSR . . . . .	13
2.5	Neutron Energy Spectra at the Beginning of Reactor Life for the (CM)FMSR . . . . .	15
2.6	Radial Distribution of Total Flux at BORL, (CM)FMSR. . . . .	16
2.7	Schematic Representation of the Fuel Management Strategy for the (CM)FMSR . . . . .	17
2.8	Details of the Fuel Management Strategy Over the Lifetime for the Sodium Cooled (CM)FMSR . . . . .	19
2.9	Reactor Isotope Inventories at the Beginning of Burnup Cycles, (CM)FMSR . . . . .	22
2.10	Variation of Subzone Power During Burnup Cycle 7, (CM)FMSR . . . . .	25
2.11	Neutron Energy Spectra at the End of Reactor Life for the (CM)FMSR . . . . .	27
2.12	Adjoint Functions at BORL and EORL in the Moderated Region, (CM)FMSR . . . . .	28
2.13	Adjoint Functions at BORL and EORL in the Fast Region, (CM)FMSR . . . . .	30
3.1	Configuration A Type (EC)FMSR Core Layout. . . . .	37
3.2	Configuration B Type (EC)FMSR Core Layout. . . . .	38
3.3	Fuel Subassembly Design. . . . .	42
3.4	Zone Map of the (EC)FMSR Core, HEX-Representation. . . . .	46
3.5	Zone Map: R-Z Representation of the (FC)FMSR Core . . . . .	48
3.6	Plutonium Isotopic Change as a Function of Time. . . . .	53
3.7	Power Density Variation with Burnup, Due to BeO Moderator. . . . .	56
3.8	Power Density Variation in Configuration B Type Subassembly. . . . .	57

LIST OF FIGURES (cont'd.)

<u>Figure</u>		<u>Page</u>
3.9	Axial Power Density Variation of (EC)FMSR. . . . .	57
3.10	Radial Power Distribution (Center to Flat) . . . . .	58
3.11	Extended-Cycle FMSR Radial Power Shape at BOL, MOL and EOL .	58
3.12	Irradiation Dependence of Sodium Void Reactivity Gain. . . .	63
3.13	Irradiation Dependence of Doppler Effect Feedback Coefficient	63
3.14	Control Subassembly Configuration. . . . .	67
3.15	Spatial Distribution of Primary Control (PC) and Safety (SC) Rods for (EC)FMSR (Tentative) . . . . .	69
3.16	Average Subzone Power Density for (EC)FMSR BOL Core. . . . .	73
3.17	Average Subzone Power Density for (EC)FMSR MOL Core. . . . .	74
3.18	Average Subzone Power Density for (EC)FMSR EOL Core. . . . .	75
3.19	Power Peaking Factors for (EC)FMSR BOL Core. . . . .	76
3.20	Power Peaking Factor for (EC)FMSR EOL Core . . . . .	77
6.1	30-Year FMSR Radial Power Distribution (Zone Average, R-Z) .	96

## EXECUTIVE SUMMARY

This is the third annual summary report on the design of the FMSR reactor concept. The principal achievement for this fiscal year has been the preliminary design of an FMSR which offers the following advantages:

- (1) a very long fuel cycle. A ten-year fuel cycle is demonstrated and a 30-year fuel cycle appears to be feasible.
- (2) a small reactivity swing over the long fuel cycle, leading to simplified control designs.
- (3) small power density changes, both locally and regionally, over the fuel cycle.
- (4) a strong Doppler effect feedback coefficient and low sodium void reactivity gain.
- (5) conventional LMFBR technology is used throughout, except for the current choice of metal fuel and the presence of some moderator, presently in the form of BeO.
- (6) proliferation-resistance resulting from the avoidance of any fuel handling, reprocessing, fabrication or enrichment activities for very long times, possibly for the full lifetime of the plant. Each of these stages offers the potential for fissile material diversion.

Reactor physics, fuel cycle, thermal-hydraulics and fuel cycle cost studies have been performed for this concept and are reported. The most serious drawback of previous FMSR designs, namely the level of irradiation damage to the stainless steel of the cladding and duct materials, has been greatly reduced by the new design. The peak fuel burnup level is also reduced.

Work continued on earlier FMSR designs, and in particular, the centrally-moderated FMSR. Emphasis was placed on defining the first core and then the total sequence of core histories over the 30-year life of the reactor. It was found possible to define a two-year fuel cycle with limited reactivity swing over the cycle.

Fuel cycle cost studies were begun. The results indicate a modest fuel cycle cost advantage for the FMSR, but the basic cost assumptions must be improved for metal fuel.

Improved thermal-hydraulic analysis capabilities have greatly improved the understanding of heat transfer behavior, particularly where the fuel approaches moderator-laden subsections.

A new treatment for fission product cross sections for LMFBR calculations predicts that previous treatments overestimated the deleterious reactivity effects by as much as 30%; sodium void calculations for LMFBRs may be seriously overestimated where the older effective fission product sets are used.



## 1. INTRODUCTION

This is the third annual report on the FMSR reactor concept. The first report (BNL-50976, Jan. 1979) introduced the concept of the Fast-Mixed Spectrum Reactor (FMSR). The major objective of that first design was to provide a breeder reactor which had important proliferation-resistance characteristics as well as a significant uranium resource conservation capability relative to the light water reactor. The reactor was to be metal-fueled and cooled by either sodium or helium. The fuel cycle was of the once-through-and-store type, with the only fuel fed to the reactor during its lifetime being either natural or depleted uranium. There would be no fuel reprocessing or enrichment operations required. The design was shown to be technically feasible but it also had some drawbacks. The most serious appeared to be that the steel cladding and ducts, on discharge, had accumulated severe irradiation damage. It was felt that advanced steel alloys currently under irradiation might be able to accommodate such levels; however, work directed toward a reduced level would be important. The peak fuel burnup was also high but less worrisome.

The second report (BNL-51225, May, 1980) described two new FMSR concepts. The first one was a design improvement of the previous concept. A number of performance parameters, such as the size of local power density swings, the reactivity change over the fuel cycle, and the length of the fuel cycle were significantly improved. Unfortunately the level of the steel irradiation damage over the fuel cycle remained high. The second FMSR concept was totally new. It is based on a strategy whereby reactor refueling is very infrequent; one or at most two reloadings are required over its lifetime. This strategy might be acceptable from a nonproliferation viewpoint if the refueling were performed in a properly controlled manner. This led to the design objective of an extended fuel cycle and the Extended Cycle FMSR, (EC)FMSR. A single core which could operate for the full 30 years of the plant lifetime would be the ultimate objective. As a design approach, it was decided that a LMFBR with a 10-year fuel cycle would be the first target, and this is the subject of the present report; this design was briefly described in Reference 1.

The (EC)FMSR study reported here concentrated on a design which was intended to serve the major national LMFBR objectives while simultaneously offering desirable proliferation-resistant characteristics. In particular, it was designed to have excellent performance by means of a very long fuel cycle, excellent local and regional power distributions, a low reactivity swing over the long fuel cycle, and a low fuel cycle cost. The sodium void reactivity worth was to be kept as low as possible and the Doppler effect reactivity feedback coefficient was to be significantly larger than in current LMFBRs.

The Centrally-Moderated FMSR first reported last year has been studied this year from the point of view of startup from the first core fueled with enriched uranium, and its operation through defined successive cycles for the full reactor lifetime. Some design improvements were achieved, such as a two-year fuel cycle instead of a one-year fuel cycle and a reduced reactivity swing. The fuel burnup level on discharge and the corresponding steel irradiation damage, however, remain high. These can be reduced, albeit at reduced resource conservation.

Important new capabilities have been achieved in the course of this work. A new treatment for fast reactor fission products will be of considerable benefit to basic LMFBR technology and should reduce computed sodium void reactivity changes for LMFBRs, particularly at the worst time in the fuel cycle, the end of core life. A new capability for two-dimensional heat transfer analysis in a subassembly has greatly reduced analytical uncertainties for systems such as the FMSR which have fuel and moderator in close proximity. Fuel cycle cost study capabilities initiated at BNL are particularly useful for design optimization. Duct dilation analyses at BNL have been improved to account for creep relaxation effects, including those at duct corners. This removes a major source of nonconservatism in these analyses.

## 2. THE CENTRALLY-MODERATED FMSR [(CM)FMSR] CONCEPT

### 2.1 INTRODUCTION

A description of the (CM)FMSR and its equilibrium fuel cycle was given in the previous progress report.<sup>(1)</sup> The (CM)FMSR uses metal fuel in subassemblies having fuel, sodium, and steel volume fractions of 0.45, 0.35 and 0.20, respectively. Moderator subassemblies containing beryllium oxide are employed to enhance the safety and performance of the reactor. The core of the (CM)FMSR can be divided into three broad regions: the central moderated region, the fast region and the outer region. The outer region contains fuel with relatively low amounts of fissile isotopes and has comparatively low power densities. The central moderated region contains moderator subassemblies interspersed among the fuel subassemblies. The relatively softer spectrum of this region leads to improved reactivity coefficients (Doppler and sodium void) and also to reduced power swings in the fuel subassemblies in this region. The fast region does not have any moderator and consequently has a very hard neutron spectrum. The fast region provides most of the power and hence the reactivity of the (CM)FMSR.

The reactor physics results described in the previous report were mainly for the equilibrium fuel cycle. The problem of approaching the equilibrium cycle, beginning with the startup core, had received only minimal attention.

The definition of the first core and the management of the fuel cycle to the end of the (CM)FMSR reactor lifetime have been the principal achievements for this period. It will be shown that two-year fuel cycles are possible for the full reactor lifetime with quite satisfactory performance.

The fissile component of the startup fuel may be either U-235 or plutonium. Only U-235 has been considered in (CM)FMSR studies, however, because of its nonproliferation advantages. According to the fuel management scheme that was described in the previous progress report, all fuel loaded into the reactor subsequent to startup consisted only of natural uranium. At the end of each burnup cycle one subzone (in this case 12 subassemblies) of fresh natural uranium fuel would be loaded into the reactor, and one subzone of burnt fuel would be discharged, presumably for storage. As the fuel builds up plutonium by captures in U-238, the subassemblies would be moved around in the reactor according to a shuffling pattern which maintains criticality and reduces power swings within the subassemblies. The equilibrium cycle is reached when all the initial enriched fuel has been discharged from the reactor. Now, the reactor is fueled solely by subassemblies which entered the reactor as fresh natural uranium subassemblies and built up their fissile plutonium in situ. After this stage each burnup cycle would essentially be a repetition of the previous cycle.

Analysis of the equilibrium cycle results provided relevant information regarding the rates of buildup of fissile isotopes and fission products in the various zones. Actual fuel shuffling strategies could then evolve from the above information. The equilibrium cycle fuel compositions in the various zones can also be used to assess the initial enrichments required for the startup fuel loading. In actual practice the time required to reach the equilibrium cycle after startup may be longer than the lifetime of the reactor, i.e., longer

than the lifetime of the reactor, i.e., longer than 30 years. The nuclear characteristics of the burnup cycles during the approach to the equilibrium cycle may vary considerably from those of the equilibrium cycle. However, the analysis of the equilibrium cycle was used as a basic reference point since it provides valuable information regarding the basic characteristics of the (CM)FMSR. The results have indicated potential problems during the approach to equilibrium, and have led to suggestions of suitable remedies.

Table 2.1 summarizes the equilibrium cycle reactor physics results (from Reference 1) for the sodium-cooled (CM)FMSR. The equilibrium cycle length is 260 full power days. During the cycle the reactivity increases by 1.27%. The high breeding ratio is typical of metal-fueled reactors. The equilibrium cycle is powered mainly by fissions in plutonium and U-238 while U-235 fissions account for less than 3% of the total fissions.

If nuclear nonproliferation is one of the major goals of the fuel cycle, the first core of the FMSR reactor will very likely be fueled with U-235 enriched fuel and operate on the once-through and store fuel cycle. In such a reactor, most of the power at the beginning of reactor life (BORL) is from U-235 fissions. As burnup proceeds, Pu-239 is produced by captures in U-238 and fissions in plutonium become increasingly more important. In high burnup metal-fueled reactors, most of the power at the end of reactor life (EORL) is derived from plutonium fissions. There are important differences between the nuclear properties of U-235 and plutonium isotopes in the neutron energy spectrum of a breeder reactor. Hence the task of designing a suitable fuel management strategy becomes more complicated, due to the transformation during the reactor lifetime from the uranium to the plutonium-based fuel cycle. To understand these differences better, a number of calculations were performed in a simple cell geometry, as described in the following section.

## 2.2 CELL BURNUP CALCULATIONS

The differences between the nuclear characteristics of U-235 enriched and plutonium enriched fuels, and the changes that take place with burnup, can be studied simply and quickly by performing simple cell burnup calculations. Such studies are useful for the design of the (CM)FMSR which uses U-235 enriched fuel as the startup fuel. Hence two series of burnup calculations on fuels with various starting enrichments were performed. The first series used U-235 enriched fuel. The second series used plutonium from light water reactors as the starting fissile fuel (plutonium composition:  $^{239}/^{240}/^{241}/^{242} = 57.7\%/22.8\%/13.9\%/5.6\%$ ). The fertile isotope was U-238 for both series. Fifty-group cross-section sets obtained from LIB-IV<sup>(2)</sup> data and the 1-DX<sup>(3)</sup> diffusion theory code were used.

The axial dimensions of the cells matched those of the FMSR fuel subassemblies, i.e., 160 cm of enriched fuel with 40 cm of natural uranium blanket on each end. Vacuum boundary conditions were used in the axial direction. In the radial direction reflective boundary conditions were used. Homogenized number densities were used in the calculations, with fuel, sodium and steel volume fractions of 0.45, 0.35 and 0.2, respectively. No moderator was used in the cells. Hence, the cell was representative of fuel in the fast region of the (CM)FMSR.

TABLE 2.1  
Equilibrium Cycle Performance,  
Sodium-Cooled, Centrally-Moderated FMSR

Number of Fuel Subassemblies	397
Number of Subassemblies Shuffled Per Cycle	84
Cycle Duration (Full Power Days)	260
Reactivity Swing Over Cycle, %	+1.27
Breeding Ratio (BOEC)	1.66
(EOEC)	1.58
Fuel Inventory	
Reactor, BOEC, kg Pu	8930
Discharge/Yr, kg Pu	530
Core Discharge Enrichment (% Pu-239)	7.6
Peak Burnup (MWD/T)	
30-Yr, Fuel Reintroduction	~184,000
*Equilibrium Fuel Cycle	237,000
Peak Fluence (E > 0.1 MeV)	
30-Yr, Fuel Reintroduction	~7.3 x 10 <sup>23</sup>
*Equilibrium Fuel Cycle	9.9 x 10 <sup>23</sup>

\*This number applies only if the fuel stays in the reactor for 33 burnup cycles.

Figure 2.1 shows the variation of  $K_{eff}$  and breeding ratio (BR) with peak burnup in the cell for two of the cases that were analyzed. Case I used LWR discharged plutonium with a fissile enrichment of 6%. Case II used U-235 enriched fuel with an enrichment of 10%. It is seen that in both the cases, high burnups of the order of 20% of heavy metal are achievable without the cells becoming subcritical. The plutonium-enriched fuel performs significantly better than the U-235 enriched fuel. At lower burnups the plutonium fuel has a significantly higher breeding ratio compared to that of the enriched uranium fuel. This is partly due to the higher values of  $\bar{\eta}$  of plutonium isotopes compared to U-235, and partly due to the higher fertile-to-fissile ratio of Case I. However, mere comparison of breeding ratios is insufficient for proper evaluation of fuel cycles. The BR (as defined here) is the ratio of the rate of fissile isotope production to the rate of fissile isotope destruction. In particular, no account is taken of the different reactivity worths of the various fissile isotopes. The reactivity worth of a fissile isotope is roughly proportional to the value of  $(\nu\sigma_f - \sigma_a)$  for that isotope. In the present case, the values of this parameter for U-235, Pu-239 and Pu-241 are, respectively, 1.87, 2.91 and 3.67. The higher reactivity worth of the bred fuel, i.e., Pu-239, compared to U-235, makes high burnups achievable in Case II, even with comparatively low breeding ratios. In Case I, the breeding ratio decreases significantly with burnup due to changes in the plutonium composition and accumulation of fission products. In Case II, on the other hand, the effect of accumulating fission products is compensated by the increasing proportion of fissions in plutonium isotopes. As a result, the breeding ratio remains almost constant with increasing burnup. The two initial breeding ratios would be closer to each other if the weighted breeding ratio had been used.

### 2.3 AIMS OF THE PRESENT STUDY

The aim of the present work is the design and study of the 30-year fuel cycle of a sodium-cooled (CM)FMSR which starts on enriched uranium fuel. With nuclear nonproliferation as an important consideration, it was decided that all fuel inputs to the reactor subsequent to startup should also be either natural or enriched uranium. The lengths of burnup cycles and fuel shuffling patterns (if used) should be designed so as to minimize the swings in reactivity of the reactor and power changes within fuel subassemblies. Another major objective is that the fuel cycle should be attractive from the point of view of uranium resource utilization, compared to the once-through fuel cycle used in LWRs. A typical 1000-MW(e) LWR requires approximately 6000 T of natural uranium (converted to enriched uranium before use) over its operating life of 30 years. To be an attractive concept, it should be demonstrated that a 1000-MW(e) (CM)FMSR would require significantly lower amounts of natural uranium.

The allowable peak fuel burnup is limited by the metallurgical characteristics of the fuel and the clad materials. Extrapolating the results of recent metal fuel experience in EBR-II, it is not unreasonable to hope that in the future it may be possible to achieve peak burnups of the order of 20% heavy metal mass. The peak burnup in a fuel subassembly, if it were to be allowed to stay in a high power region of the reactor for thirty years, could exceed 36%. One of the design objectives was to limit the peak burnup to around 20%. This design objective may be met in one of the following ways. The reactor may be operated continuously for, say, 10 or 15 years, without fuel shuffling, and in a single batch mode until the preset limit on peak burnup is reached somewhere

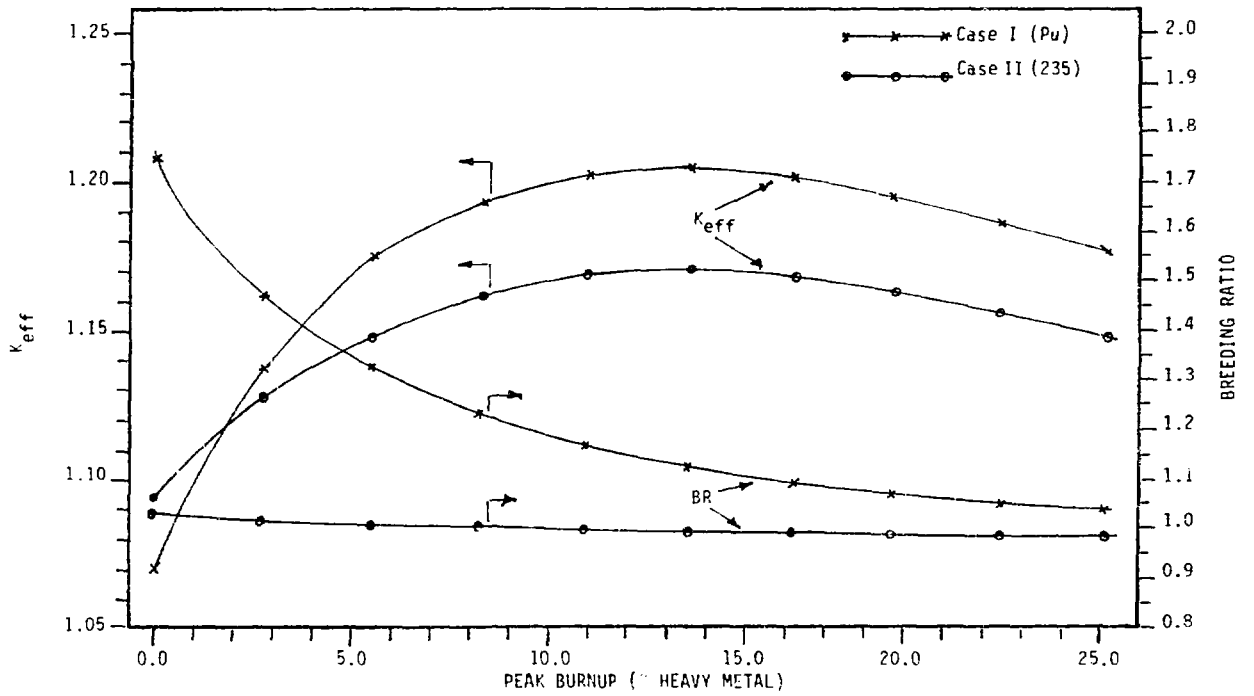


Figure 2.1 Variation of  $K_{eff}$  and Breeding Ratio with Peak Cell Burnup

in the core. At that time, the entire core may be discharged and a fresh new core brought in. Alternatively, the core size may be increased so that the peak (and the average) power density is sufficiently reduced so that the reactor may be operated on the same fuel loading for the entire 30 years without exceeding the limiting burnup. Either of the above two methods would substantially increase the uranium resource requirement because of the significant amounts of extra enriched fuel that is involved.

A third way to reduce the peak discharge burnup can be devised which would lead to a much smaller increase in the uranium resource requirement. The method involves in-core fuel shuffling. Natural uranium subassemblies would be introduced into low power density regions of the reactor where plutonium is built up by captures in U-238. When a sufficiently high level of plutonium is built up, the fuel subassemblies would be moved to higher power density regions where they would produce substantial amounts of energy prior to being discharged. In this way the burden of energy production (over the life of the reactor) is shared by a larger number of fuel subassemblies, thus reducing the peak burnup. If the peak burnup is still found to be too high, a limited number of enriched fuel subassemblies could be introduced into the high power density regions at predetermined times to achieve the same end.

Since high resource utilization (or low resource requirement) is an important objective, the fuel management strategy for this study involves in-core fuel shuffling. In actual practice, a fuel subassembly may have to be moved several times within the reactor prior to the final discharge.

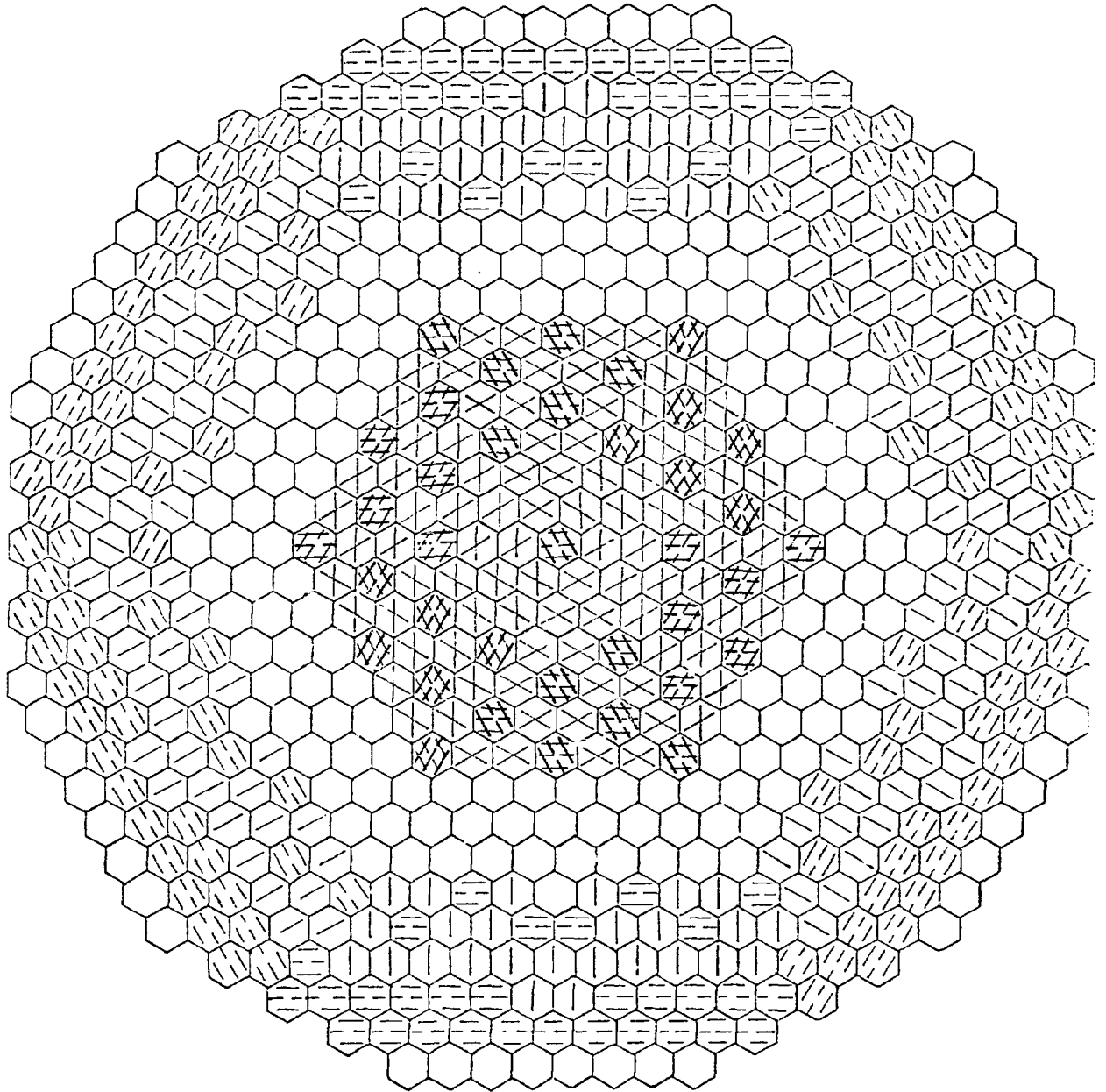
## 2.4 (CM)FMSR DESIGN AND CALCULATIONS

### 2.4.1 Reactor Configuration

Figure 2.2 shows the schematic layout of the (CM)FMSR in the X-Y plane. The (CM)FMSR can be divided into three broad regions, i.e., the central moderated region, the fast region, and the outer region. The outer region is a low power density region where low enrichment (or natural uranium) fuel subassemblies build up their fissile inventories by capturing neutrons leaking radially outwards. This region contains some moderator subassemblies which help soften the neutron spectrum and enhance neutron capture in U-238. When a sufficient level of plutonium is built up, the fuel subassemblies are moved into the central moderated region.

The central moderated region contains 37 moderator subassemblies. These are arranged so that each moderator subassembly is surrounded by fuel subassemblies on all sides. Beryllium oxide is chosen as the moderator material. The moderator subassemblies serve many purposes. They enhance the safety of the reactor by reducing the sodium void reactivity coefficient and increasing the Doppler reactivity coefficient. The relatively softer spectrum in this region also reduces the rate of plutonium buildup, and hence, reduces the power swings in the subassemblies in this region. In order to prevent excessively high power densities and too rapid swings in power, it is desirable to prevent the flux from peaking at the center of the reactor. Use of the moderator subassemblies in the central region is also helpful in this regard.











- |   |                           |   |                      |
|---|---------------------------|---|----------------------|
|  | REFLECTOR                 |  | FUEL, OUTER REGION   |
|  | MODERATOR, OUTER REGION   |  | FUEL, FAST REGION    |
|  | MODERATOR, CENTRAL REGION |  | FUEL, CENTRAL REGION |

Figure 2.2 Schematic View of the Centrally-Moderated FMSR  
in the X-Y Plane

An additional potential advantage of the (CM)FMSR is the possibility of employing some of the moderator subassemblies in the central region for reactor control. Withdrawal of the moderator from the core leads to a hardening of the neutron spectrum in the central region. This effect, along with the changes in the shapes of neutron flux and adjoint functions, leads to an increase of reactivity. Inserting the moderator back into the reactor has the opposite effect. Preliminary calculations in R-Z geometry indicate that it may be possible to use the moderator subassemblies to control reactivity swings during a burnup cycle. However, the reactivity worth of the moderator changes substantially during the life of the reactor due to accumulation of fission products and changes in the fissile composition of the fuel. Hence, more detailed calculations will be needed to fully establish this feasibility.

The fast region provides the bulk of the power, and hence, reactivity of the reactor. Fuel in the moderated region, after a prescribed period of residence, is to be moved into the fast region. In actual practice a fuel subassembly may be moved once or twice within a region in order to facilitate more even plutonium buildup or to avoid excessive power swings in the subassembly.

Table 2.2 compares the (CM)FMSR and the Clinch River Breeder Reactor design parameters. In order to take maximum advantage of current fast reactor development, the FMSR design parameters were selected to be reasonably close to the CRBR design parameters but to also represent design trends of 1000-MW(e) studies. The larger fuel pin diameter shown for the FMSR reflects the advantage to be gained from the higher thermal conductivity of metal fuel of the FMSR compared to the oxide fuel of the CRBR. For the present analysis, it is assumed that the moderator subassemblies contain beryllium oxide, steel, and sodium coolant with the volume fractions of 0.7, 0.15 and 0.15, respectively. The beryllium oxide is at 50% theoretical density in the central region and 80% theoretical density in the outer region.

Figure 2.3 shows the details of the reactor layout in the X-Y plane. A 60° sector of the reactor is shown. The reactor contains 33 fuel subzones, each containing 12 subassemblies. In a 60° section of the reactor, each fuel subzone is represented by two hexagonal fuel subassemblies. In the R-Z geometry representation shown in Figure 2.4, the fuel subzones are represented by rings of fuel. Moderator subassemblies are grouped together and represented by moderator rings. Each half of the reactor, above and below the midplane, is divided into three axial layers. In the first and second layers, the 33 radial fuel subzones are explicitly represented. The top layer, i.e., axial blanket, is represented by only seven subzones because of constraints in computer storage. All reactor physics calculations in this study were performed in the R-Z geometry.

#### 2.4.2 Startup Core Calculations

All burnup calculations were performed using 20-group cross-section sets. The group structure is described in Section 3. These sets were collapsed from 50-group sets (obtained from LIB-IV data) using the 1-DX diffusion theory code. Cross-section sets were obtained for different compositions chosen to reflect not only the different regions of the reactor but also changes in composition due to burnup. Burnup calculations were performed in R-Z geometry using the 2DB<sup>(4)</sup> diffusion theory code. In the present calculations, four fission products with appropriate yields were used. They are Sm-149 and three lumped

TABLE 2.2  
Thermohydraulic Parameters  
Sodium-Cooled (CM)FMSR and CRBR

<u>REACTOR CORE</u>	<u>FMSR</u> <u>(REFERENCE CASE)</u>	<u>CRBR</u> <u>(300 MW(e))</u>
Thermal Power, MW	2780	975
Inlet Temperature, °C	380	388
Outlet Temperature, °C	540	535
Total Pressure Drop, MPa	0.77	0.77
Average Flow, kg/hr-cm <sup>2</sup>	$2.36 \times 10^3$	$1.72 \times 10^3$
 <u>FUEL ASSEMBLIES</u>		
Rods Per Assembly	331	217
Volume Fraction		
Fuel	0.45	0.325
Coolant	0.35	0.419
Steel	0.20	0.234
Rod Outside Diameter, cm	0.869	0.5842
Fuel Diameter, cm	0.783 (metal)	0.4915 (oxide)
Clad Thickness, cm	0.043	0.0381
Wire-Wrap O.D., cm	0.149	0.142
Pitch, wrap	30.0	30.23
Rod Triangular Pitch, cm	1.018	0.7308
P/D Ratio	1.171	1.251
Rod Length, cm	270	290.6
Fuel-Clad Gap, cm	0	0.0082
Duct Flat Distance, cm	18.692	11.011
Duct Wall Thickness, cm	0.254	0.3048

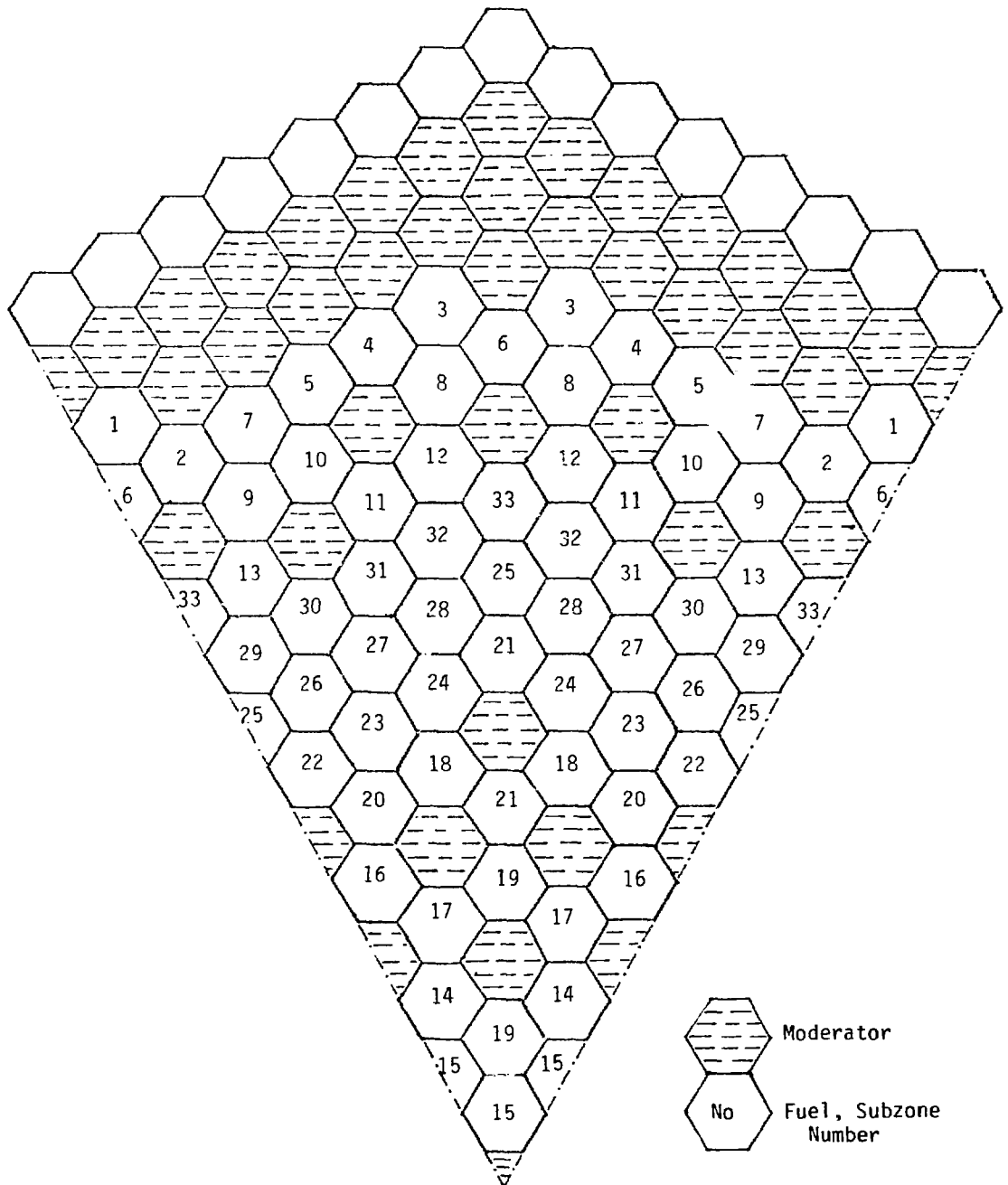


Figure 2.3 Reactor Layout in the X-Y Plane for the (CM)FMSR



fission products, i.e., Rapidly Saturating Fission Product (RSFP), Slowly Saturating Fission Product (SSFP) and Non-Saturating Fission Product (NSFP). Fission product isotopes, in general, transmute to other isotopes of lower absorption cross sections upon neutron absorption. In the present calculations, these transmutations were approximated by the following scheme. RSFP were assumed to transmute to SSFP, SSFP to NSFP and Sm-149 was assumed to transmute to NSFP. Fission products of both U-235 and Pu-239 were employed. These were taken from the LIB-IV cross-section set. A recent evaluation of fission product cross sections, described in Section 3 of this report, indicates that use of LIB-IV fission product cross sections may lead to negative reactivities which may be too high (as much as 30%).

An initial estimate of the startup U-235 enrichments was made by inspecting the equilibrium cycle plutonium contents of the different subzones. By combining groups of subzones together and averaging, the number of initial enrichments to be used in these studies was reduced to eight. Using these enrichments, a concentration search was performed to obtain the desired  $K_{eff}$ . Thus, the actual enrichments that go into the startup core were obtained. In addition, it is important to avoid excessive power and reactivity swings during burnup. These swings in turn depend on the initial enrichments, burnup cycle length and the fuel shuffling pattern. Hence, many iterations may be needed before optimum, or close to optimum, values of initial enrichments were found.

Table 2.3 shows the U-235 enrichments selected for the startup core. The enriched uranium is contained in the 160 cm core region of the fuel subzones (all except subzones 1 to 4). Subzones 1 to 4 and the upper and lower axial blankets of all the subzones contain natural uranium. The enrichments vary from 2% to 11.26%. The total amount of U-235 in the reactor is 10,899 kg, of which 10,284 kgs are in the enriched uranium. The total heavy metal loading is 209.5 tonnes.

Figure 2.5 compares the 20-group neutron spectra in the moderated region (subzone 17) and the fast region (subzone 27). It can be seen that even though the spectrum in the moderated region is softer than in the fast region, it is still "hard," with a considerable fraction of neutrons above 1 keV. The flux depression due to the sodium resonance at 2.85 keV can be clearly seen in Figure 2.5.

Figure 2.6 shows the radial total flux distribution in the fuel subzones corresponding to the reactor midplane. It is seen that the total flux is relatively flat in the moderated and the fast regions, but drops off rapidly in the outer region, much as it does in the analogous radial blanket of any LMFBR. Because of the slightly lower fuel enrichments and the presence of moderator sub-assemblies in the moderator region, there is a slight drop in the total flux. As more fissile fuel is built up during burnup, the flux tends to peak at the center and may lead to unacceptably high power densities. The fuel shuffling scheme is designed to counter this tendency.

#### 2.4.3 Fuel Management Strategy

Figure 2.7 schematically represents the broad fuel management strategy. The 33 fuel subzones are grouped under six broad zones. In Figure 2.7 the number of subzones grouped under each broad zone are marked. In the outer region

TABLE 2.3  
Startup Reactor Loading,  
Centrally-Moderated FMSR

Subzone Number	% of U-235	kg of U-235
1-4 (plus axial blankets of all subzones)	0.71	616 (nat. U)
5-7	2.00	254
8-10	3.50	444
11-12	5.50	465
13	7.00	296
14-17	8.80	1490
18-19	9.30	787
20-21	9.80	829
22-33	11.26	5718

Total U-235 = 10,899 kg  
 Total Heavy Metal = 209.5 tonnes

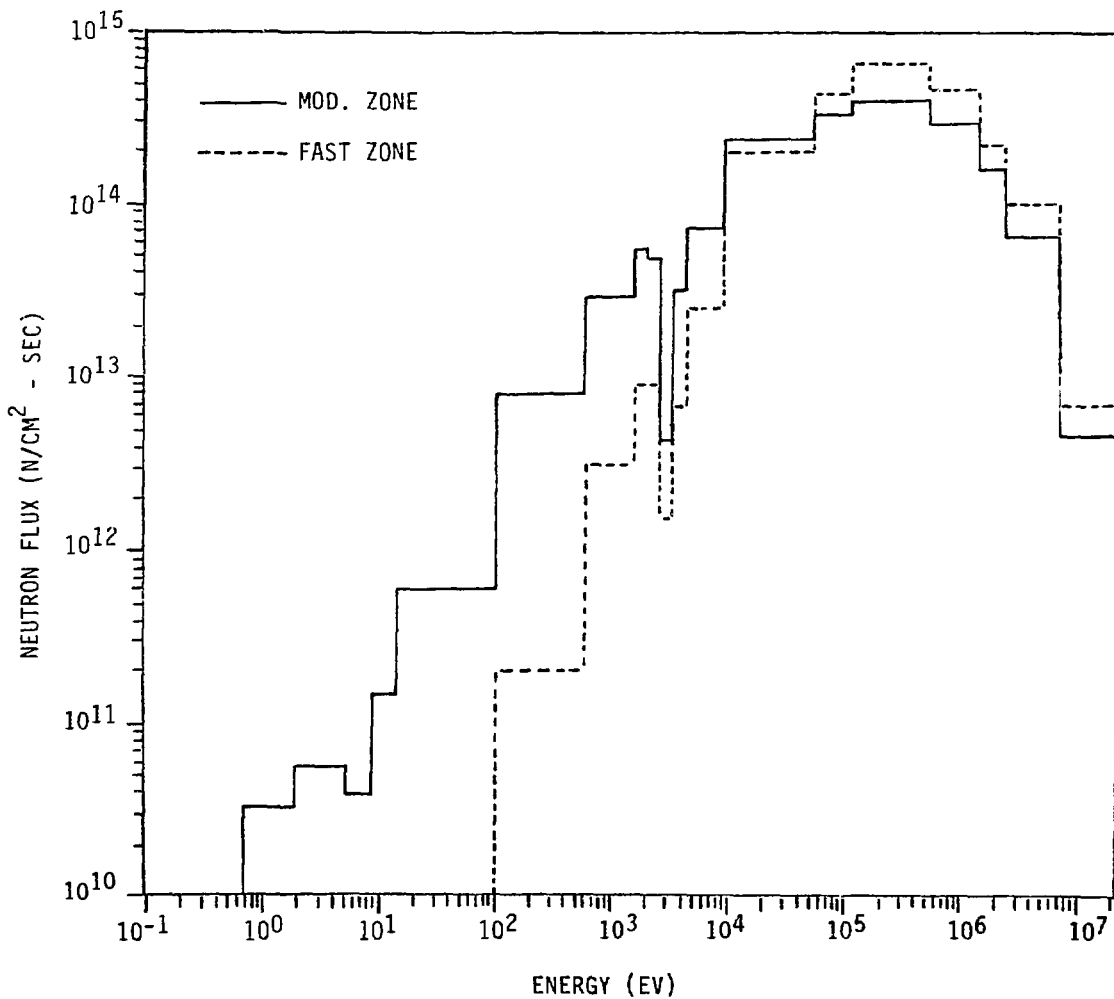


Figure 2.5 Neutron Energy Spectra at the Beginning of Reactor  
 Life for the (CM)FMSR

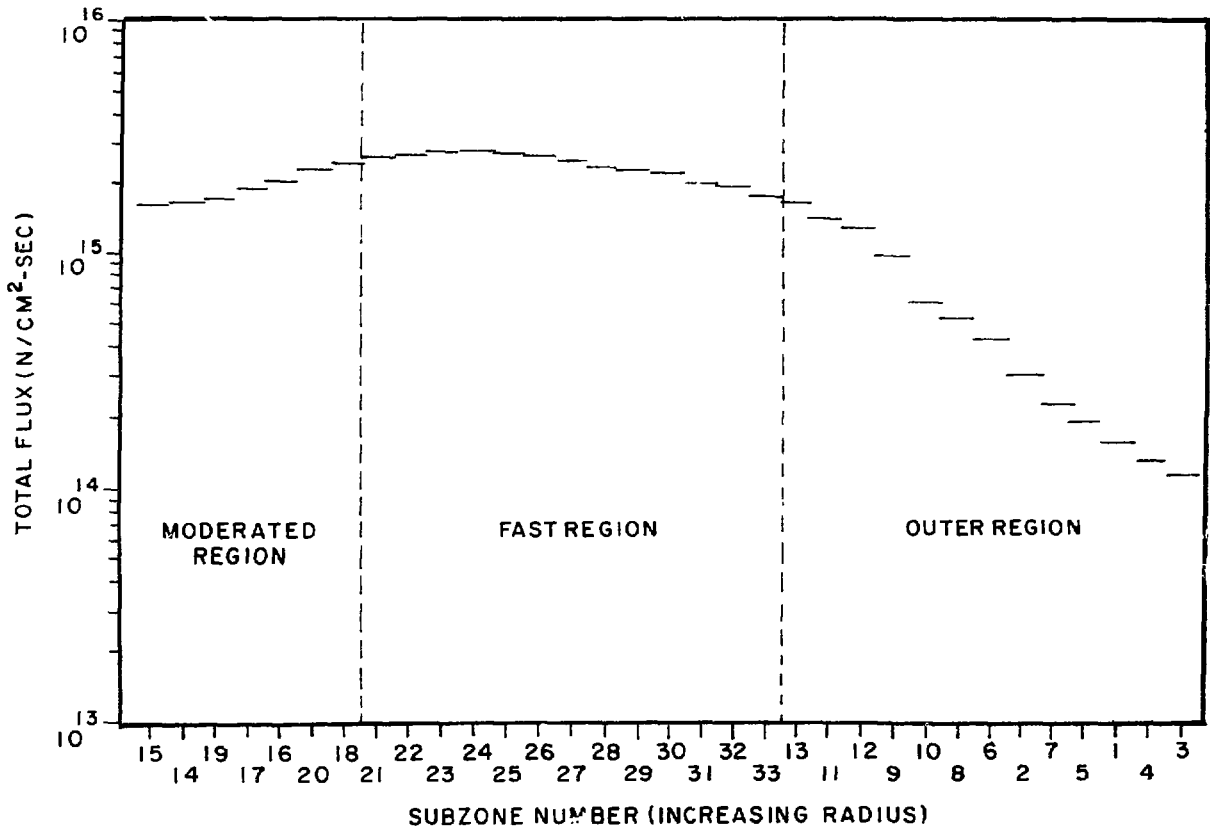


Figure 2.6 Radial Distribution of Total Flux at BORL, (CM)FMSR



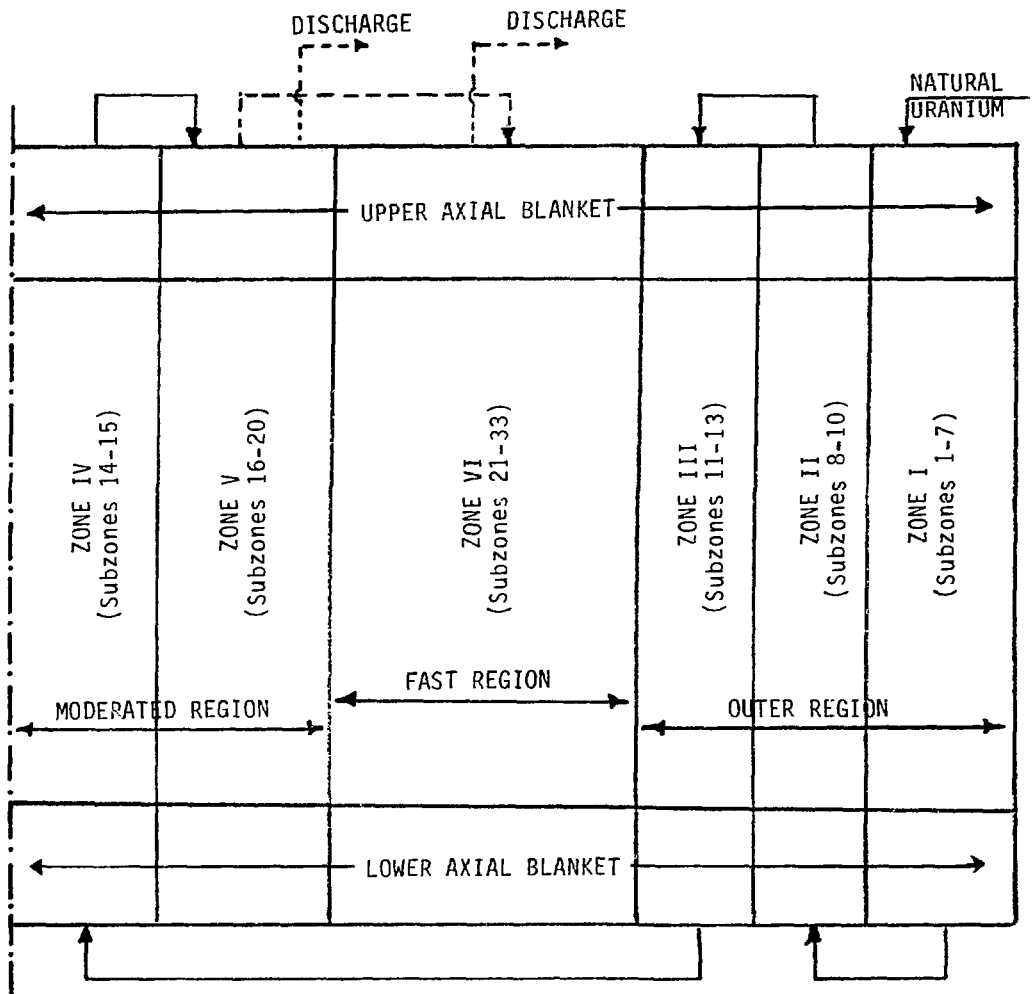


Figure 2.7 Schematic Representation of the Fuel Management Strategy for the (CM)FMSR

of the reactor (subzones 1 to 13) each broad zone roughly corresponds to one hexagonal ring of fuel. The outer region is divided into three broad zones. At the end of each burnup cycle one fresh subzone of natural uranium fuel is brought into Zone I. One subzone from Zone I is moved to Zone II and one subzone from Zone II is moved to Zone III. This progressive movement inwards facilitates an even buildup of plutonium in the fuel before it is moved to Zone IV. A fuel subzone in Zone IV resides there for only two burnup cycles before moving to Zone V. This is done to prevent excessive plutonium buildup near the center which would result in flux peaking at the center. At the end of each burnup cycle one subzone from Zone IV is usually moved to Zone V. Depending on the burnup level, one subzone from Zone V may or may not be moved into Zone VI. If it is moved into Zone VI, one subzone from Zone VI is discharged from the reactor. If not, one subzone from Zone V is discharged from the reactor, sometimes for storage until a subsequent reintroduction.

The actual fuel management strategy is further complicated because of the need to limit the peak burnup to around 20%. A fuel subzone which resides in a high power producing region for the whole 30-year period may experience a peak burnup of as much as 36%. On the other hand, a fuel subzone that is discharged from the reactor at the end of the first burnup cycle, for example, has a peak burnup of only about 2.9%. This fuel may be brought back into the reactor at a later time to replace a subzone which has reached the maximum allowable burnup. In the fuel management scheme to be described, (see Figure 2.8) fuel subzones discharged at the end of the first five cycles are brought back into the reactor at the end of the seventh and eighth cycles. In addition, four subzones of fresh enriched (11.26% U-235) fuel are brought into the fast region at the end of the third cycle. As a result of these fuel management maneuvers, the actual peak burnup at the time of discharge was found to be 20.8%. With further fine tuning of the fuel management scheme, this number can be brought below 20%. Further substantial reduction of the peak discharge burnup is possible if more subzones of enriched fuel (11.26% U-235) are brought into the reactor at appropriate times. However, this would also increase the total uranium resource requirement for the fuel cycle.

The details of the adopted fuel management strategy are shown schematically in Figure 2.8. Details for Zones IV, V and VI are shown in the figure (subzones 14-33). Corresponding details for the outer region consisting of Zones I, II and III (subzones 1 to 13) are not shown. These, however, are very simple. One subzone of fuel is always shuffled to the next zone at the end of each cycle. All fuel transfers, into and out of the reactor, or within the reactor are performed at the end of burnup cycles. All transfers take place in units of subzones (12 subassemblies).

The symbols used in Figure 2.8 are explained below.

- (x) : indicates that a fuel subzone from a lower numbered zone is moved into that position while the fuel that was in that position is moved into a higher numbered zone.
- (x)→ : indicates that a fuel subzone from a lower numbered zone is moved into that position while the fuel that was in that position is moved out of the reactor into external storage.

EOC No.	Zone IV		Zone V					Zone VI												
	Subzones		Subzones					Subzones												
	15	14	19	17	16	20	18	21	22	23	24	25	26	27	28	29	30	31	32	33
1	(x)					(x)										(x)→ A				
2		(x)	(x)												(x)→ B					
3	(x)						(x)							(x)→ C		(x)↘ NF D	(x)↘ NF E	(x)↘ NF F	(x)↘ NF G	
4		(x)		(x)									(x)→ H							
5	(x)				(x)→ I															
6		(x)				(x)→														
7	(x)		(x)→					(x)↘ G	(x)↘ F	(x)↘ E	(x)↘ D	(x)↘ A	(x)↘ B							
8		(x)					(x)→							(x)↘ C	(x)↘ H	(x)↘ I				
9	(x)			(x)→																
10		(x)			(x)→															
11	(x)					(x)→														
12						E	O	L												

Figure 2.8 Details of the Fuel Management Strategy Over the Lifetime for the Sodium Cooled (CM)FMSR

(x)↕: indicates that a fuel subzone from external storage is brought into that position while the fuel that was in that position is moved out of the reactor into external storage.

Letters near the arrows (A,B,C, etc.), when used, identify the fuel subzones that are brought into or taken out of the reactor.

Letter NF denotes fresh new enriched fuel (11.26% U-235 subzones).

Looking at Figure 2.8, at the end of cycle 3, for example, one subzone from Zone III is moved to subzone 15 of Zone IV. The fuel that was in subzone 15 is moved to subzone 18 of Zone V, while that fuel, in turn, is moved to subzone 27 of Zone VI. The fuel that was under subzone 27 is tagged C and moved into external storage. In addition, four fresh subzones of enriched fuel (NF) are brought into subzones 30, 31, 32 and 33. The fuel subzones that were in these positions are tagged D, E, F and G, respectively, and moved to external storage. D, E, F and G are brought back into the reactor at the end of the seventh cycle. C is brought back into the reactor at the end of the eighth cycle.

In the actual reactor physics calculations, the above fuel management strategy was slightly modified for the sake of calculational convenience.

#### 2.4.4 Results of Burnup Calculations

The single burnup cycle length required to maintain the criticality of the reactor throughout the 30-year lifetime was found to be about 640 full power days. Table 2.4 tabulates the values of  $K_{eff}$  and breeding ratio at the beginning of each of the 12 burnup cycles. The values at the end of cycles 1, 4, 8 and 12 are also given. The breeding ratio is found to increase with burnup as the importance of plutonium fissions increases. The reactivity swing over the cycle is the largest for the first cycle (1.1%) and becomes smaller at higher burnups.

Figure 2.9 shows the changes in the reactor inventories of U-235, Pu-239, and total fission products with successive burnup cycles. The figure shows the inventories at the beginnings of cycles. Discontinuities at the beginning of the fourth and the eight cycles reflect the particular fuel management scheme employed (see Figure 2.8).

Table 2.5 tabulates the changes in the isotope inventories during cycles 1, 4, 8 and 12. Also, the percentage of the total fissions occurring in U-235 (approximate) during each of the cycles is shown. It is seen that even during the last cycle 9.1% of the fissions take place in U-235. Corresponding numbers for the equilibrium cycle are also shown for the sake of comparison.

During a burnup cycle the power produced by the fuel subzones near the center of the reactor tends to increase due to buildup of plutonium in this region. Since the total reactor power is held constant, the power produced in the other zones falls if there is no compensating control rod action. The subassembly orifices are set to cool the highest power that will be produced by the subassembly during the cycle. Hence, for better thermal efficiency the power swing during a cycle should be kept as low as possible. The magnitude of the power swing varies from cycle to cycle. Figure 2.10 shows the power swings

TABLE 2.4

Sodium-Cooled (CM)FMSRResults of Burnup Calculations Over Reactor Life

Time	$K_{eff}$	Breeding Ratio	$\Delta K$ Over Cycle
BOC 1	1.0118	1.095	.011
EOC 1	1.0228	1.095	
BOC 2	1.0136	1.123	
BOC 3	1.0144	1.148	
BOC 4	1.0197	1.164	.0069
EOC 4	1.0266	1.153	
BOC 5	1.0189	1.182	
BOC 6	1.0165	1.198	
BOC 7	1.0108	1.221	
BOC 8	1.0180	1.20	
EOC 8	1.0246	1.183	.0066
BOC 9	1.0163	1.218	
BOC 10	1.0148	1.226	
BOC 11	1.0111	1.237	
BOC 12	1.0047	1.253	
EOC 12	1.0083	1.232	.0036

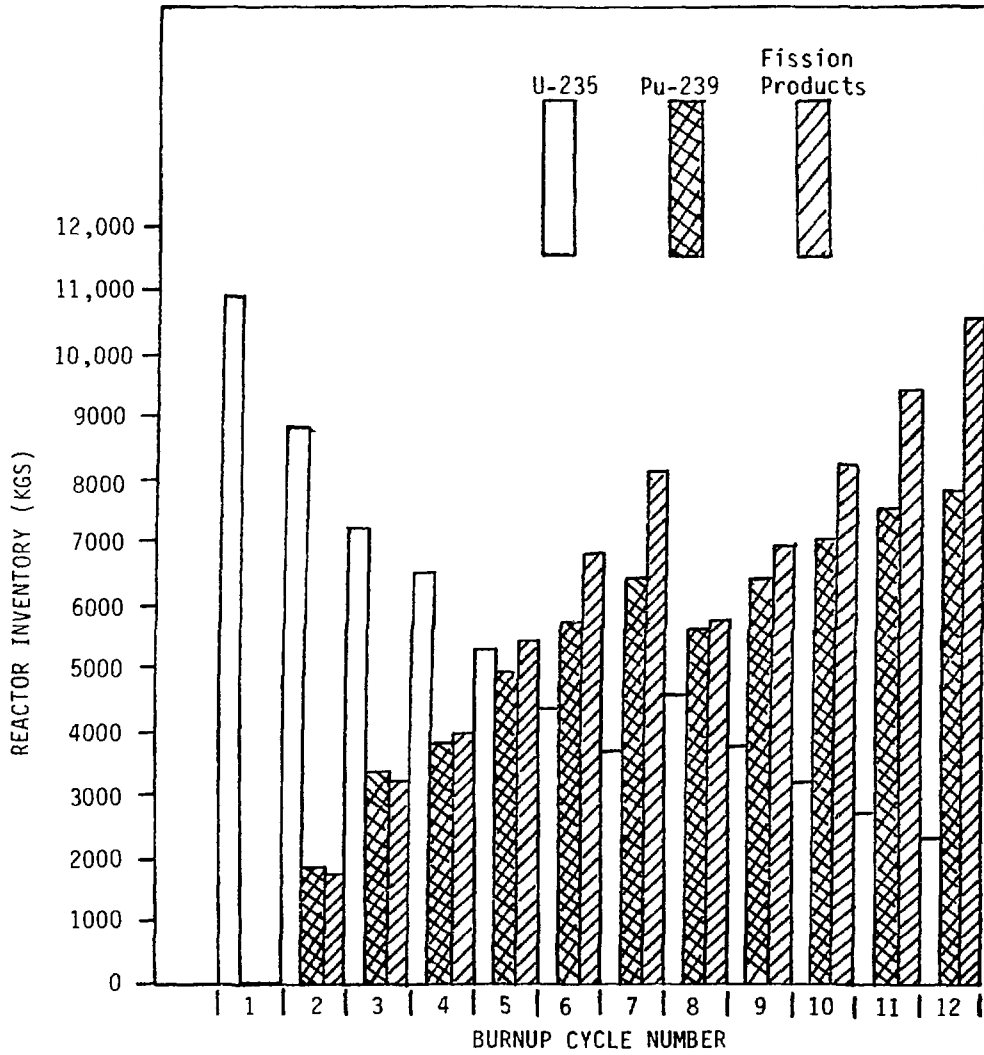


Figure 2.9 Reactor Isotope Inventories at the Beginning of Burnup Cycles, (CM)FMSR

TABLE 2.5

Changes in Isotope Inventories During Selected Burnup Cycles  
[Sodium-Cooled (CM)FMSR]

Time	U-235 (kg)	Pu-239 (kg)	Fission Product (kg)	% Fissions in U-235 (approximate)
BOC 1	10,899	0	0	75.8
EOC 1	9,184	1,912	1,766	
BOC 4	6,482	3,840	3,948	44.1
EOC 4	5,474	5,140	5,728	
BOC 8	4,538	5,696	5,708	32.6
EOC 8	3,808	6,766	7,500	
BOC 12	2,316	7,790	10,562	9.1
EOC 12	2,112	8,510	12,360	
BOEC	884	7,804	7,820	2.9
EOEC	852	8,220	8,612	

for cycle 7, which has the worst swing among all the cycles. The subzones of zones IV, V and VI only are shown in Figure 2.10. The largest power swings occur in subzones near the reactor center. These swings, which are without adjustment by control rods, are more than satisfactory.

Table 2.6 summarizes some of the important results of reactor physics calculations. The peak discharge burnup is 20.8% and the peak fast fluence ( $E > 0.1$  MeV) is  $7.7 \times 10^{23}$  n/cm<sup>2</sup>. The  $\beta_{eff}$  (which is equal to one dollar of reactivity) at the beginning of reactor life (BORL) is approximately 70% higher than at the end of reactor life (EORL). This is because at BORL most of the fissions occur in U-235 whereas at EORL most fissions occur in Pu-239. The delayed neutron fraction for U-235 is approximately twice as large as for Pu-239. The values of  $\beta_{eff}$  were calculated using the perturbation code PERT-V.

#### 2.4.5 Reactivity Coefficients

Table 2.6 also gives the Doppler reactivity coefficients and preliminary values of the sodium void reactivity gain for full core voiding, at BORL and at EORL. The reactivity coefficients were obtained from 50-group calculations in R-Z geometry.

The Doppler reactivities are calculated for two temperature ranges, 300 K-975 K and 975 K-1500 K. The Doppler reactivity coefficients at BORL are significantly larger than those for typical oxide-fueled reactors (which are of the order of 0.006). This is due to comparatively large amounts of low energy flux (below 25 keV) in the moderated region of the (CM)FMSR and to the comparatively large reactivity worth of neutrons in this region. The Doppler reactivity coefficients at EORL are considerably smaller than at BORL. This is due to the depletion of the low energy flux due to the buildup of large amounts of fission products.

Figure 2.11 shows the 20-group neutron spectra in the moderated region (subzone 17) and the fast region (subzone 27) at EORL. A comparison with the spectrum at BORL (Figure 2.5) shows that the low energy fluxes at EORL are smaller and, thus, that the spectrum has become harder compared to that at BORL.

The relatively low sodium void reactivity at BORL (\$1.38) is typical of U-235 fueled reactors. The variation of  $\eta$  with energy (at higher energies) for U-235 is comparatively flatter than for Pu-239. As a result the positive spectral component of sodium void reactivity is smaller for U-235 fueled reactors. Also, the value of  $\beta_{eff}$  at BORL is approximately 70% higher than at EORL. As a result, the dollar value of the sodium void reactivity at BORL is comparatively smaller. At EORL, fissions in Pu-239 are much more numerous than fissions in U-235 while the value of  $\beta_{eff}$  at EORL is smaller than at BORL. Also, the effect of accumulated fission products is to increase the sodium void reactivity coefficient. These factors combine to give a large positive sodium void reactivity at EORL. These sodium void calculations should be considered as preliminary. They are very sensitive and may change with further study. Application of the recently created fission product cross-section set, for instance, will significantly lower these values at EORL.

The change in the sodium void reactivity between BORL and EORL can also be explained from comparing the respective adjoint spectra. Figure 2.12 compares



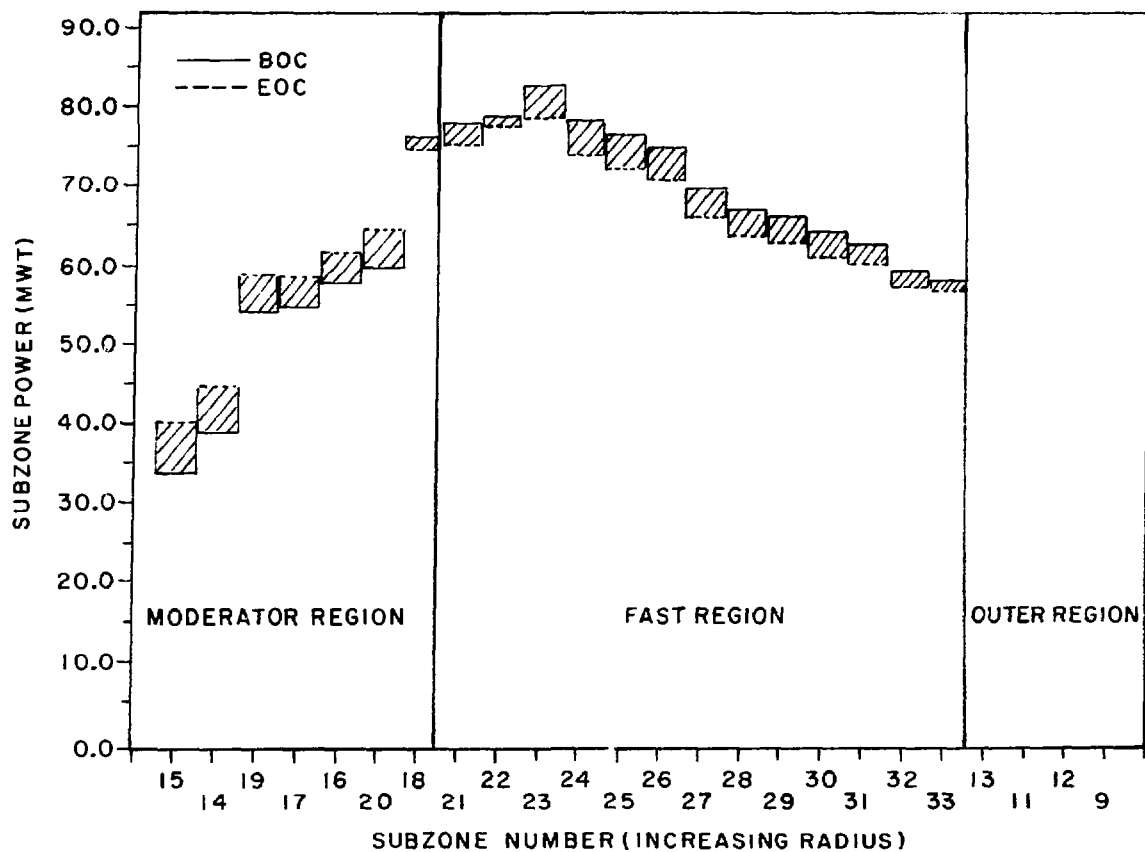


Figure 2.10 Variation of Subzone Power During Burnup Cycle 7, (CM)FMSR

TABLE 2.6

Summary of Reactor Physics Calculations,  
Sodium-Cooled (CM)FMSR

Cycle Length = 640 fpd, all cycles

Peak Discharge Burnup = 20.8%

Peak Fast Fluence (E>0.1 MeV) =  $7.7 \times 10^{23}$  n/cm<sup>2</sup>

Effective Delayed Neutron Fraction,  $\beta_{eff}$

Beginning of Reactor Life (BORL) = 0.0072

End of Reactor Life (EORL) = 0.0042

Sodium Void Reactivity

BORL = 1.38\$

EORL = 7.42\$

Doppler Reactivity (T dK/dT)

Between 300 K and 975 K:

BORL = -0.0122

EORL = -0.0073

Between 975 K and 1500 K:

BORL = -0.0112

EORL = -0.0070

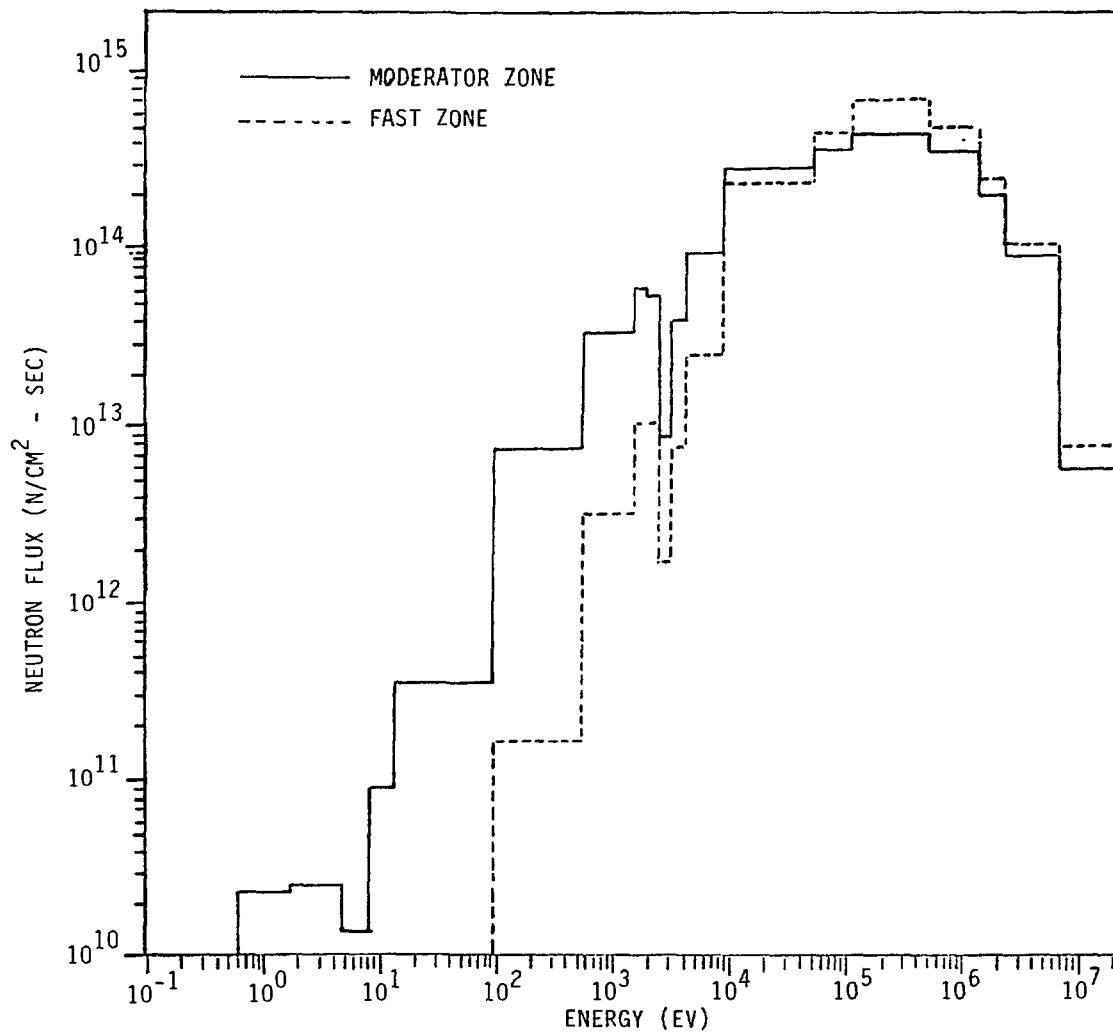


Figure 2.11 Neutron Energy Spectra at the End of Reactor Life for the (CM)FMSR

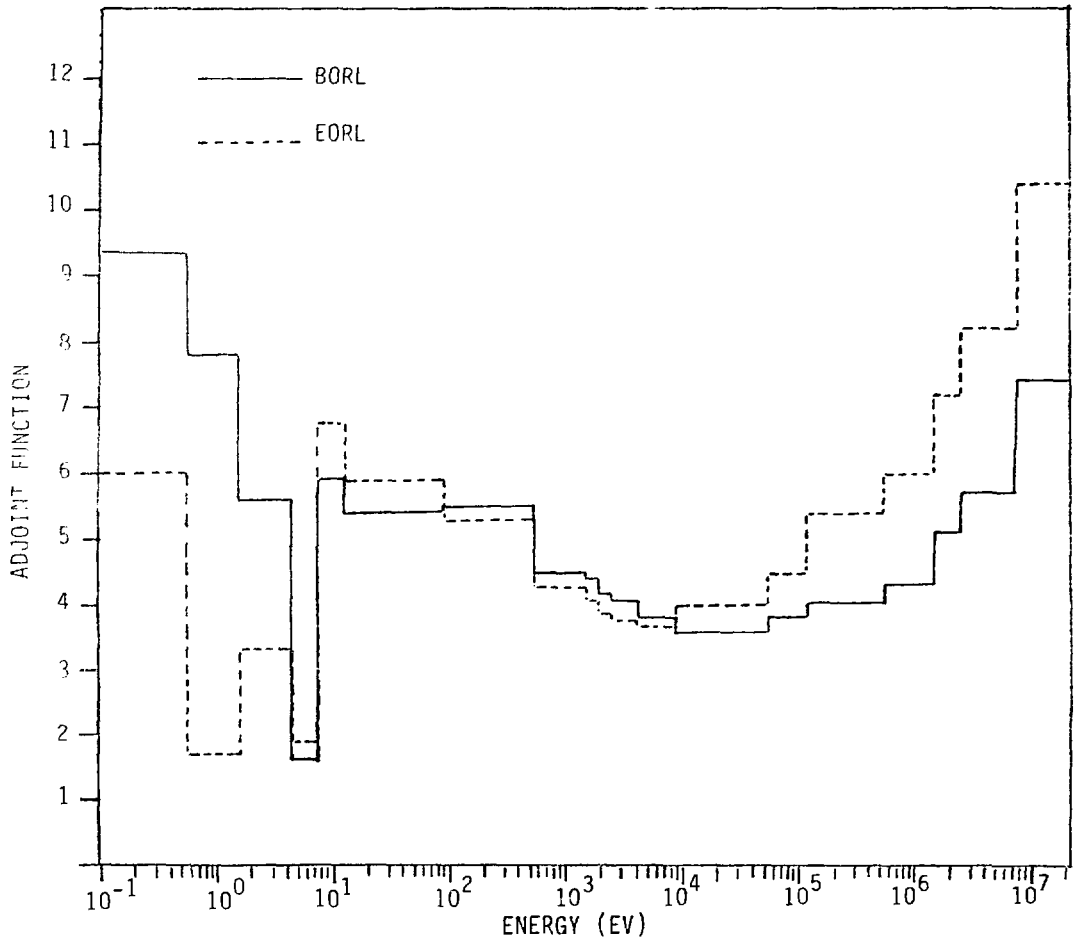


Figure 2.12 Adjoint Functions at BORL and EORL in the Moderated Region, (CM)FMSR

the 20-group adjoint spectra in the moderated region (subzone 17) at BORL and EORL. Figure 2.13 compares the adjoint spectra in the fast region (subzone 27). In both the regions the adjoint function in the energy range  $E > 5$  keV is steeper (larger positive slope) at EORL than at BORL. This is principally due to the larger number of plutonium fissions at EORL. The adjoint spectra at EORL are seen to be flatter (smaller negative slope) in the energy range below 5 keV than at BORL. This is principally due to the buildup of fission products which have relatively high absorption cross sections for low energy neutrons. The combined effect of these factors is a higher sodium void reactivity at EORL.

#### 2.4.6 Reactor Control During Burnup Cycles

During the first burnup cycle the reactivity of the (CM)FMSR increases by 1.1% (see Table 2.4). From preliminary calculations in R-Z geometry, it is found that at BORL the reactivity worth of withdrawing the central moderator subassemblies is only 0.64%. Hence, for the first burnup cycle at least, the moderator subassemblies will not be able to provide the required reactivity control.

The reactivity swings during the later cycles are considerably smaller. During the final burnup cycle the reactivity increases by only 0.36%. It is found that the reactivity worth of the central moderator subassemblies increases with burnup. This is due to the changes in the fissile composition of the fuel and to the accumulation of fission products. At EORL, for example, the reactivity worth of the central moderator subassemblies is found to be about 6.8%, much more than is required to control the reactivity swing during the final cycle.

Hence, during the later part of the reactor life, the central moderator subassemblies may be used to control the reactivity variations. In the early part, on the other hand, poison control rods may have to be used. More detailed calculations, however, are needed.

#### 2.4.7 Thermal-Hydraulic Calculations

Detailed results of thermal-hydraulic calculations for the (CM)FMSR were presented in Reference 1. Thermal-hydraulic calculations were performed with the SATURN<sup>(1)</sup> code which is a flexible, one-dimensional, multichannel steady-state code developed at BNL for the FMSR program. The coolant inlet temperature was 380°C and the inlet pressure was 140 psi. The mean temperature rise of the coolant was 160°C. Some of the important thermal-hydraulic parameters can be seen in Table 2.2. Metallurgical considerations set the maximum fuel centerline temperature and fuel clad contact temperature at 850°C and 625°C, respectively. Calculations indicated that these temperature limits will not be exceeded even when hot spot factors are included. The total pressure drop across the core was 113 psi and the total pumping power was 13.5 MW. These results were calculated for the equilibrium cycle and are also roughly applicable to any of the twelve burnup cycles, since the design parameters are unchanged and the peak power densities and radial and axial power shapes are approximately similar for all the cycles.

Recent preliminary calculations using the two-dimensional thermal-hydraulic code COBRA-IV<sup>(5)</sup> have reaffirmed the basic validity of the results obtained

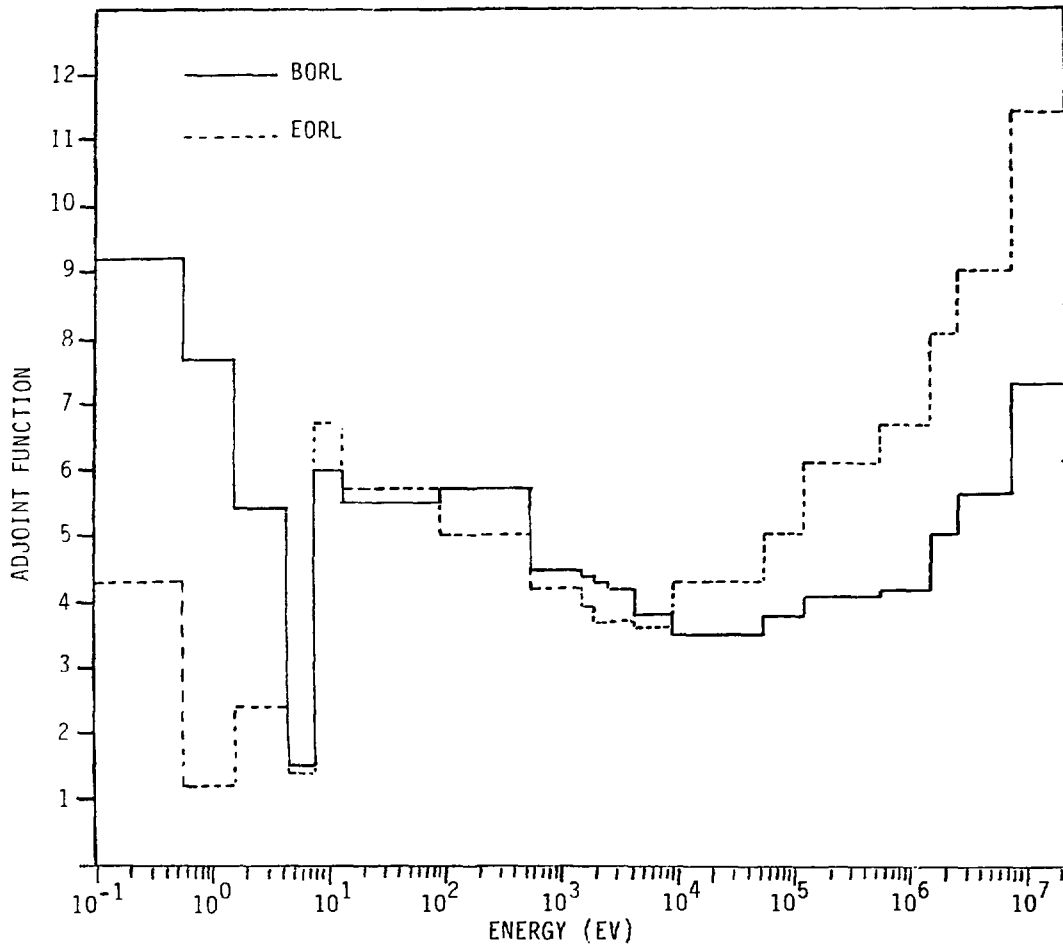


Figure 2.13 Adjoint Functions at BORL and EORL in the Fast Region, (CM)FMSR

by the simpler SATURN code. In the inner moderated region and the fast region, the temperature predictions made by COBRA for the peak channels agree well with those made by SATURN. The fuel subassemblies in the above two regions are characterized by high power densities and low radial power gradients. In the outer region, on the other hand, the fuel subassemblies have low power densities and large radial power gradients. Here, the temperatures predicted by COBRA for the peak channel are considerably lower than those predicted by SATURN. The peak channels in this region occur at the edges of fuel subassemblies. The enhanced cooling effect of cross flow for the edge pins can be taken into account in COBRA calculations but cannot be included in SATURN calculations. Hence, the results obtained by SATURN for the outer region are overly conservative. Improved modeling of the peak channel in the outer region, to achieve better agreement with COBRA-IV, will result in a higher mixed-mean coolant temperature at the core exit.

## 2.5 URANIUM RESOURCE REQUIREMENTS

Table 2.7 lists the natural uranium needs for the 30-year life of the (CM)FMSR. The natural uranium needed for the startup reactor is by far the largest part of the total requirement, i.e., 2055 T. Most of the natural uranium is converted to enriched uranium prior to use. It is assumed that the depleted uranium tails in the enrichment plant contain 0.2% U-235. During the 30 years, 11 subzones of natural uranium are fed into the reactor. The amount of natural uranium for this totals 70 tonnes. At the end of the third burnup cycle four subzones of 11.26% enriched uranium fuel are fed into the reactor. This requires 375 T of natural uranium. The total natural uranium requirement over the life of the reactor is 2500 T.

At the time of discharge many of the fuel subzones still contain significant amounts of U-235, for which credit may be taken. The U-235 content of the fuel for which credit is taken varies from 1% to 3.7%, the average being 2.2%. This credit is equivalent to 370 T of natural uranium. After 30 years of operation, when the FMSR is decommissioned, the outer region of the reactor (subzones 1-13) can be used in a second FMSR. These subzones have low burnups but significant amounts of fissile fuel. This transfer does not significantly alter the fuel cycle of the second reactor. This arrangement would reduce the amount of uranium needed for the second reactor by an amount corresponding to the first 13 subzones. The credit for this is equivalent to 292 T of natural uranium. The total credit over the 30 years is 662 T of natural uranium. Hence, the net amount of natural uranium required over the life of the sodium-cooled (CM)FMSR is 1838 T. This represents a significant resource saving relative to that required for generation of the same amount of energy by a LWR.

TABLE 2.1

Natural Uranium Resource Requirements of the (CM)FMSR

Natural Uranium for the Startup Reactor	= 2055 T
Natural Uranium Feed for the 30-Year Life	= 70 T
Natural Uranium for Four Enriched (11.26%) Fuel Subzones (Needed at EOC 3)	= <u>375 T</u>
Total Natural Uranium Requirement	= <u>2500 T</u>
<u>Credits</u>	
Credit for U-235 in Discharged Fuel	= 370 T
Credit for Subzones 1-13 at EOL	= <u>292 T</u>
Total Credits	= <u>662 T</u>
Net Requirement for Natural Uranium	= 2500-662 = <u>1838 T</u>



### 3. THE EXTENDED FUEL CYCLE FMSR [(EC)FMSR] CONCEPT - PHYSICS ANALYSIS

#### 3.1 INTRODUCTION

The Extended Fuel Cycle FMSR [(EC)FMSR] is a new design concept which offers the potential for excellent performance and cost characteristics while also providing attractive nuclear weapons proliferation resistance and major resource utilization advantages. Like the Centrally-Moderated FMSR, <sup>(1)</sup> metal fuel is used in this sodium-cooled reactor to take advantage of its high density of fertile atoms as well as its excellent burnup characteristics. A fuel design based largely on the EBR-II reactor MARK-II fuel is used in order to achieve extensive fission product gas release and therefore excellent burnup performance. A moderator is used to enhance design flexibility and improve safety characteristics.

The principal design strategy is to exploit the inherently high conversion ratio of metal-fueled breeders by adding sufficient moderator, in this case BeO, so that the reactivity gain resulting from breeding new fissile material slightly exceeds the reactivity losses due to fission product buildup at the start of the fuel cycle. Under these conditions there is a very small reactivity change over a very long fuel cycle, until losses due to fission products dominate and the fuel cycle is ended. A very long fuel cycle has immediate operating advantages for the operating utility and leads to reduced fuel cycle costs.

Major safety advantages of this design approach, which result from employment of some moderator, are a relatively low sodium void reactivity worth and a significantly larger (approximately a factor of 3) Doppler feedback. These two factors enhance the safety of the plant without compromising either performance or economics.

The proliferation-resistance advantage of an (EC)FMSR stems from the fact that the reactor has to be refueled only once or twice over its 30-year plant life. In this way fuel handling, fuel reprocessing, fabrication, or enrichment are minimized. Each of these steps would offer some potential for diversion. If the nation which operated an (EC)FMSR would agree to buy its fresh fuel and sell its spent fuel to an internationally managed agency, then the nation would not need to have within its borders fuel reprocessing, fuel enriching, or fuel fabrication facilities. An (EC)FMSR has been designed and shown to operate for 30 years with excellent neutronic and thermal-hydraulic performance. The sodium void reactivity gain at end of life of the core, however, was found to be in the range of that of a conventional oxide-fueled LMFBR, such as the French Super-Phenix Reactor or the British Commercial Fast Reactor. Since there is a considerable licensing advantage for reactors with smaller sodium void reactivity gain, an important design objective of the (EC)FMSR is to achieve long fuel cycle lifetimes with minimum end-of-life sodium void worths.

Analytic and design studies to more fully understand the origins of reactivity changes associated with sodium voiding are now under way at Brookhaven National Laboratory. These tend to indicate that modest changes in geometry and composition ratios as well as improved fission product cross sections can lead to a considerable reduction of the computed sodium void reactivity gain

for the (EC)FMSR. Thus, further design studies for the 30-year FMSR may lead to improved sodium void characteristics. The present report will focus on those studies for (EC)FMSR fuel cycles of shorter length (around ten years) which offer major advantages.

The particular design described in the present report is only one of the many design options which can be achieved through the judicious use of metal fuel and moderator. Primary emphasis in the design studies reported here was directed toward achieving a design which had a long fuel cycle with excellent thermal hydraulics and neutronic performance, low fuel cycle costs, and enhanced safety features. Other designs are equally feasible which could emphasize, as examples, very short doubling times or symbiotic operation to generate U-233 for HTGR needs, if these should be in the national interest. Other fuels are now being examined for use in FMSR-type designs. These should be capable of providing many of the above objectives, but probably at a somewhat reduced level of performance.

The (EC)FMSR has been conceived to achieve as far as is practicable the following objectives:

- a. an extended fuel cycle (presently 10 years),
- b. a small reactivity change over the fuel cycle,
- c. small power density changes over the fuel cycle, locally and regionally,
- d. competitive fuel cycle costs,
- e. a low sodium void reactivity gain,
- f. strong Doppler effect feedback safety coefficients,
- g. proliferation resistance through use of one or possibly two core loadings over full plant lifetime (three for present study),
- h. use of conventional breeder reactor technology as far as possible. The balance-of-plant outside of the core should be identical to that of any other fast breeder, use essentially the same core radius, pressure drop, same inlet and outlet temperatures, etc. The metal fuel should operate in the manner of the MARK-II fuel used in EBR-II as far as possible. The scale-up of the fuel to prototypical 1000-MW(e) reactor dimensions represents a concern to be resolved by experimental testing and design studies.

The extended fuel cycle objective has a number of implications with regard to design decisions. Since metal fuel has very roughly somewhat less than twice as many heavy metal atoms per unit volume as an oxide or a carbide fuel, the same total number of fissions would require a proportionately smaller fractional heavy metal burnup for the same core volume, same fuel volume fraction, etc. This is a major advantage if core size is to be minimized in order to reduce reactor capital costs and when the allowable heavy metal burnup is a major concern. An (EC)FMSR which operates on carbide or oxide fuel

may be feasible, although some degree of compromise, such as a reduced fuel cycle length or larger core volume, may be necessary.

The core radius of the (EC)FMSR has been designed to be close to that of a typical heterogeneous oxide-fueled LMFBR with the objective of having an (EC)FMSR core someday operate as a replacement core in a demonstration 1000-MW(e) LMFBR. The core radius is kept to reasonable dimensions by increasing the core height. This change automatically improves the breeding performance of the reactor but it also worsens the sodium void effect by lowering the negative axial neutron leakage reactivity component on voiding. For the (EC)FMSR, larger core heights are possible since the BeO moderator provides an alternative means for reducing the sodium void reactivity gain. In addition, a relatively modest power density for the metal fuel, along with a correspondingly generous sodium fraction, tends to keep the pressure at the core mid-height down, and thereby also reduce the distortion of the duct due to pressure-driven creep over the long fuel cycle.

Small initial differences in the fissile enrichment and moderator-to-fuel ratios tend to maintain the conversion ratios of the two core zones, and therefore, to preserve the radial dependence of the power density across the core over the years of operation. Control requirements and attendant control rod location problems are consequently minimized. Since there is no region in the (EC)FMSR in which there are any strong changes in power density over extended periods of time, thermal-hydraulics design problems are also greatly reduced. A thermal-hydraulics evaluation for the ten-year (EC)FMSR is provided in Section 4.

Most of the current section is devoted to the reactor physics and fuel cycle aspects of the (EC)FMSR, which are the subjects of Section 3.4, which also includes the results of a preliminary study of the control and shutdown rods design.

Fuel cycle cost studies which were performed in cooperation with the Massachusetts Institute of Technology are summarized in Section 5.

The metal fuel and materials aspects of the (EC)FMSR design are not discussed in this report. These have been described to some degree in two previous reports<sup>(1,6)</sup> and will not be repeated here. An advantage of the (EC)FMSR design is that the anticipated peak fuel burnup can now be made significantly less than that required for the (CM)FMSR and close to that which has already been achieved with about 1000 metal fuel pins in EBR-II. The expected peak fluence damage to the steel of the duct and cladding may be brought within the range of capability of the near-term D-9 steel and well within the capability of ferritic steels now under irradiation. Safety aspects of the (EC)FMSR design are not discussed in this report, in spite of their importance, but were briefly discussed in the same two previous reports. Since it is anticipated that the safety analysis of the (EC)FMSR and related safety experiments with metal fuel could lead to attractive safety conclusions, some near-term efforts in this area are needed.

### 3.2 (EC)FMSR DESIGN CONSIDERATIONS

Design of the (EC)FMSR core requires the determination of the moderator to fuel ratio and the geometrical arrangement of the moderator in the core. The radial power peaking factor within the subassembly as well as the swing in radial and axial power over the full fuel cycle are principally controlled by these decisions. Other design concerns relate to the radial blanket management over the long fuel cycle as well as the design and location of control and safety rods.

Experience gained from the Feasibility Study of the (CM)FMSR<sup>(6)</sup> indicated that the optimal value of the moderator to fuel volume ratio is near 1:3. In core optimization studies two parameters were varied: the moderator volume fraction and the moderator density. The maximum amount of moderator which can be used is determined by the minimum conversion ratio needed to sustain reactor criticality over the fuel cycle, so that enough fissile plutonium is bred to compensate for fission product buildup. Use of a dense moderator will cause power peaking at the fuel-moderator interface while utilization of a low density moderator requires an increase of moderator volume at the expense of a decrease in fuel volume. Other constraints which affect the design are the maximum fuel power density, fuel and coolant volume fractions, and allowable core pressure drop.

Two configurations were considered along with different geometrical arrangements of the moderator, namely configuration A and configuration B (see Figures 3.1 and 3.2). In configuration A, the moderator occupied the entire subassembly and was symmetrically surrounded by subassemblies filled entirely with fuel, such that the volume ratio of 1:3 was achieved. In configuration B the moderator was placed in the center of each fuel subassembly and occupied about 25% of the total volume, to yield the same 1:3 ratio.

Preliminary calculations for both configurations indicated some advantages of configuration B over configuration A. The radial power peaking near the fuel-moderator interface of configuration A was significantly higher than for configuration B, for which the moderator lumps have smaller widths. In order to decrease the peaking factors, the moderator density employed in configuration A was lowered, resulting in a higher sodium worth and smaller Doppler coefficient; these effects are undesirable from a safety point of view.

Most of the following discussion and results relate to configuration B, which was selected for the reference design studies. However, it should be noted that since the peripheral fuel pins are typically overcooled, modest power peaking near the fuel-moderator interface may be tolerable. This suggests that the overall core performance of configuration A should be compared with that of configuration B, and a final choice of core layout should be made at a later stage. There are also some practical design and economic advantages in favor of configuration A.

The design of the (EC)FMSR core and fuel subassembly followed, as closely as possible, conventional LMFBR design strategy. The (EC)FMSR core, however, is designed for a very long fuel cycle, somewhat higher burnup and a higher fast neutron fluence damage to steel than conventional LMFBRs. The smeared density of the metal fuel was taken to be exactly that used in the MARK-II

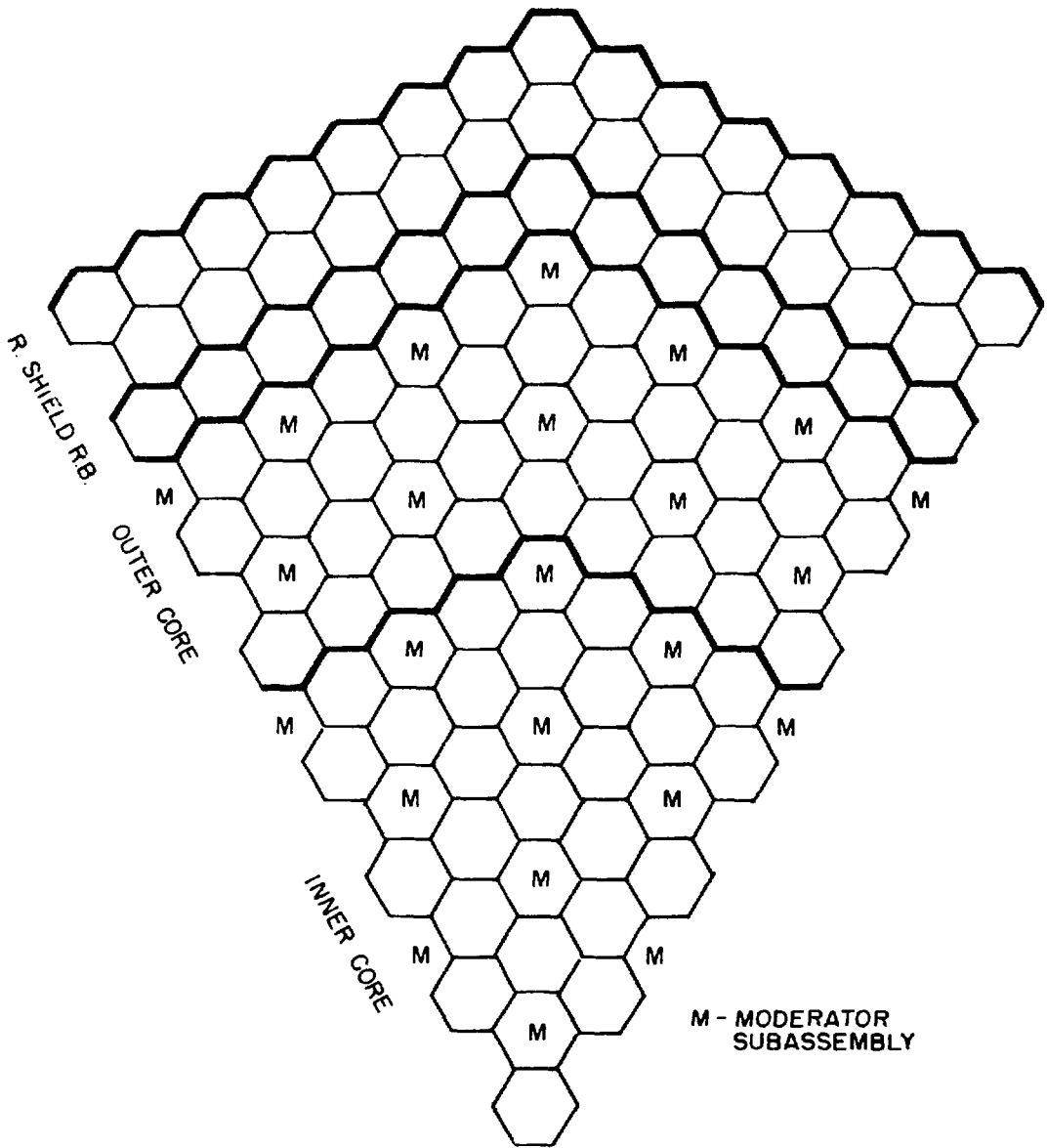


Figure 3.1 Configuration A Type (EC)FMSR Core Layout

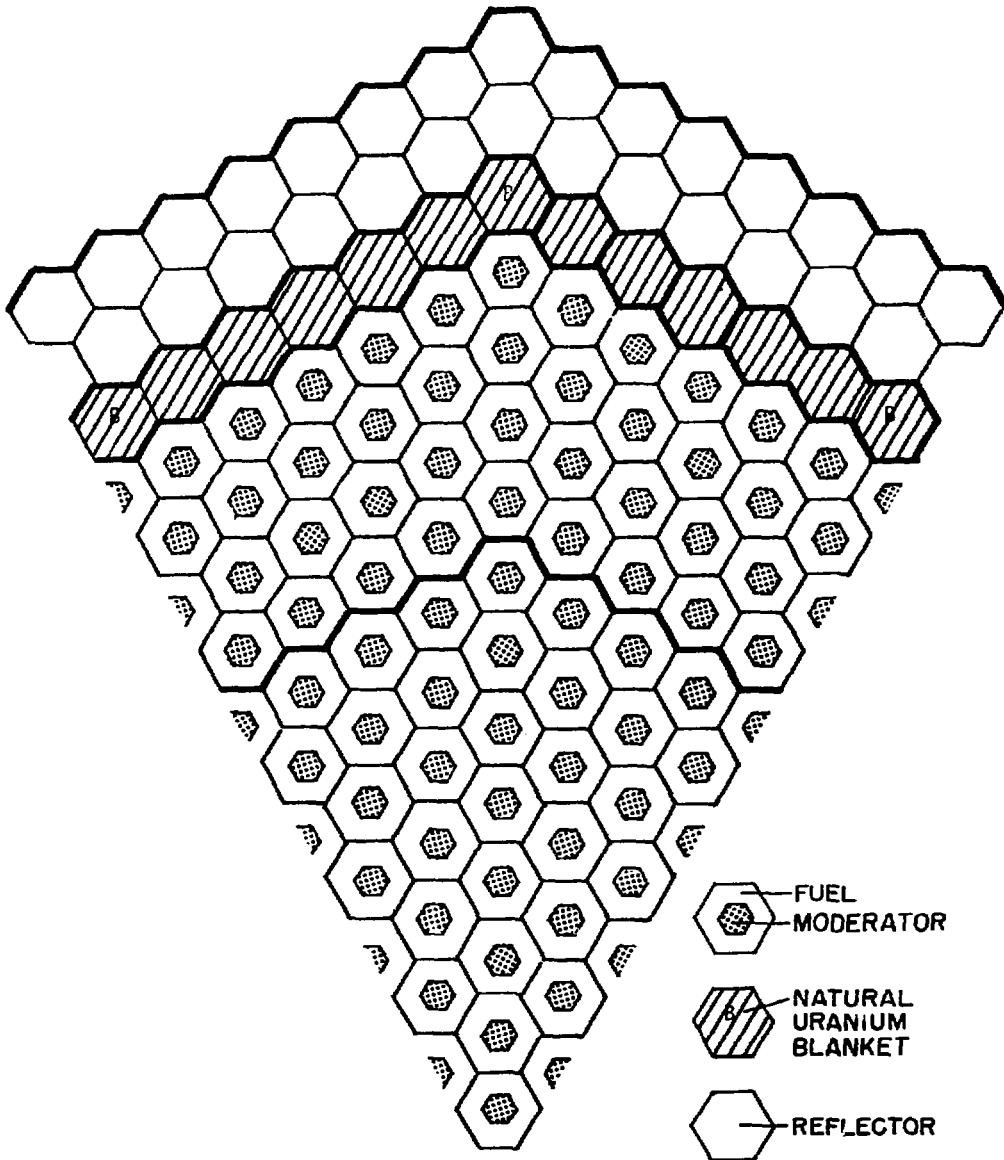


Figure 3.2 Configuration B Type (EC)FMSR Core Layout

design employed for the metal driver fuel used in EBR-II. The MARK-II fuel has already demonstrated that irradiations of 100,000 MWD/MT are attainable through irradiation of about 1000 pins to or beyond this limit. Failure at about 160,000 MWD/MT tends to occur as a result of a design feature of the EBR-II fuel which can be removed without any operating drawbacks. Therefore, concerns about performance of the proposed FMSR metal fuel are more often related to the dimensional changes required to bring the (EC)FMSR metal fuel to dimensions which are prototypical of 1000-MW(e) LMFBR designs. Particular duct designs may allow specification of the near-term D-9 steel for the (EC)FMSR ducts. The advanced ferritic steels currently under irradiation offer significantly greater swelling and creep resistance, but may not be needed for (EC)FMSR objectives. For the present design, the gap between subassemblies is set unusually large and will be redefined in future work.

Core and fuel subassembly design data are summarized in Tables 3.1 and 3.2 along with comparable data for a typical heterogeneous LMFBR design.<sup>(7)</sup> The proposed (EC)FMSR subassembly design is shown in Figure 3.3.

The fuel subassembly design shown in Figure 3.3 contains 240 fuel pins with an outer diameter of 0.776 cm and a cladding thickness of 0.035 cm. The wrapper wire has a diameter of 0.13 cm. The outer subassembly wall thickness is 0.318 cm and the inner duct, surrounding the moderator zone, is 0.250 cm thick. The fuel pin theoretical density was chosen as 0.75, in agreement with the design convention of the MARK-II fuel employed in the EBR-II reactor by ANL. This density provides the means for extensive fission gas release and reduction of fuel swelling. The need to cool the moderator was taken into account: a sintered block of BeO is anticipated for purposes of enhanced helium gas release, reduced swelling, and good thermal conductivity. Previous work at other laboratories indicates that if the temperature of the BeO can be kept above 900°C by means of a large temperature drop across the helium bond to the moderator duct wall, the BeO will have an excellent irradiation stability<sup>(8)</sup>.

### 3.3 CALCULATIONAL METHODS

#### 3.3.1 Cross-Section Generation

The 1DX code<sup>(3)</sup> was used to generate multigroup cross-section sets from the LIB-IV cross-section library,<sup>(2)</sup> which is based on ENDF/B-IV data. 1DX calculations were performed in cylindrical geometry for a two-region "unit-assembly" cell. The "unit-assembly" cell dimensions were chosen to represent a single hexagonal subassembly with inner moderator region. Reflective conditions were imposed on the left and right boundaries of the cell. Heterogeneous corrections were introduced to take into account "pin-cell" heterogeneity and "assembly-cell" heterogeneity. The "inverse fuel" correction, with moderator inside and fuel on periphery, was introduced into the 1DX code, following Reference (9).

Burnup calculations were performed in 20 groups whose group structure is presented in Table 3.3. Collapsing of the LIB-IV cross sections (50 groups) to 20 groups was performed for both the moderator and fuel regions using region-averaged fluxes. For the sodium-void reactivity and Doppler coefficient

TABLE 3.1  
General Core Data

	<u>(EC)FMSR</u>	<u>Heterogeneous LMFBR (TC-CC40-36)</u>
Power, MW(e)	1000	1000
No. of rings in core (including radial blanket)	14	17
Initial fissile inventory (Pu-239 + Pu-241), kg	7260	4268
Core height, cm	160	81
Core radius, cm	243	254
Fuel volume fraction	.43	.44
Steel volume fraction	.20	.19
Sodium volume fraction	.37	.37
Number of fuel subassemblies	468	354
Number of radial blanket subassemblies	78	210
Number of internal blanket subassemblies	-----	169
Total:	546	733
Number of control rod positions	42 (tentative)	24
Moderator core fraction, %	25*	-----
(BeO) moderator density, % T.D.		
Inner Core	65	
Outer Core	57	

\*First 4 rings of subassemblies have moderator volume fraction of 35%.



TABLE 3.2  
Fuel Subassembly Data

	<u>(EC)FMSR</u>	<u>Heterogeneous LMFBR (TC-CC40-36)</u>
Lattice pitch, cm	18	15
Duct wall thickness, cm	.318	.282
Sodium gap between subassemblies, cm	.800	.500
Number of fuel pins per subassembly	240	271
Fuel pin OD, cm	0.776	0.711
Fuel pin pitch, cm	0.908	0.839
Pitch/OD ratio	1.17	1.18
Fuel density, % T.D.	75	88
Fissile fraction, % fissile Pu		
Inner Core	7.4	17.7
Outer Core	7.8	18.1
Moderator duct thickness, cm	0.25	-----

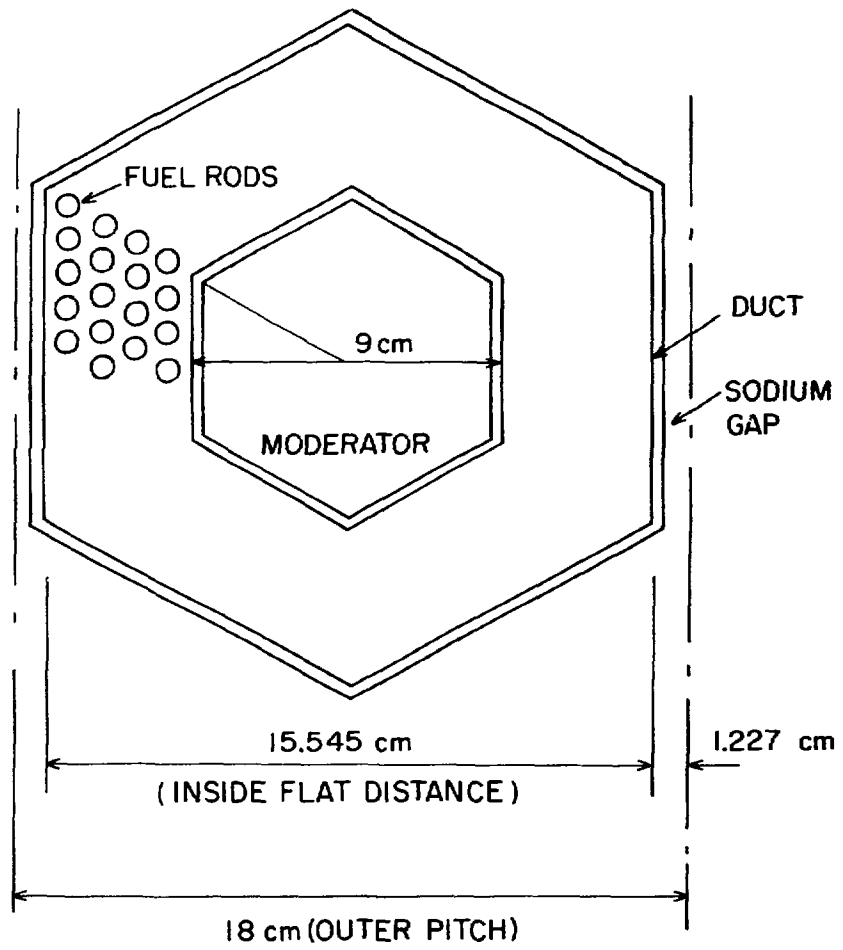


Figure 3.3 Fuel Subassembly Design

TABLE 3.3  
BNL 20-Group Structure

Group	LIB-IV Groups	Energy Range	Lethargy Width, $\Delta U$	Fission Source Fraction
1	1-2 (2)	20 MeV-6 MeV	1.192	0.035058
2	3-4 (2)	6 MeV-2.2 MeV	1.0	0.331826
3	5 (1)	2.2 MeV-1.3 MeV	0.5	0.222367
4	6-7 (2)	1.3 MeV-0.49 MeV	1.0	0.282496
5	8-13 (6)	0.49 MeV-0.11 MeV	1.5	0.112383
6	14-16 (3)	0.11 MeV-52 keV	0.75	0.010589
7	17-23 (7)	52 keV-9 keV	1.75	0.004898
8	24-26 (3)	9 keV-4.3 keV	0.75	0.000264
9	27 (1)	4.3 keV-3.3 keV	0.25	0.000040
10	28 (1)	3.3 keV-2.6 keV	0.25	0.000027
11	29 (1)	2.6 keV-2.0 keV	0.25	0.000019
12	30 (1)	2.0 keV-1.5 keV	0.25	0.000013
13	31-34 (4)	1.5 keV-582 eV	1.0	0.000022
14	35-39 (5)	582 eV-101 eV	1.75	0.000005
15	40-43 (4)	101 eV-13.7 eV	1.5	0.0
16	44 (1)	13.7 eV-8.3 eV	0.5	0.0
17	45 (1)	8.3 eV-5.0 eV	0.5	0.0
18	46-47 (2)	5.0 eV-1.8 eV	1.0	0.0
19	48-49 (2)	1.8 eV-0.68 eV	1.0	0.0
20	50 (1)	0.68 eV- $10^{-5}$ eV	11.31	0.0

calculations, a 50-group library was generated by the 1DX code for the fuel and moderator regions without collapsing. The LIB-IV group structure is shown in Table 3.4. A separate cross-section set was generated for the blanket fuel composition. In addition, cross-section sets were generated for different fuel temperatures (465 K and 1400 K), as well as a reference temperature of 875 K, and for fuel compositions with voided sodium.

The fission product treatment includes three lumped fission products in addition to Xe-135 and Sm-149. These fission lumps are Slowly Saturating Fission Products (SSFP), Rapidly Saturating Fission Products (RSFP) and Non-Saturating Fission Products (NSFP), all from the LIB-IV library. Neutron capture by a rapidly saturating fission product atom transformed that atom into a slowly saturating fission product atom. SSFP atoms transform into NSFP atoms and NSFP atoms do not transform on capture. Separate fission product yield sets were used for plutonium and uranium isotopes.

### 3.3.2 Hexagonal and R-Z Models of the (EC)FMSR Core

The principal neutronic calculations were carried out with the 2DB code.<sup>(4)</sup> 2DB is a two-dimensional (X-Y, R-Z) diffusion theory code with a triangular mesh capability. Both R-Z and hexagonal X-Y geometries were used in the present work. Hexagonal geometry calculations were performed to obtain the critical plutonium concentrations and radial power shapes within each subassembly. Because the (EC)FMSR layout was planned with a twelve-fold symmetry, these calculations could be performed economically using only a 30° sector of the core to represent the whole core. This allowed increased detail, with each hexagonal subassembly being divided into 24 triangular mesh points. Duct material and stagnated sodium (between subassemblies) were smeared over the fuel region, and the material of the duct surrounding the moderator was smeared over the moderator region.

Because of the 30° symmetry, each fuel zone represents 12 hexagonal subassemblies. The numbered zone map is shown in Figure 3.4. The calculational procedure included two steps. First, a critical plutonium concentration search was performed by the 2DB code in HEX geometry for the two zones of enrichment. In the second step the critical plutonium concentration is used in R-Z fuel cycle calculations. The core is represented in the R-Z model, with reflective conditions imposed on the left (core center) and mid-height boundaries, and with vacuum on the top and right boundaries. An R-Z representation of the core is necessary for depletion calculations, where the axial component of the power distribution is important, as well as for sodium void effect calculations. On the other hand, the correct radial power shape across the core and within the fuel subassembly can be determined only from HEX-geometry calculations. Summarizing, HEX and R-Z modeling was used for determining the core parameters as follows:

BOL critical Pu concentrations	- HEX
Radial power shape, radial peaking factors	- HEX
Doppler coefficients	- HEX,R-Z
Sodium void effect	- R-Z
Fuel cycle calculations	- R-Z

TABLE 3.4

LIB-IV Group Structure

<u>Group</u>	<u>Energy Range (eV)</u>		<u>Lethargy</u>	<u>Fission Source Fraction</u>
1	1.9971+7	1.0000+7	0.692	2.66500-3
2	1.0000+7	6.0653+6	0.5	3.23930-2
3	6.0653+6	3.6788+6	0.5	1.21445-1
4	3.6788+6	2.2313+6	0.5	2.10381-1
5	2.2313+6	1.3534+6	0.5	2.22367-1
6	1.3534+6	8.2085+5	0.5	1.72323-1
7	8.2085+5	4.9787+5	0.5	1.10173-1
8	4.9787+5	3.8774+5	0.25	3.60350-2
9	3.8774+5	3.0197+5	0.25	2.65500-2
10	3.0197+5	2.3518+5	0.25	1.92630-2
11	2.3518+5	1.8316+5	0.25	1.38100-2
12	1.8316+5	1.4264+5	0.25	9.80900-3
13	1.4264+5	1.1109+5	0.25	6.91600-3
14	1.1109+5	8.6517+4	0.25	4.84900-3
15	8.6517+4	6.7379+4	0.25	3.38500-3
16	6.7379+4	5.2475+4	0.25	2.35500-3
17	5.2475+4	4.0868+4	0.25	1.63400-3
18	4.0868+4	3.1828+4	0.25	1.13100-3
19	3.1828+4	2.4788+4	0.25	7.82000-4
20	2.4788+4	1.9305+4	0.25	5.45000-4
21	1.9305+4	1.5034+4	0.25	3.72000-4
22	1.5034+4	1.1709+4	0.25	2.57000-4
23	1.1709+4	9.1188+3	0.25	1.77000-4
24	9.1188+3	7.1017+3	0.25	1.22000-4
25	7.1017+3	5.5308+3	0.25	8.40000-5
26	5.5308+3	4.3074+3	0.25	5.80000-5
27	4.3074+3	3.3546+3	0.25	4.00000-5
28	3.3546+3	2.6126+3	0.25	2.70000-5
29	2.6126+3	2.0347+3	0.25	1.90000-5
30	2.0347+3	1.5846+3	0.25	1.30000-5
31	1.5846+3	1.2341+3	0.25	9.00000-6
32	1.2341+4	9.6112+2	0.25	6.00000-6
33	9.6112+2	7.4852+2	0.25	4.00000-6
34	7.4852+2	5.8295+2	0.25	3.00000-6
35	5.8295+2	4.5400+2	0.25	2.00000-6
36	4.5400+2	3.5358+2	0.25	1.00000-6
37	3.5358+2	2.7536+2	0.25	1.00000-6
38	2.7536+2	1.6702+2	0.5	1.00000-6
39	1.6702+2	1.0130+2	0.5	0.
40	1.0130+2	6.1442+1	0.5	0.
41	6.1442+1	3.7267+1	0.5	0.
42	3.7267+1	2.2603+1	0.5	0.
43	2.2603+1	1.3710+1	0.5	0.
44	1.3710+1	8.3153+0	0.5	0.
45	8.3153+0	5.0435+0	0.5	0.
46	5.0435+0	3.0590+0	0.5	0.
47	3.0590+0	1.8554+0	0.5	0.
48	1.8554+0	1.1254+0	0.5	0.
49	1.1254+0	6.8256-1	0.5	0.
50	6.8256-1	1.0000-5	11.31	0.



The HEX-geometry search calculations were usually performed with axial leakage evaluated by introducing a geometrical buckling (axial). In order to validate this approximation, the GA version of the PERT-V code (10) was used to calculate group- and zone-dependent bucklings. The R-Z calculated fluxes were used as input for the PERT-V run. Then the HEX calculation was repeated with the calculated group-dependent bucklings for each zone. The critical concentration of plutonium was then compared with that resulting from a calculation with geometrical buckling. This procedure was performed for a reference (EC)FMSR design. It was found that both critical compositions of plutonium were close (less than 0.1% difference), and that use of geometrical buckling at this stage was adequate.

A heterogeneous arrangement of the moderator lumps in the core presents a special problem in the R-Z modeling of the core. The amount of moderator, geometrical form, i.e., optical thickness of the moderator regions, total surface, etc., determines the amount of moderation, and eventually, the neutron spectrum and its spatial dependence. This, in turn, determines values and spatial variations of the conversion ratio, Doppler reactivity coefficient and sodium void effect, as well as the local power shape across the core. A "correct" R-Z representation means that the above-mentioned core parameters are as close as possible to the hexagonal geometry values, which are considered "exact" for present purposes. Plutonium buildup and its spatial distribution depend upon values of the local conversion ratio and power level and their spatial shape across the core. Fuel and moderator zones in the hexagonal core must be properly modeled by the arrangement of fuel and moderator in the circular rings used in the R-Z model of the core. As a means of defining the moderator and fuel ring dimensions, the fuel and moderator from every hexagonal row of fuel (see Figure 3.4) were projected on the R-axis as rings of either fuel or moderator while conserving their respective volumes. Conservation of the total fuel and moderator volumes is achieved in this model. All fuel and moderator ring thicknesses are approximately the same, except the first moderator ring. In order to avoid overmoderation of the central part of the fuel as a result of the thick moderator zone, that particular moderator ring was split into two rings.

It was observed that the zonal conversion ratio, as calculated in hexagonal geometry, followed a spatial dependence corresponding to the spectral shift from the center of the core (harder) to the periphery of the core (softer) because of greater leakage of higher energy neutrons. The same effect was achieved in the proposed ring geometry utilized in the R-Z model. The conversion ratio and power fraction values for the inner core, outer core and radial blanket, as calculated by the hexagonal and R-Z geometry, were compared to assure a close match between the two representations. Comparison between effective multiplication factor calculations showed differences of up to 0.5%  $\Delta K$ , which are attributed to the approximation of the axial component of the leakage by the geometrical buckling.

The R-Z representation of the half-core is shown in Figure 3.5. There are 15 rings, including 9 rings of the inner core, 4 rings of the outer core, a radial blanket ring and a radial shield ring. In the axial direction, each radial ring was divided into two parts of equal length. The axial blanket is followed by the plenum and axial shield. Note that zone numbers in the HEX and R-Z representations are related but not identical. The relation between

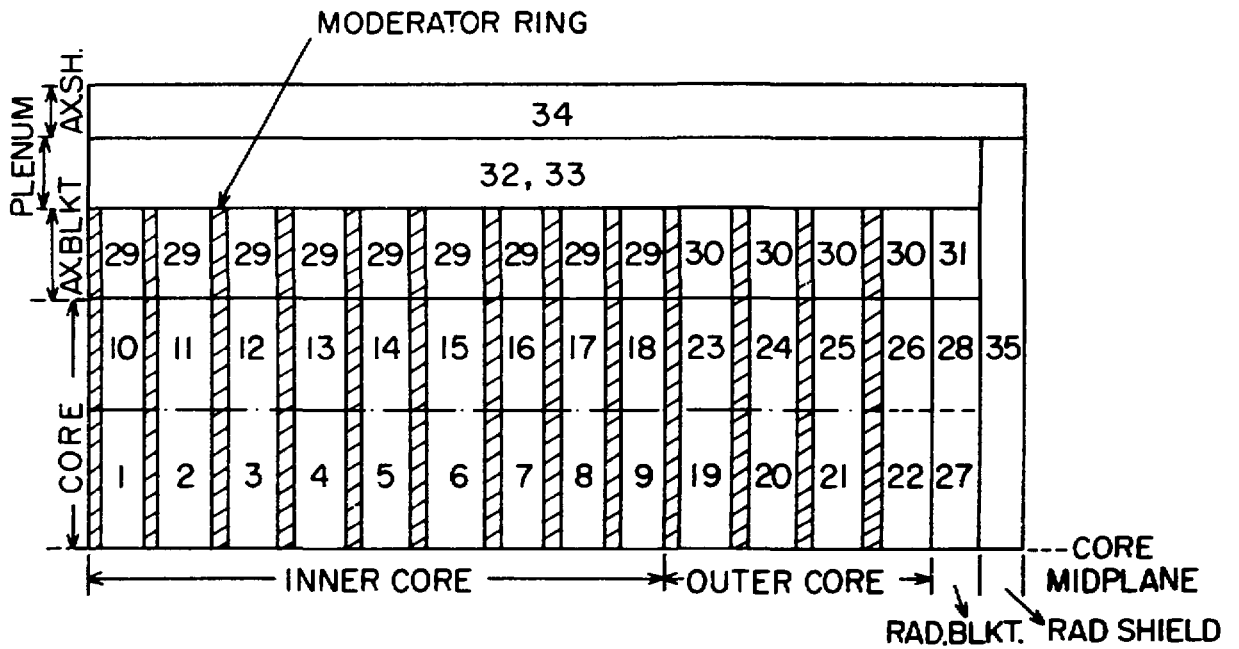


Figure 3.5 Zone Map: R-Z Representation of the (EC)FMSR Core



HEX and R-Z zones identification numbers (Figs. 3.4 and 3.5) may be interpreted as follows:

<u>HEX Zone Number</u>	<u>R-Z Zone Number</u>
half of 1	1 and 10
half of 1 and 2	2 and 11
half of 2 and 3	3 and 12
4 and 5	4 and 13
.....	.....
40	27 and 28

### 3.4 RESULTS OF THE (EC)FMSR PHYSICS ANALYSES

The physics performance of the (EC)FMSR core is summarized in this section. The identification of the zone numbers for HEX and R-Z geometry representations was given in the previous section and zone maps were shown in Figures 3.4 and 3.5 of that section.

#### 3.4.1 Reactivity Swing and Plutonium Concentrations During the Fuel Cycle

One of the most important advantages of the (EC)FMSR core is its very low reactivity swing over a very long fuel cycle. The time dependence of the effective multiplication factor, conversion ratios and plutonium inventories is presented in Table 3.5. The  $K_{eff}$  change over the 10-year irradiation is less than 1%  $\Delta K$ . The time behavior of the effective multiplication factor, conversion ratios and fissile plutonium inventories is responsible for meeting one of the design objectives of the (EC)FMSR concept. Plutonium buildup is limited to that which is necessary to sustain criticality of the core. In particular, the reactivity gain of the added plutonium compensates for the reactivity lost due to fission product buildup.

Utilization of the moderator in the core provides sufficient design flexibility to control plutonium buildup in the core and its spatial distribution. This is achieved by varying the density and geometry of the moderator, which leads to variations in the conversion ratios and power levels for different parts of the core. It should be noted that depletion calculations at this stage were performed without control rods. Control rods would be utilized as an additional tool for flattening the power shape across the core. For the present design, taking into account a very small reactivity swing over the fuel cycle, the BOL excess reactivity is only about 1%  $\Delta K$ , so that the amount of poison material needed to control it will be very small. A description of the proposed control system is presented in Section 3.4.6.

It was found that in order to achieve a flat power shape across the core at the beginning of life (BOL), the initial fissile plutonium fractions (Pu-239 and Pu-241) should be 7.4% HM and 7.8% HM for the inner and outer cores, respectively. The gain in the fissile inventory of the fuel after 10 years of operation is 2000 kg (or ~28% of the initial fissile inventory). The plutonium

TABLE 3.5

Multiplication Factor, Fissile Inventory and Conversion Ratios  
as a Function of Time

Full Power Days (Years)	$K_{eff}$	Conversion Ratios				Fissile Pu Inventory (239 + 241), kg				
		Inner Core	Outer Core	Radial Blanket	Axial Blanket	Inner Core	Outer Core	Radial Blanket	Axial Blanket	Total
0	1.0102	1.303	1.230	-----	-----	3152	4110	-----	-----	7262
550(2)	1.0072	1.277	1.199	21.2	14.0	3340	4190	94	178	7782
825(3)	1.0072	1.194	1.185	14.6	9.6	3416	4226	138	264	8044
1375(5)	1.0072	1.139	1.158	9.2	6.1	3534	4286	220	426	8466
1650(6)	1.0072	1.117	1.146	7.9	5.2	3578	4312	258	504	8652
2200(8)	1.0057	1.079	1.123	6.2	4.1	3640	4356	332	654	8982
2750(10)	1.0027	-----	-----	-----	-----	3672	4390	404	796	9262

isotopic composition for the initial fissile loading was that of discharged LWR fuel<sup>(11)</sup>:

Pu-239 - 57.7%  
Pu-240 - 22.8%  
Pu-241 - 13.9%  
Pu-242 - 5.6%

The change of plutonium isotopic composition with fuel burnup is presented in Table 3.6 and shown in Figure 3.6. The results indicate that while the total plutonium concentration in the core is increasing with irradiation, the Pu-241 fraction is decreasing. This effect influences significantly such core parameters as the conversion ratio and the sodium void reactivity effect.

#### 3.4.2 Power Shape and Power Swing

In addition to the requirement of a flat radial power profile across the core, another design objective was to minimize the power swing in each assembly over the 10-year fuel cycle. The larger the change in assembly power, the greater the penalty in the thermal performance of the reactor due to overcooling during the low power density portion of the fuel cycle. In addition, sodium flow adjustments to compensate for power peaking lead to overcooling of many of the rods within the subassembly. It was found that a certain tradeoff exists between the flatness of the power shape across the core and the minimum power swing of each subassembly. Flattening of the power shape is achieved by increasing the fissile fraction of the fuel in the outer core. This increase leads to a lower conversion ratio in that part of the core. In order to avoid a decrease in power density with time due to the lower conversion ratio, the moderator density in the outer core was decreased, and thus, the conversion ratio was increased once more.

Values in Table 3.7 demonstrate a relatively low power density swing in the inner and outer core; the maximum change in power density for any individual subassembly is about 11% of maximum, while most of the subassemblies have power density swings under 10%. The high power density swings in the radial and axial blankets are due to the significant plutonium buildup from zero at BOL (natural uranium) to about 2% fissile fraction at EOL. The power swing in the radial blankets will not result in a significant penalty in thermal efficiency because the power fraction in both the radial and axial blankets is only about 7% of the total power at EOL.

Another important characteristic parameter of core performance is the peaking factor for each subassembly, i.e., ratio of maximum to average power. Maximum power density occurs at the fuel-moderator interface due to the increased fission rate in the vicinity of the moderator. The increase in the fission rate is due to an increase in the effective fission cross sections of the fissile isotopes caused by the softening of the spectrum. This softening also causes a reduction of the conversion ratio near the moderator surface. A combination of those two factors, an increase in power density and a decrease in conversion ratio, was investigated by performing depletion calculations in HEX geometry. The spatial distribution of the plutonium buildup and its effect on time dependence of the subassembly peaking factors was evaluated. For this purpose, configuration A geometry (see Figure 3.1) was employed in order

TABLE 3.6

Plutonium Isotopic Composition of (EC)FMSR Fuel

Full Power Days (Years)	Inner Core % HM			Outer Core % HM			Radial Blanket % HM			Axial Blanket % HM		
	Pu-239	Pu-240	Pu-241	Pu-239	Pu-240	Pu-241	Pu-239	Pu-240	Pu-241	Pu-239	Pu-240	Pu-241
0 (0)	6.0	2.4	1.4	6.2	2.5	1.6	0.	0.	0.	0.	0.	0.
825 (3)	7.1	2.7	1.0	7.1	2.7	1.2	0.6	0.	0.	0.7	0.	0.
1650 (6)	7.7	3.0	0.8	7.5	2.9	0.9	1.2	0.	0.	1.4	0.	0.
2750 (10)	8.0	3.4	0.6	7.9	3.1	0.7	1.9	0.	0.	2.2	0.1	0.

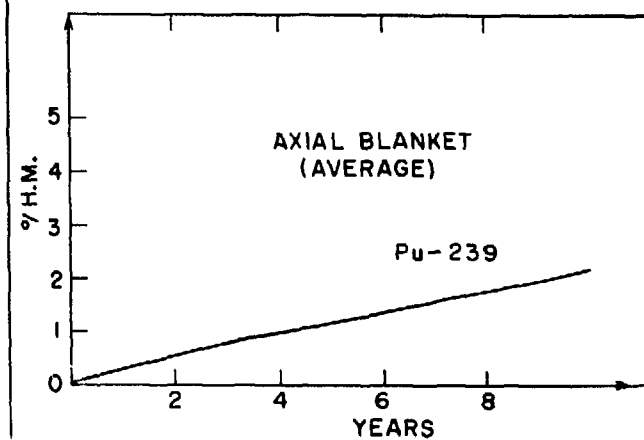
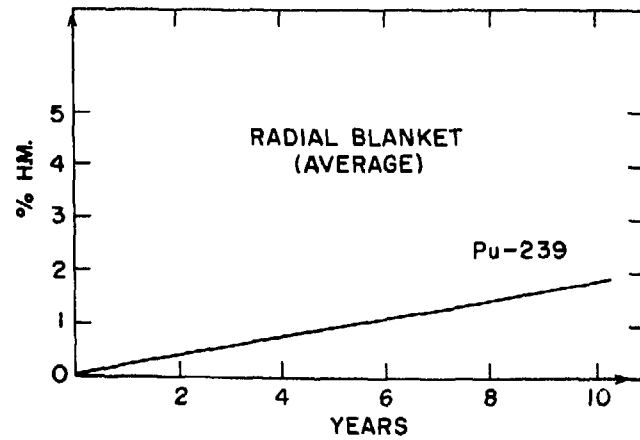
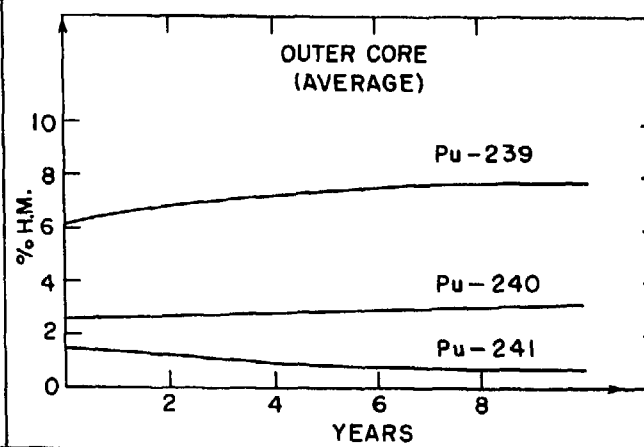
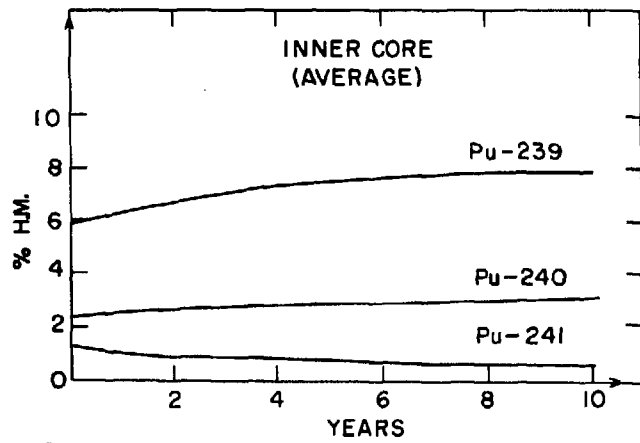


Figure 3.6 Plutonium Isotopic Change as a Function of Time

TABLE 3.7

Zone-Averaged Power Densities (MWT/L)  
R-Z Representation

Full Power Days (Years) R-Z Zone No.	0	1375 (5)	2750 (10)	$\Delta = \frac{P_{max} - P_{min}}{P_{max}}$ (%)	
1	.267	.287	.268	7	
2	.270	.283	.262	7	
3	.291	.293	.267	9	
4	.302	.296	.270	11	
5	.307	.301	.277	10	
6	.286	.293	.276	6	
7	.269	.285	.274	6	
8	.263	.277	.268	5	
9	.256	.260	.252	3	
10	.160	.172	.175	9	
11	.161	.171	.172	6	
12	.174	.178	.178	2	
13	.181	.181	.179	1	
14	.184	.184	.184	0	Core
15	.171	.177	.181	2	
16	.160	.170	.177	10	
17	.157	.165	.172	4	
18	.153	.155	.160	4	
19	.249	.235	.225	10	
20	.210	.193	.187	11	
21	.159	.144	.141	11	
22	.100	.091	.090	10	
23	.148	.141	.142	5	
24	.125	.116	.116	7	
25	.095	.086	.087	9	
26	.060	.054	.055	10	
<hr style="border-top: 1px dashed black;"/>					
27	.007	.012	.016	56	Radial
28	.005	.006	.008	38	Blanket
<hr style="border-top: 1px dashed black;"/>					
29	.010	.023	.036	72	Axial
30	.006	.010	.014	57	Blanket

to stress the effect of the spatial spectrum shift. Values of the power densities for each mesh point within the subassembly are shown in Figure 3.7 for BOL and EOL fuel compositions. Each triangular node was evaluated as a separate fuel zone. The combined effect of the spatial distributions of the power density and conversion ratio leads to a lower buildup of plutonium, as well as a greater buildup of fission products near the moderator interface, and consequently, to a flattening of the power shape within the subassembly during the fuel cycle. An example of the power shape within the fuel subassembly of the reference core (configuration B) is shown in Figure 3.8.

Power distributions in the axial direction for BOL and EOL are shown in Figure 3.9. The buildup of plutonium in the axial blanket and shift of power is explicitly demonstrated. It should be noted that the shift of power toward the axial blanket results in the flattening of the axial power shape and a decrease in the axial peaking factor.

The radial power shape for the mesh points along the right boundary of the segment of the core shown in Figure 3.4 is given in Figure 3.10 and represents BOL power distributions calculated in HEX geometry without control rods. The power shift during the 10-year fuel cycle (R-Z geometry and average power distributions) is shown in Figure 3.11 and presents the radial power shape for BOL, mid-life (5 years) and EOL calculated in R-Z geometry, again without control rods.

#### 3.4.3 Burnup and Fast Fluence Damage

The (EC)FMSR fuel cycle does not employ any shuffling of the fuel, so that every subassembly remains in place for the full 10-year cycle. As a result, the accumulated burnup level and fast fluence value for each zone follows the spatial power distribution and spatial spectrum shift in the core. Tables 3.8 and 3.9 summarize the burnup and fast fluence levels for each zone during the whole fuel cycle. The higher values of burnup and fast fluence occur in zones 1 to 5, i.e., the central part of the core. The highest value of the burnup for any zone is 137,000 MWD/T, and taking into account the axial peaking factor of 1.1 for any zone, it can be concluded that the maximum burnup level in the core for any point in the reactor is 150,000 MWD/T. Similarly, the maximum fast fluence for any point in the reactor is about  $3.4 \times 10^{23}$ . These values are subject to reduction with further design study. For instance, since the total amount of power generated at any radius of the core varies with the square of that radius, a modest increase in power density at the outer core radii (see Figure 3.11) will allow a large corresponding reduction in power density at the current location of the burnup and fluence peak. (The zones are not of equal volume.)

#### 3.4.4 Reactivity Coefficients

The Doppler reactivity coefficient was calculated using effective multiplication factors at two temperatures. The Doppler coefficient,  $\alpha$ , is defined as

$$\alpha = -T \frac{dK}{dT},$$

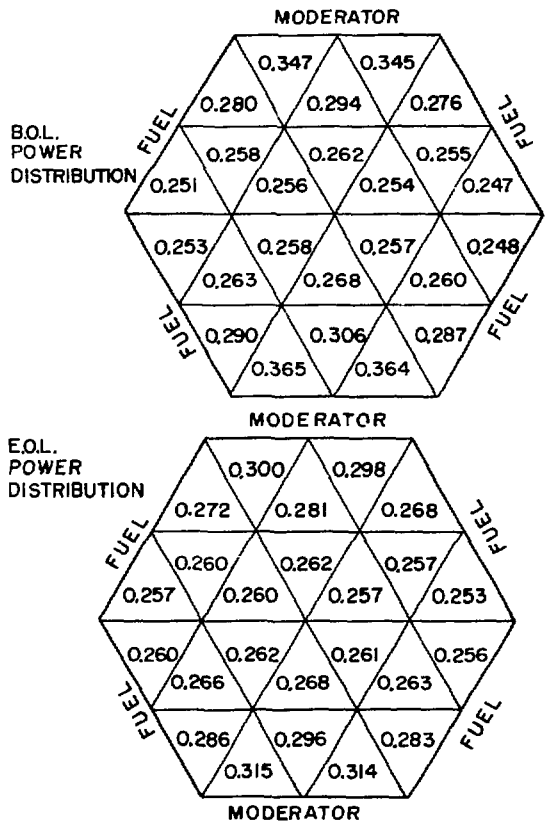


Figure 3.7 Power Density Variation with Burnup, Due to BeO Moderator



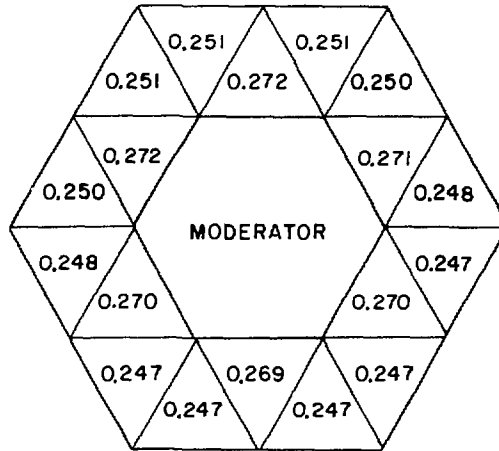


Figure 3.8 Power Density Variation in Configuration B Type Subassembly

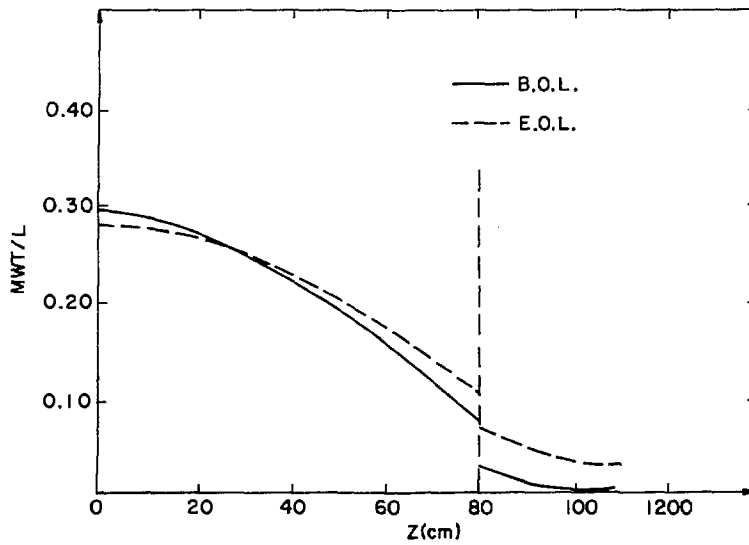


Figure 3.9 Axial Power Density Variation of (EC)FMSR

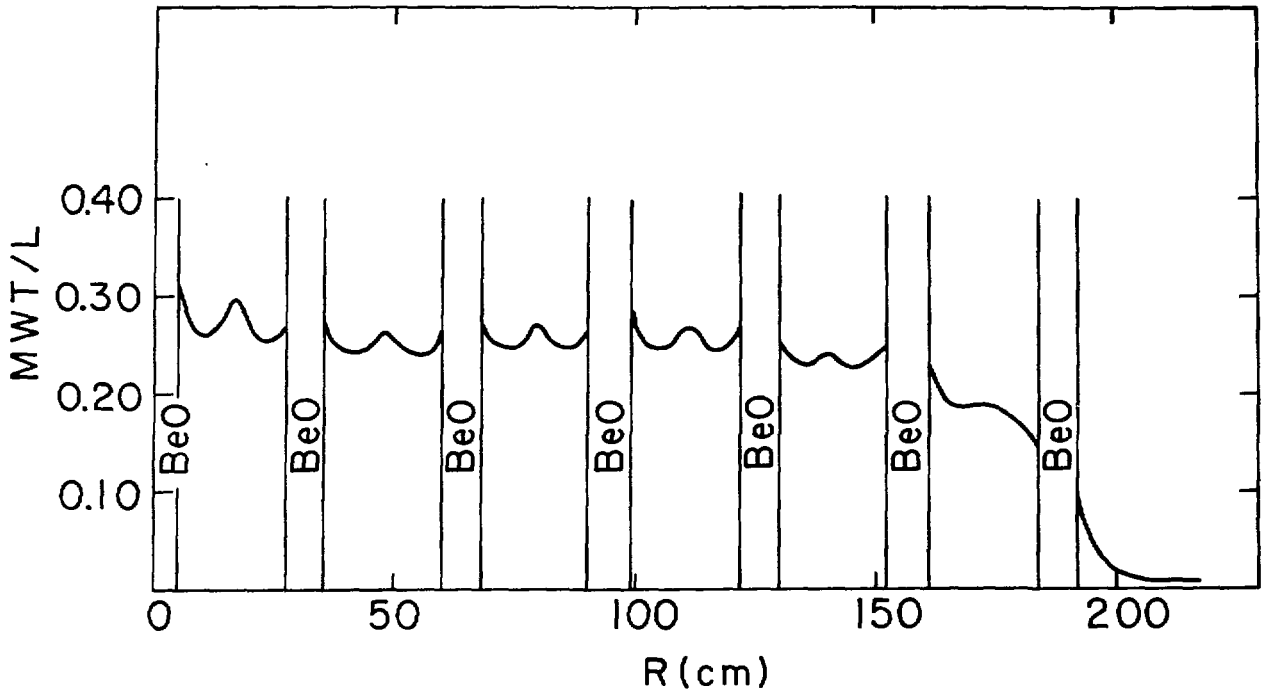


Figure 3.10 Radial Power Distribution (Center to Flat)

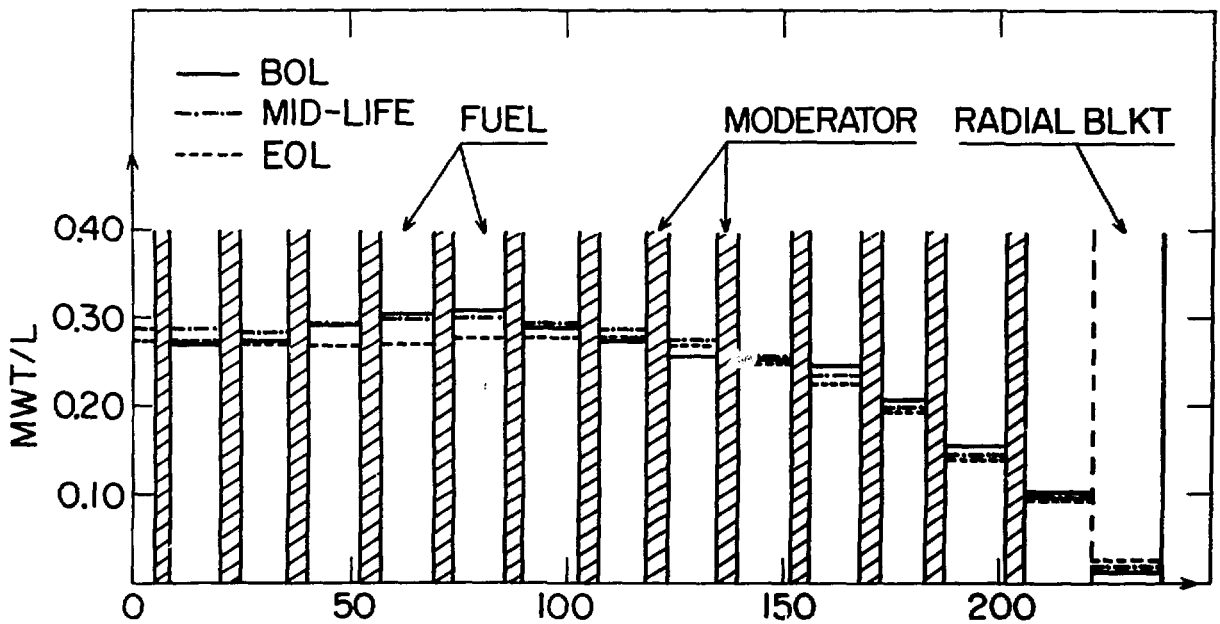


Figure 3.11 Extended-Cycle FMSR Radial Power Shape at BOL, MOL and EOL

TABLE 3.8

Zone-Averaged Burnup Increments (MWD/kg), R-Z Representation

Zone No. Full Power Days(y)	1 (10)	2 (11)	3 (12)	4 (13)	5 (14)	6 (15)	7 (16)	8 (17)	9 (18)	19 (23)	20 (24)	21 (25)	22 (26)	Core Average
0	---	---	---	---	---	---	---	---	---	---	---	---	---	---
550(2)	26 (16)	25 (15)	27 (16)	28 (17)	28 (17)	26 (16)	25 (15)	24 (14)	23 (14)	22 (13)	19 (11)	14 (9)	9 (5)	20 (2)
825(3)	14 (8)	13 (8)	14 (8)	14 (8)	14 (8)	13 (8)	13 (8)	13 (8)	12 (7)	11 (7)	9 (5)	7 (4)	4 (3)	10 (6)
1375(5)	27 (17)	26 (16)	27 (16)	27 (17)	28 (17)	27 (16)	26 (15)	25 (15)	24 (14)	22 (13)	18 (11)	13 (8)	8 (5)	20 (12)
1650(6)	14 (8)	13 (8)	14 (8)	14 (8)	14 (8)	13 (8)	13 (8)	13 (8)	12 (7)	11 (6)	9 (5)	7 (4)	4 (2)	10 (6)
2200(8)	28 (17)	26 (16)	27 (17)	27 (17)	27 (17)	27 (17)	26 (16)	25 (15)	24 (14)	21 (13)	17 (11)	13 (8)	8 (5)	21 (12)
2750(10)	28 (18)	25 (16)	26 (17)	26 (17)	26 (17)	26 (17)	26 (16)	25 (16)	23 (15)	21 (13)	17 (11)	13 (8)	8 (5)	20 (12)
<u>TOTAL</u>	137 (84)	128 (79)	135 (82)	136 (84)	137 (84)	132 (82)	129 (78)	125 (76)	118 (71)	108 (65)	89 (54)	67 (41)	41 (25)	101 (60)

NOTE: Integers with parenthesis refer to the outer axial region.  
Integers without parenthesis refer to the inner axial region.

TABLE 3.9

Zone-Averaged Fast Fluence Increments ( $10^{23}$  n/cm<sup>2</sup> > 0.1 MeV), R-Z Representation

Zone No. Full Power Days (y)	1 (10)	2 (11)	3 (12)	4 (13)	5 (14)	6 (15)	7 (16)	8 (17)	9 (18)	19 (23)	20 (24)	21 (25)	22 (26)	Core Average
550(2)	.63 (.37)	.63 (.32)	.59 (.35)	.57 (.34)	.57 (.34)	.61 (.32)	.62 (.35)	.60 (.35)	.57 (.33)	.52 (.31)	.44 (.26)	.33 (.20)	.20 (.12)	.47 (.29)
825(3)	.32 (.18)	.32 (.19)	.30 (.18)	.29 (.17)	.29 (.17)	.31 (.18)	.30 (.19)	.30 (.18)	.28 (.17)	.26 (.15)	.22 (.13)	.16 (.10)	.10 (.06)	.24 (.14)
1375(5)	.64 (.38)	.63 (.38)	.59 (.36)	.57 (.34)	.57 (.35)	.61 (.37)	.63 (.33)	.61 (.36)	.57 (.33)	.51 (.30)	.43 (.25)	.32 (.19)	.20 (.12)	.48 (.28)
1650(6)	.32 (.19)	.32 (.19)	.29 (.18)	.28 (.17)	.28 (.17)	.31 (.18)	.32 (.19)	.31 (.18)	.28 (.17)	.25 (.15)	.21 (.13)	.16 (.09)	.10 (.06)	.24 (.14)
2200(8)	.62 (.39)	.62 (.39)	.57 (.36)	.55 (.35)	.56 (.35)	.61 (.38)	.63 (.39)	.61 (.38)	.56 (.34)	.50 (.30)	.42 (.25)	.31 (.19)	.19 (.12)	.48 (.28)
2750(10)	.60 (.39)	.60 (.39)	.55 (.36)	.53 (.34)	.54 (.35)	.59 (.38)	.62 (.39)	.60 (.38)	.56 (.35)	.50 (.31)	.42 (.26)	.31 (.19)	.20 (.12)	.47 (.28)
<b>TOTAL</b>	3.13 (1.90)	3.12 (1.91)	2.89 (1.79)	2.79 (1.71)	2.81 (1.73)	3.04 (1.85)	3.12 (1.91)	3.03 (1.83)	2.82 (1.69)	2.54 (1.52)	2.04 (1.28)	1.59 (0.96)	0.99 (0.60)	2.38 (1.41)

NOTE: Integers with parenthesis refer to the outer axial region.  
Integers without parenthesis refer to the inner axial region.

where T is temperature in K. After integrating and rearranging,

$$\alpha = \frac{K(T_2) - K(T_1)}{\ln(T_1/T_2)},$$

where  $K(T_1)$  and  $K(T_2)$  are effective multiplication factors at temperature  $T_1$  and  $T_2$ .  $K(T_1)$  and  $K(T_2)$  were calculated for both R-Z and HEX geometries, and it was found that values of the Doppler coefficients were in satisfactory agreement (difference less than 5%). Similar Doppler coefficient calculations were performed for EOL compositions, as well as for sodium voided cores.

Results of the Doppler coefficient calculations are presented in Table 3.10. The temperatures  $T_1$  and  $T_2$  were taken as 875 K and 1400 K, respectively.

The values of the Doppler coefficient indicate a significant decrease of the Doppler coefficient with fuel depletion due to the replacement of the U-238 atoms by the atoms of fission products. In addition, the Doppler coefficient is about 30% smaller for the sodium voided core due to hardening of the neutron spectrum in the absence of sodium. Both of these results were as expected. Generally, the (EC)FMSR Doppler coefficient is about 3-4 times larger than for conventional LMFBRs. This can be attributed to the relatively softer neutron energy spectrum of the (EC)FMSR.

Calculations of the sodium void reactivity effect were performed in R-Z geometry by voiding all sodium from the core, as well as the radial and axial blankets. It is important to note that in the present calculations the stagnated sodium between subassemblies was smeared with flowing sodium over the fuel region, and both types of sodium were removed. In some evaluations of the sodium void effect, only the flowing sodium is removed. The values of the sodium void effect reported here would be reduced if this practice were followed.

Results of the calculations with fully voided core, radial and axial blankets are presented in Table 3.11 where  $\Delta K_{Na,v}$  is the reactivity shift due to sodium voiding.

An increase of the sodium void reactivity shift with fuel depletion may be attributed to (1) an increase in the positive spectral contribution due to the fission products formed during the fuel cycle, (2) changes in plutonium isotopic composition, i.e., a decrease in the Pu-241 fraction and an increase in the Pu-239 fraction, and (3) decrease of the negative leakage contribution due to buildup of plutonium in the radial and axial blankets. The effect of plutonium buildup in the axial and radial blankets was evaluated by repeating the EOL composition calculations with BOL radial or axial blanket compositions (i.e., natural uranium). Results of these calculations indicated that the "sodium void reactivity worths" of plutonium buildup in the radial and axial blankets are \$0.2 and \$0.1, respectively. The time dependence of the sodium void effect and Doppler coefficients are shown in Figures 3.12 and 3.13.

The sodium void calculations reported here are preliminary. A more intensive study of this effect has begun and will be reported in the following progress report.

TABLE 3.10  
Doppler Coefficients

BOL (Sodium In)	BOL (Sodium Voided)	EOL (Sodium In)	EOL (Sodium Voided)
0.0270	0.0180	0.0175	0.0110

TABLE 3.11  
Sodium Void Reactivity Effect  
(\$1 = 0.0041  $\Delta K$ )

BOL	$\Delta K_{Na.V.} = \$1.8$
Mid-Life (5y)	$\Delta K_{Na.V.} = \$3.7$
EOL (10y)	$\Delta K_{Na.V.} = \$5.0$

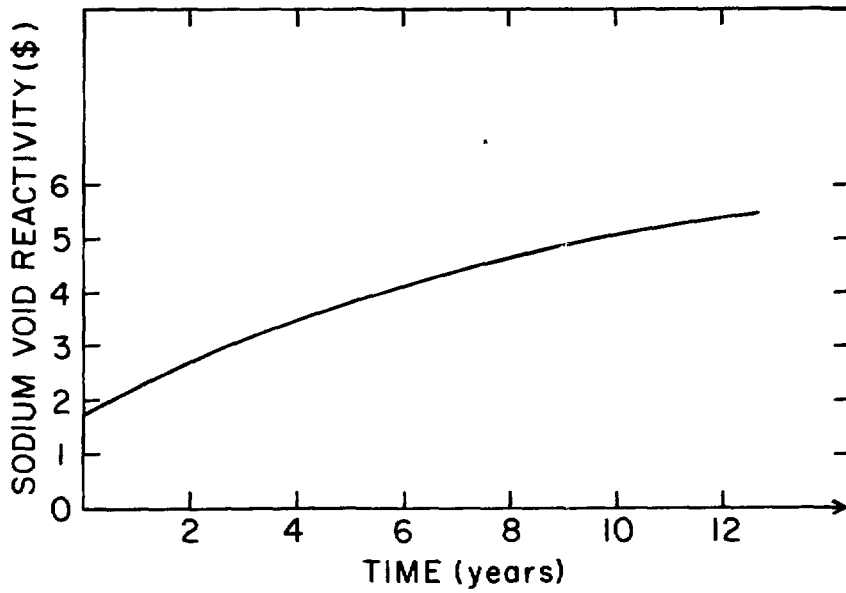


Figure 3.12 Irradiation Dependence of Sodium Void Reactivity Gain

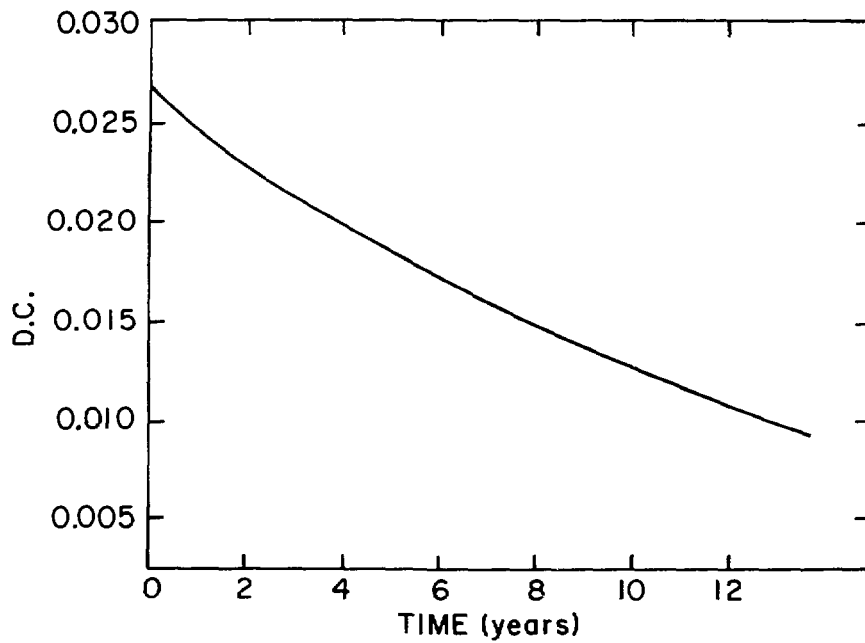


Figure 3.13 Irradiation Dependence of Doppler Effect Feedback Coefficient

#### 3.4.5 Radial and Axial Blankets

The sizes of the radial and axial blankets in the reference design of the (EC)FMSR were chosen by considering two factors: (1) the reactivity gain due to the plutonium buildup in the blankets and (2) the contribution of the plutonium buildup in the blankets to the sodium void reactivity effect as a result of the decreased leakage component of the sodium void reactivity shift. Calculations performed in R-Z geometry for different values of the axial blanket height indicated that no significant reactivity penalty occurs at EOL when the height of the axial blanket (upper and lower) is decreased from 40 cm (usually accepted for LMFBRs) to 25 cm. Similarly, the radial blanket was decreased from 2 rings (162 subassemblies) to 1 ring (78 subassemblies). The reactivity penalty for the decrease in the blanket sizes did not exceed 0.3%  $\Delta K$  at EOL. The sodium void reactivity effect was decreased by \$0.3 at BOL for the decreased size blankets. The main advantage of smaller blankets will be realized in the decrease of the core volume and fuel fabrication and reprocessing requirements. Further (EC)FMSR core analyses, with economic optimization and doubling time sensitivity analyses, will lead to later decisions for radial and axial blanket design.

#### 3.4.6 Reactivity Control Systems

Two independent reactivity control systems are utilized in the reference design (EC)FMSR core. The primary system serves both a safety and a control function. This system must have sufficient reactivity worth at any time in the reactor cycle, assuming one stuck primary rod, to shut down the reactor from any operating condition and to maintain subcriticality down to the refueling coolant temperature. In addition, the primary system is designed to compensate for the cold startup reactivity loss, provide the excess reactivity needed at BOL, and provide for criticality and fissile content uncertainties.

The secondary control system must have sufficient worth at any time in the reactor cycle, assuming one stuck secondary rod, to independently shut down the reactor from any operational condition to the hot shutdown temperature of the coolant (hot standby temperature). These are conventional LMFBR design requirements.

The primary and secondary control systems operate independently, such that the capability of either system to fulfill its functions is not dependent on the operation of the other system.

The control and safety rod design calculations reported here are in the nature of a preliminary evaluation. In future studies the number of control and safety rods, for instance, probably will be significantly reduced.

A set of fuel temperatures was adopted in order to represent the working, refueling and hot standby conditions of the core. The refueling and hot standby temperatures for all the fuel of the core were assumed to be 460 K and 560 K, respectively. These values are usually used in calculations of the control requirements due to the Doppler effect. The average fuel temperature for full power condition was taken as 875 K. The  $\Delta K$  values needed to bring the core from 465 K and 560 K to 875 K were calculated from direct  $K_{eff}$  calculations.



The control requirements were calculated by the 2DB code in R-Z geometry. Burnup calculations provided the BOL excess reactivity value and direct  $K_{eff}$  calculations at different temperatures provided cold-to-hot reactivity shifts. It should be noted that the Doppler effect decreases with depletion so the BOL cold-to-hot reactivity shifts calculated are conservative.

The control rod reactivity worths were calculated using the 2DB code HEX geometry. The absorber used in the control and shutdown rods ( $B_4C$ ) was homogenized over the moderator region; this approximation leads to an overestimation of the reactivity worth of the control rods. All control rods were grouped according to their location, i.e., radial position of the ring. Therefore, at this stage the mutual shadowing of the control rods in the same ring was neglected. A number of calculations, representing different combinations of the control rods inserted, were performed in order to evaluate mutual shadowing of the control rods located in different rings.

Radial and axial expansion of the fuel, as well as subassembly bowing, were neglected at this preliminary stage.

Due to the number of approximations made and effects neglected, the individual uncertainty in the hot-to-cold reactivity swing was taken as  $\pm 35\%$ ; criticality uncertainty and fissile tolerance were taken as  $0.3\% \Delta K$  each.

Control requirements calculations were performed by the 2DB code in R-Z geometry. Direct  $K_{eff}$  calculations were performed for three temperatures: 875 K - working temperature, 560 K - hot standby, and 465 K - refueling temperature. Those calculations gave hot-to-cold reactivity shifts for primary and secondary control systems requirements. The item-by-item reactivity requirements for the primary and secondary control systems are listed in Table 3.12.

The maximum reactivity requirements, including uncertainties, are  $3.87\% \Delta K$  and  $1.63\% \Delta K$  for primary and secondary control systems, respectively. Hot-to-cold requirements for the primary and secondary systems are  $1.58\% \Delta K$  and  $1.12\% \Delta K$ , respectively. Those values are relatively high compared with homogeneous and heterogeneous LMFBRs due to the higher Doppler coefficient of the (EC)FMSR core.

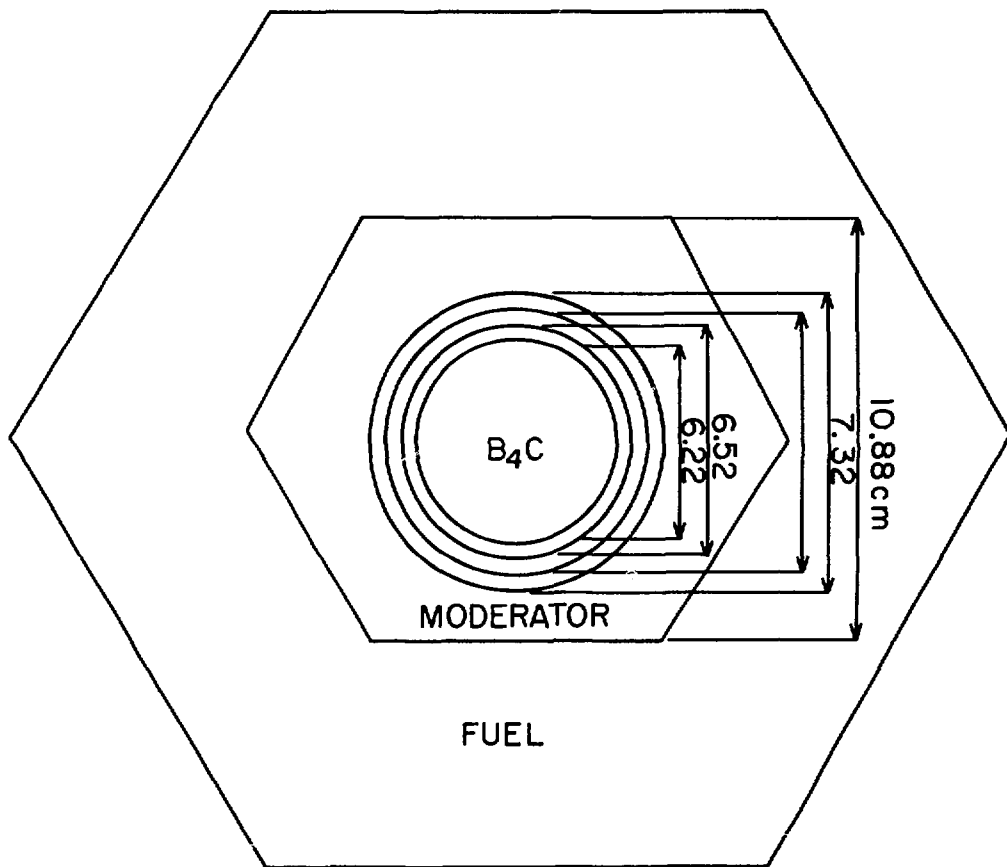
In the control subassembly the moderator volume fraction was increased from 25% to 37% of the total volume compared with the basic fuel subassembly. The control rod is located in the center of the subassembly (see Figure 3.14).

The control rod neutron absorber is a cylindrical metal tube containing  $B_4C$  (92% B-10 enriched). A summary of the tentative control subassembly design is given in Table 3.13. The primary control system consists of 24 rods and the secondary system of 18 rods. Control rod assignments are summarized in Table 3.14. This preliminary design feature should change as a result of future studies.

The layout of the core with control rod locations is shown in Figure 3.15. The available control rods reactivity worths were calculated for a variety of control rod positions by performing direct  $K_{eff}$  calculations. Axial movement of the control rod was represented by the equivalent changes in absorber number densities.

TABLE 3.12  
Control Systems Reactivity Requirements (% ΔK)

	<u>Primary System</u>	<u>Secondary System</u>
1. Hot-to-cold shift (Doppler only)	1.58 ± 0.55	1.12 ± 0.39
2. Max. reactivity fault	0.12	0.12
3. BOL excess reactivity	1.02	
4. Criticality uncertainty	± 0.30	
5. Fissile tolerance	± 0.30	
Total	2.72	1.24
+ Uncertainties	3.87	1.63



ALL DIMENSIONS IN cm

Figure 3.14 Control Subassembly Configuration

TABLE 3.13  
Control Subassembly Design Data

Moderator volume, cm <sup>2</sup>	102.5	(37% of V <sub>TOT</sub> )
Moderator flat-to-flat, cm	10.88	
BeO volume, cm <sup>2</sup>	61.73	(≈ 22% of V <sub>TOT</sub> )
Control rod volume, cm <sup>2</sup> (including guide tube)	42.09	
Guide tube outer D, cm	7.32	
Guide tube thickness, cm	0.15	
Gap, cm	0.25	
Absorption rod outer D, cm	6.25	
Volume B <sub>4</sub> C, cm <sup>2</sup>	30.89	

TABLE 3.14  
Control Rod Assignments

<u>Ring</u>	<u>Primary System</u>	<u>Secondary System</u>
3	6	----
5	----	12
7	6	6
11	12	----
Total	24	18

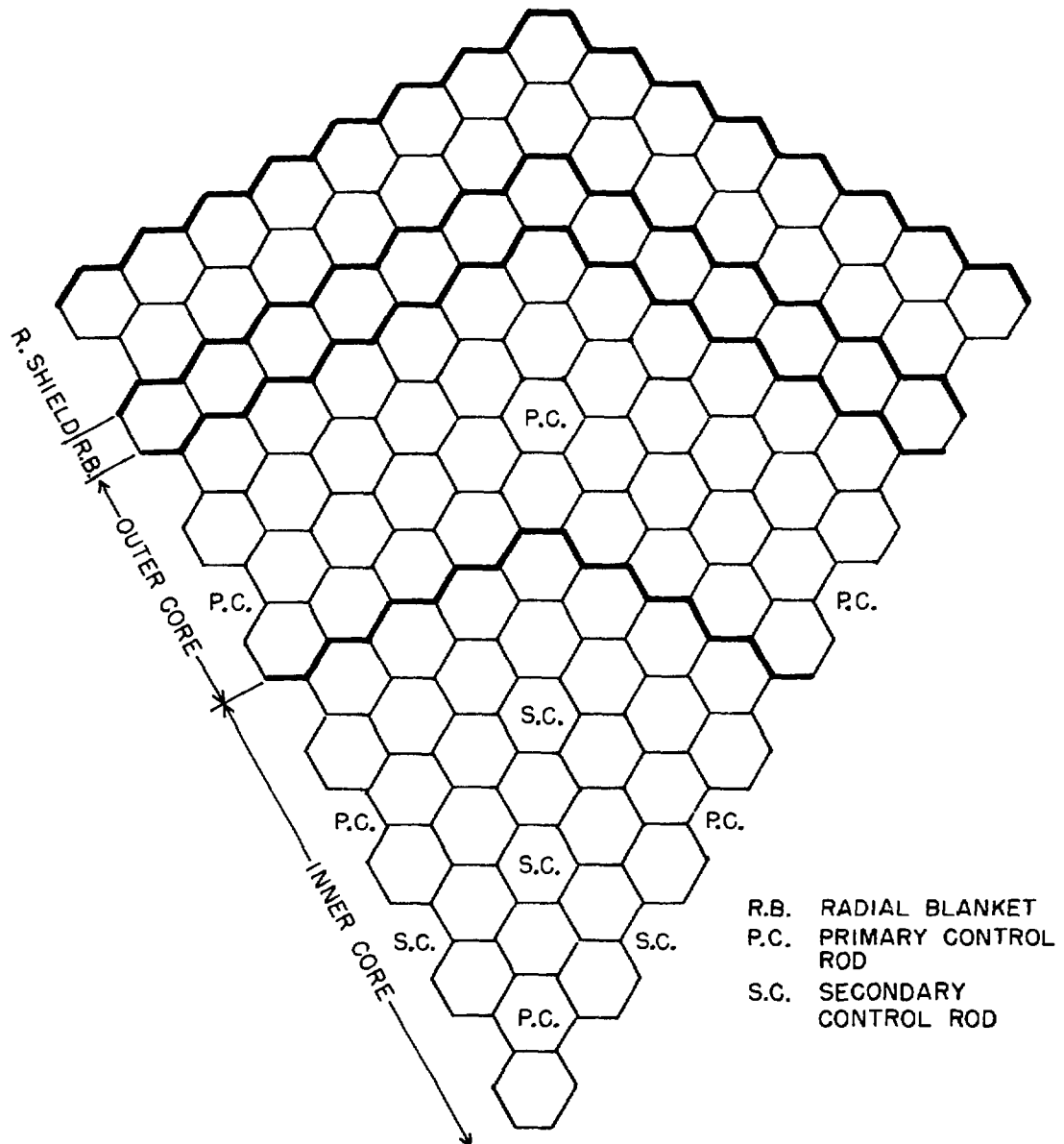


Figure 3.15 Spatial Distribution of Primary Control (PC) and Safety (SC) Rods for (EC)FMSR (Tentative)

Results of the calculations are summarized in Tables 3.15 and 3.16. The reactivity worth of each ring of control rods was evaluated as well as the total reactivity worth available for primary and secondary control systems. A maximum reactivity worth of one control rod was calculated for each ring, neglecting mutual shadowing of the control rods from the same ring. Finally, the total reactivity worth for the primary control system was calculated as 6.29%  $\Delta K$  versus 3.87% required, and for the secondary control system, 2.75%  $\Delta K$  available versus 1.63%  $\Delta K$  required.

Average power densities and peaking factors for each subassembly for BOL and EOL compositions, and with control rods inserted, are shown in Figures 3.16-3.20. It should be noted that EOL HEX calculations were performed with number densities from R-Z depletion calculations. Therefore, the material composition was smeared over every radial ring of the subassemblies.

The main conclusion of this section is the feasibility of the control system for the (EC)FMSR core with the proposed design. Though reported calculations are of a preliminary nature and include a number of approximations, the results indicate the possibility of a design in which the control rods do not occupy the whole fuel subassembly, but are located in the moderator region of the subassembly. Proposed design and geometrical patterns of the primary control system show flat radial power distribution in the presence of the control rods.

TABLE 3.15

Multiplication Factor as a Function of Control Rod Position

Run Number	Control Rods Position (% Insertion)				K <sub>eff</sub>
	R3	R7	R11	R5	
1	out	out	out	out	1.0147
2	100% in	out	out	out	1.0058
3	10% in	out	out	out	1.0095
4	out	6 rods, 100%	out	out	1.0019
5	out	6 rods, 10%	out	out	1.0091
7	out	out	6 rods, 100%	out	1.0108
8	out	out	6 rods, 10%	out	1.0129
9	out	12 rods, 100%	out	out	0.9900
10	out	12 rods, 10%	out	out	1.0032
11	out	out	12 rods, 100%	out	1.0040
12	out	out	12 rods, 10%	out	1.0097
13	50%	50%	50%	out	0.9684
14	10%	10%	10%	out	0.9906
15	5%	5%	5%	out	0.9981
16	50%	50%	50%	100%	0.9587
17	10%	10%	10%	100%	0.9771
18	5%	5%	5%	100%	0.9832
19	5%	6 rods, 5%	5%	out	1.0023
20	100%	6 rods, 100%	100%	out	0.9518

TABLE 3.16

Control Rod Reactivity Worths

(R3 + R7 + R11) 50% insertion	$\Delta K = 4.63\%$
(R3 + R7 + R11) 10% insertion	$\Delta K = 2.41\%$
(R3 + R7 + R11) 5% insertion	$\Delta K = 1.66\%$
(R3 + 6 rods R7 + R11) 5% insertion	$\Delta K = 1.24\%$
(R3 + 6 rods R7 + R11) 100% insertion	$\Delta K = 6.29\%$
(R5) with (R3 + R7 + R11) inserted 5%	$\Delta K = 1.56\%$
(R7) 6 rods with (R3,R11) inserted 5%	$\Delta K = 1.19\%$

Maximum Reactivity Worth of 1 Rod:

R3	$\Delta K/\text{rod} = 0.15\% \approx \$ .37$
R5	$\Delta K/\text{rod} = 0.21\% \approx \$ .50$
R7	$\Delta K/\text{rod} = 0.21\% \approx \$ .50$
R11	$\Delta K/\text{rod} = 0.07\% \approx \$ .20$

Primary control system reactivity worth	$\Delta K = 6.29\%$	$\Delta K$
Primary control system required worth	$\Delta K = 3.87\%$	$\Delta K$
Secondary control system reactivity worth	$\Delta K = 2.75\%$	$\Delta K$
Secondary control system required worth	$\Delta K = 1.63\%$	$\Delta K$



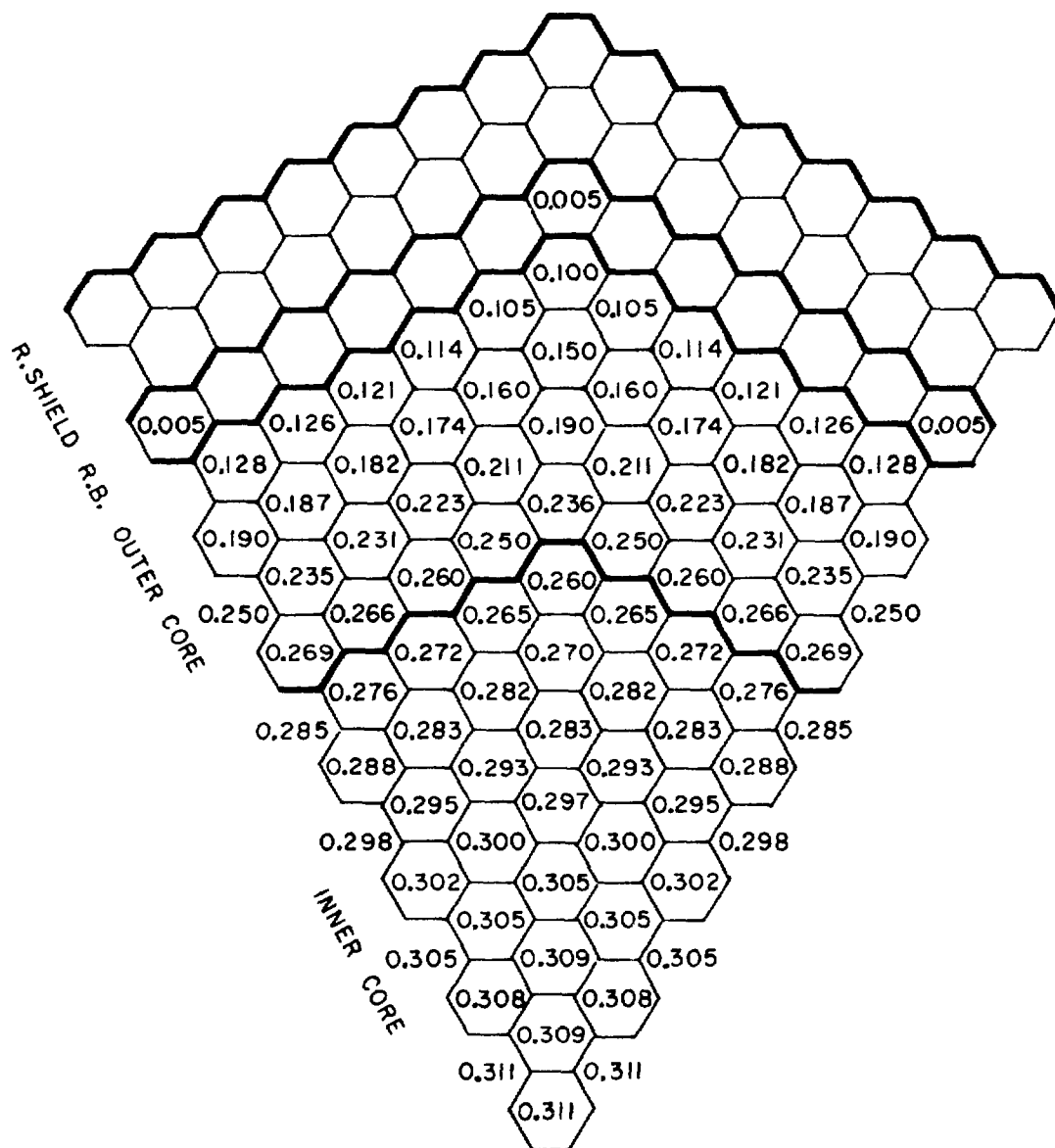


Figure 3.16 Average Subzone Power Density for (EC)FMSR BOL Core

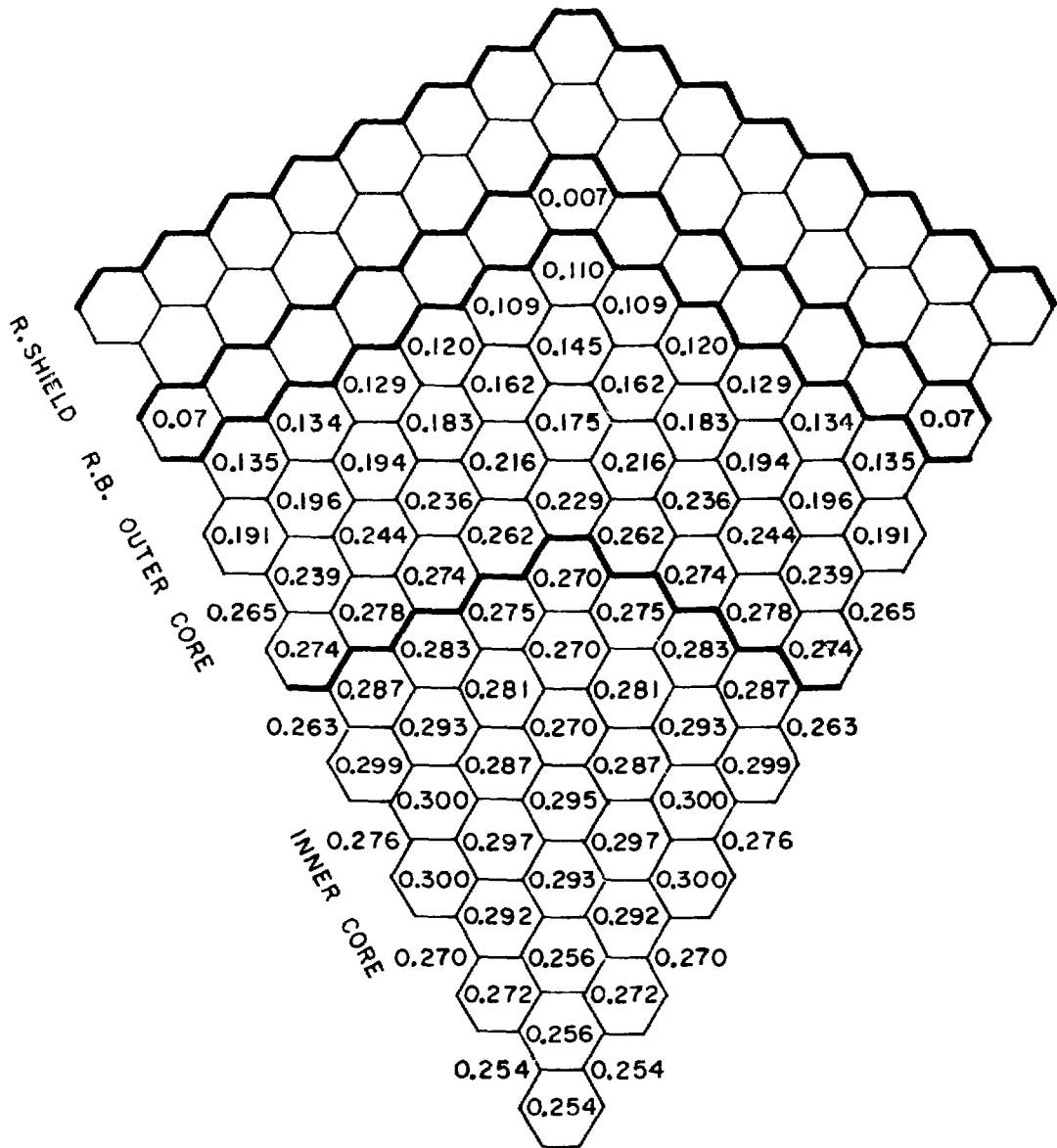


Figure 3.17 Average Subzone Power Density for (EC)FMSR MOL Core

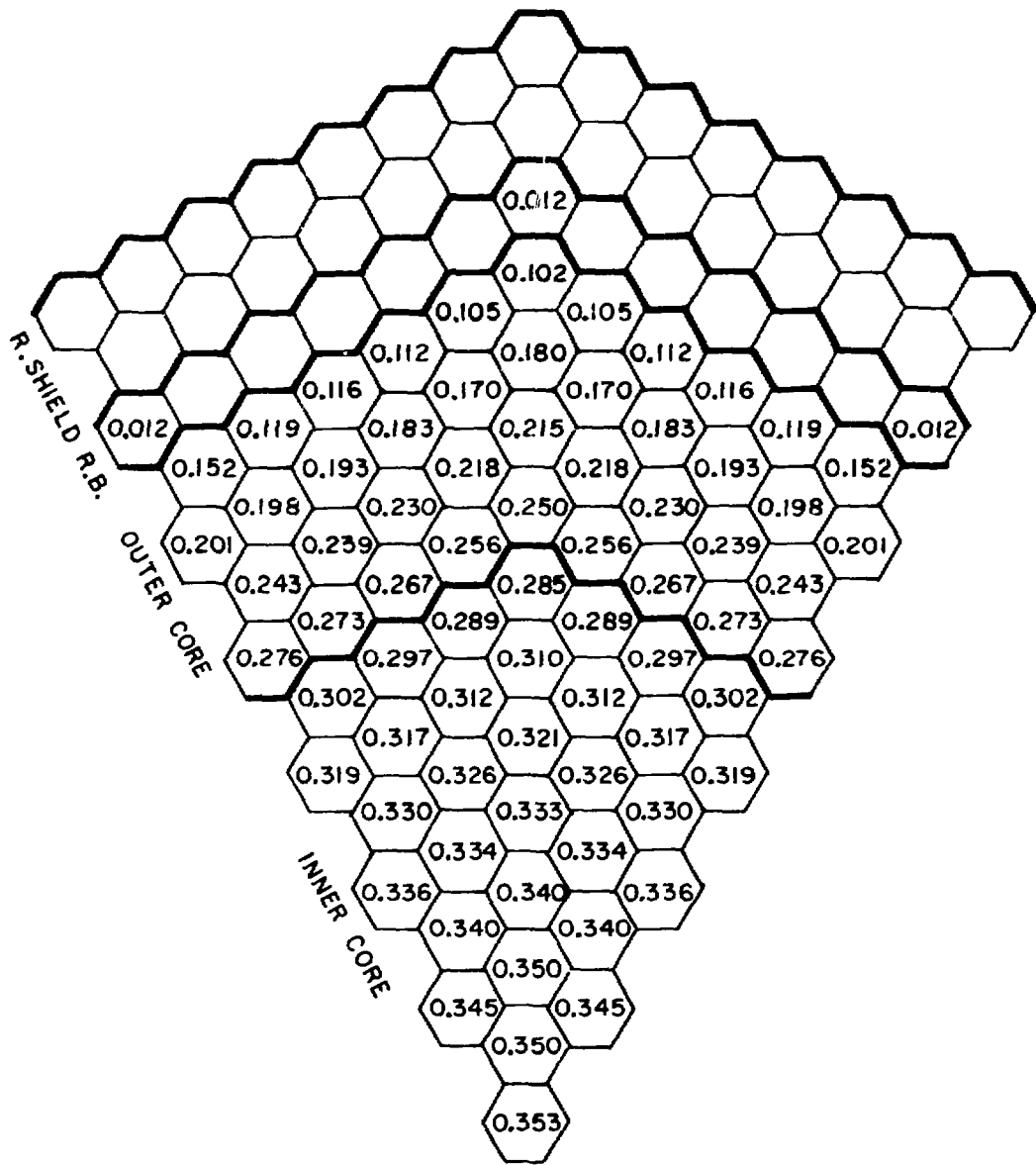


Figure 3.18 Average Subzone Power Density for (EC)FMSR EOL Core

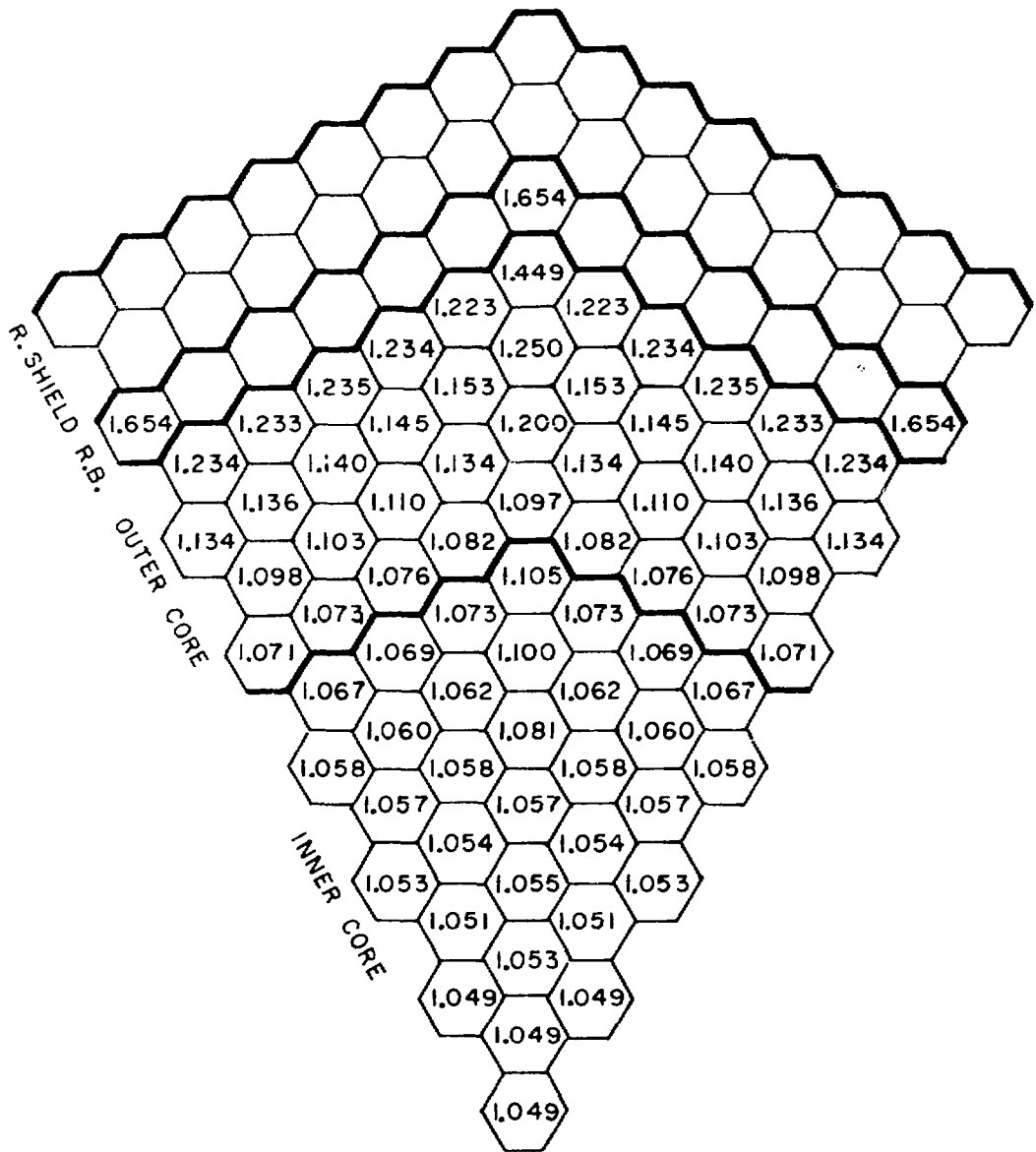


Figure 3.19 Power Peaking Factors for (EC)FMSR BOL Core

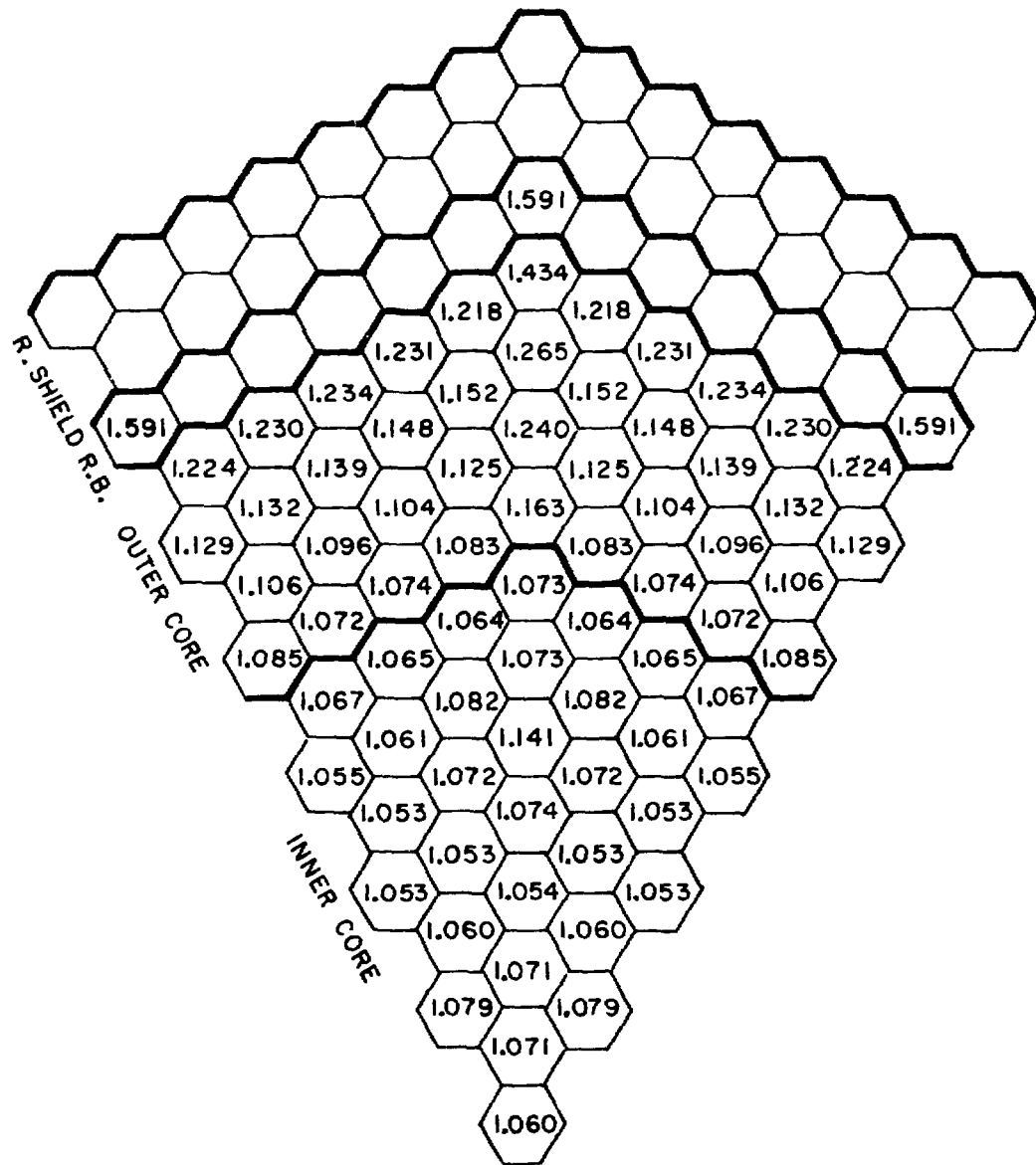


Figure 3.20 Power Peaking Factor for (EC)FMSR EOL Core

## 4. THERMAL-HYDRAULIC ANALYSIS OF THE (EC)FMSR

### 4.1 GENERAL DESIGN CONSIDERATIONS

The thermal-hydraulic design of the (EC)FMSR core closely follows that of the conventional LMFBR. The sodium enters the core region from the lower plenum, flows through the core inlet section, including the orifice, and then flows upward along the fuel rod bundles. The fuel rods are assumed to be helically wire wrapped along their entire length. Axial shielding is assumed both above and below the core, within the subassembly. The present study focuses on thermal-hydraulic computations for the core region only. Heat transport processes in the intermediate loop and steam-water loop are not included. Because the (EC)FMSR is designed to operate with essentially the same pressure drop across the core and the same inlet and outlet temperatures as a conventional LMFBR, the balance-of-plant external to the core may be assumed to be unchanged. Also, an (EC)FMSR core of this type design could be considered as being able to replace a conventional core in a 1000-MW(e) LMFBR.

Metallurgical considerations set the maximum fuel centerline and fuel-clad contact temperatures at 850°C and 625°C, respectively. Thus, one objective is to achieve a thermal-hydraulic design consistent with these metallurgical limitations. In addition, the mixed mean coolant outlet temperature is also a major factor in the thermal-hydraulic design; the coolant inlet temperature and the temperature rise in the core region are closely related to the thermodynamic efficiency of the power plant. For the present design, the coolant inlet temperature was set at 380°C and the temperature rise is, nominally, 150°C. A preliminary study of the overall plant balance has shown that these temperatures yield good performance for conventional designs of the IHX and the steam generator, with an achievable thermodynamic efficiency of 36%. The pressure drop across the core selected for the present study is 90 psi. The fuel pin design used in the (EC)FMSR employs the same operating principle as the EBR-II MARK-II fuel pin, which is a sodium-bonded metal fuel. According to the operating experiences of the EBR-II, the fuel-cladding gap is practically closed after about 3 atom percent burnup, at which time a state of interconnected porosity is achieved. Fission product gas is released through this porosity from that point onward, and fuel swelling is correspondingly greatly reduced. A closed fuel-cladding gap is assumed in the present design calculations. The thermal impedance of the porosity was taken into account.

The rod bundle of the core is divided into four axial sections: the lower axial blanket (25 cm), the active core (160 cm), the upper axial blanket (25 cm) and the upper vented plenum (30 cm). It is one of five thermal-hydraulic regions defined below which make up the full core segment of the hydraulic loop.

### 4.2 METHOD OF CALCULATION

The thermal-hydraulic design evolved from several iterations which were interfaced with physics and materials requirements. Thermal-hydraulic computations were performed with the SATURN code which is a flexible, one-dimensional, multichannel, steady-state code for thermal-hydraulic design analysis of sodium-cooled fast reactors developed at BNL for the FMSR Program. The code

uses the same radial and axial zoning for heat generation as those used in the fuel cycle calculations. The SATURN code first establishes the pin geometry by computing fuel and clad dimensions and hydraulic parameters based on the input design specifications. With these initial conditions established, the code then computes individual channel coolant flow rates to achieve a specified temperature rise, using the same pressure drop for all radial zones. The total pressure drop consists of pressure drops due to friction, gravity, acceleration and flow area changes. Detailed pressure drops in five axial regions are computed for each channel. The five regions are the core support module, inlet nozzle, orifice plate and shield, rod bundle, and assembly outlet. To achieve a consistent pressure drop for all radial zones, an iteration procedure is used in the code to adjust the loss coefficient of the orifice plate in each zone.

ANL has shown that the thermal conductivity of the metal fuel depends on the fuel temperature, fission product content, and porosity.<sup>(14)</sup> Empirical correlations of the thermal conductivity, which were developed by ANL, were used in this design study. The physical properties of sodium, such as enthalpy, density, viscosity and thermal conductivity, as functions of temperature, are taken from Reference 13. The correlation of frictional pressure drop for turbulent flow in triangular rod bundles developed by Novendstern<sup>(15)</sup> is adopted in the SATURN code. These correlations are well developed for LMFBRs and are given in Appendix A of Reference 6.

The detailed temperature distributions in fuel and clad, as well as the pressure and temperature of the coolant in each axial node, are computed in SATURN for all radial channels. The computations are for the average and hot pin in each channel under the nominal operating conditions. Hot spot and hot-channel calculations are also performed.

The impact of uncertainties on the thermal-hydraulic performance is represented by the application of hot spot factors. The hot spot factors were defined according to conventional LMFBR practice.<sup>(16)</sup> These factors represent the statistical and other uncertainties of theoretical and experimental analyses, instrumentation accuracy, manufacturing tolerances, physical properties and correlations. Descriptions of the hot spot factors are given in Appendix B of Reference 6. The hot spot analysis was applied to the peak power channel only. It is referred to as the hot channel. The hot channel represents the hot pin in the peak power assembly affected by the simultaneous occurrence of all uncertainties. Preliminary results for the (EC)FMSR calculation are presented in the following section.

#### 4.3 THERMAL-HYDRAULIC PERFORMANCE

To perform the multichannel thermal-hydraulic analysis, the 40 radial subzones, (Figure 3.4), for which two-dimensional power density distributions were determined by physics computations, were used in this study. Each channel represented the average fuel pin of twelve subassemblies. The computed results are summarized in Table 4.1. The (EC)FMSR is designed to operate at a rated power level of 2776 MW(t), which yields 1000 MW(e) for a 36% thermodynamic efficiency. It is noted in Table 4.1 that Zone 1 (marked by an \*) is the peak power channel. The average linear power and maximum power density of Zone 1

TABLE 4.1

Summary of Core Fuel Thermal Hydraulics for the (EC)FMSR

SUMMARY OF RESULTS

UNIFORMLY MODERATED - HE COOLANT - TWO-PHASE BULKY - HFC

TOTAL FLOW = 1371405 CM/3  
 TOTAL POWER = 24174 MW  
 TOTAL PUMPING HEAD = 9342401 MM  
 TOTAL PRESSURE DROP = 91.65 PSI  
 MEAN COOLANT TEMPERATURE = 548.35 C

ZONE	NO OF ASSEMBLY	MAX POWER KW/3	LINEAR POWER KW/F1	POW-FR FRACTION	FLOW FRACTION	--AVERAGE P1H-- (NOMINAL)		----- PEAK POWER P1H ----- (HOT CHANNEL EFFECT)		COOLANT T (C)	
						MAX CLAD T (C)	MAX FUEL T (C)	PEAKING FRACTOR	MAX CLAD T (C)		MAX FUEL T (C)
1	12	3011.6	6.01	0.290	0.035	527.4	6524.7	1.049	0.514	728.0	551.5
2	12	299.7	5.97	0.228	0.014	521.7	6511.5	1.053	0.511	727.6	551.5
3	12	296.4	5.96	0.218	0.010	522.4	6511.0	1.040	0.514	727.0	551.5
4	12	296.4	5.96	0.218	0.010	522.4	6511.0	1.051	0.511	725.9	551.5
5	12	295.1	5.89	0.214	0.011	521.4	6491.7	1.055	0.511	726.2	551.5
6	12	293.1	5.83	0.211	0.007	521.7	6481.0	1.053	0.511	724.6	551.0
7	12	281.1	5.74	0.216	0.006	521.0	6461.1	1.054	0.511	724.1	551.0
8	12	280.4	5.74	0.200	0.003	521.0	6461.1	1.057	0.511	722.0	551.0
9	12	280.4	5.74	0.200	0.003	521.0	6461.1	1.057	0.511	722.1	551.5
10	12	279.1	5.72	0.211	0.004	521.1	6461.0	1.055	0.511	721.2	551.5
11	12	279.1	5.72	0.211	0.004	521.1	6461.0	1.058	0.511	719.3	551.5
12	12	279.1	5.72	0.211	0.004	521.1	6461.0	1.060	0.511	718.6	551.2
13	12	279.1	5.72	0.211	0.004	521.1	6461.0	1.062	0.511	716.9	551.0
14	12	274.4	5.45	0.200	0.005	520.2	6381.0	1.081	0.511	719.5	551.7
15	12	257.7	5.12	0.282	0.028	527.0	6281.0	1.106	0.512	714.5	551.1
16	12	267.5	5.33	0.293	0.028	527.0	6281.0	1.107	0.511	714.5	551.0
17	12	267.5	5.33	0.280	0.025	526.0	6251.2	1.109	0.511	713.2	551.0
18	12	257.7	5.25	0.282	0.027	526.0	6251.2	1.107	0.511	710.1	551.5
19	12	257.7	5.25	0.282	0.027	526.0	6251.2	1.107	0.511	710.1	551.5
20	12	257.7	5.25	0.282	0.027	526.0	6251.2	1.107	0.511	710.1	551.5
21	12	257.7	5.25	0.282	0.027	526.0	6251.2	1.107	0.511	710.1	551.5
22	12	257.7	5.25	0.282	0.027	526.0	6251.2	1.107	0.511	710.1	551.5
23	12	257.7	5.25	0.282	0.027	526.0	6251.2	1.107	0.511	710.1	551.5
24	12	229.1	4.50	0.281	0.026	524.4	6181.2	1.109	0.512	697.3	551.2
25	12	229.1	4.50	0.281	0.026	524.4	6181.2	1.109	0.512	697.3	551.2
26	12	216.7	4.47	0.286	0.024	524.5	6161.2	1.109	0.512	697.6	551.2
27	12	216.7	4.47	0.286	0.024	524.5	6161.2	1.107	0.512	694.0	548.7
28	12	216.7	4.47	0.286	0.024	524.5	6161.2	1.110	0.512	694.0	548.7
29	12	184.7	4.67	0.292	0.025	526.1	6061.9	1.136	0.512	692.1	548.5
30	12	184.7	4.67	0.292	0.025	526.1	6061.9	1.136	0.512	692.1	548.5
31	12	184.7	4.67	0.292	0.025	526.1	6061.9	1.136	0.512	692.1	548.5
32	12	184.7	4.67	0.292	0.025	526.1	6061.9	1.136	0.512	692.1	548.5
33	12	184.7	4.67	0.292	0.025	526.1	6061.9	1.136	0.512	692.1	548.5
34	12	184.7	4.67	0.292	0.025	526.1	6061.9	1.136	0.512	692.1	548.5
35	12	184.7	4.67	0.292	0.025	526.1	6061.9	1.136	0.512	692.1	548.5
36	12	184.7	4.67	0.292	0.025	526.1	6061.9	1.136	0.512	692.1	548.5
37	12	184.7	4.67	0.292	0.025	526.1	6061.9	1.136	0.512	692.1	548.5
38	12	184.7	4.67	0.292	0.025	526.1	6061.9	1.136	0.512	692.1	548.5
39	12	184.7	4.67	0.292	0.025	526.1	6061.9	1.136	0.512	692.1	548.5
40	12	184.7	4.67	0.292	0.025	526.1	6061.9	1.136	0.512	692.1	548.5



are 6.01 kw/ft and 301.6 w/cm<sup>3</sup>, respectively. The hot channel peak centerline temperature of the fuel is 728°C and of cladding 625°C (Table 4.3).

Detailed thermal-hydraulics results for Zone 1, a high power zone under nominal conditions, are given in Table 4.2. The coolant temperature and pressure distributions, fuel and clad temperatures, heat transfer rate, friction factor and Reynolds numbers are listed for all axial nodes. The coolant enters the core region at 380°C; its temperature rapidly increases in the active core region, reaching 556°C at the core exit. The inlet temperature is an input parameter. The clad outer surface temperature is slightly higher than the coolant temperature along the entire length of the fuel pin. This small temperature difference is due to the high heat transfer rate possible with sodium. Inspection of the temperatures at the clad inner surface and in the fuel region shows that the radial temperature variation of the fuel pin is relatively small; this is due to the high thermal conductivity of the metal fuel and the low contact resistance at the sodium-bonded fuel-clad interface. Using the cosine-type axial power profile obtained from the physics calculations for the average pin in Zone 1, the maximum fuel centerline temperature (653°C) occurs 30 cm above the core mid-height position. The maximum clad temperature (562°C) at the clad inner surface occurs near the top of the active core. The coolant saturation temperatures based on the local pressure were computed in SATURN and are also included in Table 4.2. Comparison of the saturation temperature with the coolant temperature indicates that the sodium is highly subcooled, as is common in LMFBR design. The highly subcooled sodium provides a large temperature margin for safety considerations.

The above discussion and the results shown in Tables 4.1 and 4.2 correspond to the average pin under nominal conditions. To account for the design uncertainties, the hot spot factors were applied to the peak power channel, i.e., Zone 1. In general, a reasonable estimate of hot spot factors requires a complete knowledge of the reactor core and subassembly design and the interaction of the heat transport systems. Since these data are not presently available for the FMSR, the hot spot factors used in this preliminary study were largely based on a modification of CRBRP hot channel factors. This treatment is discussed in Appendix B of BNL-51225 (Reference 1). The computed maximum clad and fuel temperatures are given in Table 4.3.

The main conclusion which can be drawn from this initial study is that for the reference (EC)FMSR design, fuel and clad temperatures can be maintained below the current maximum temperature limits even when hot spot factors are included in computations. The mixed mean outlet temperature of 530°C can be achieved, thereby assuring a 36% thermodynamic efficiency using conventional components.

TABLE 4.2

Thermal-Hydraulic Results for Average Pin at Nominal Conditions in Zone I of (EC)FMSR

ZONE I--AVERAGE PIN AT NOMINAL CONDITION		S A T U R N		HYDRAULIC DIAMETER = .3086 (CM)		P/D RATIO = 1.173		MASS FLOW PER ASSEMBLY = .347E+05 GMS/SEC			
AXIAL NODE	HEIGHT (CM)	LOWER PLENUM PRESSURE (PSI)	SATURATION TEMPERATURE (C)	CLAD OUTER SURFACE	CLAD INNER SURFACE	FUEL PELLETT SURFACE	FUEL PELLETT INNER SURFACE	FUEL CENTERLINE	HTX (BTU/HR /FT**2/F	REYNOLDS NUMBER	FRICTION FACTOR
LOWER PLENUM		100.00									
COBE INLET		99.02									
COBE SUPPORT MOD		92.64									
INLET NOZZLE		80.74									
SHIELD/ORIFICE		64.20									
1	4.17	65.30	107.48	380.44	380.84	380.87	384.17	384.62	31951.15	0.0213	
2	12.50	63.71	106.10	381.12	381.50	381.42	386.37	386.92	31945.89	0.0213	
3	27.49	63.71	106.10	381.12	381.50	381.42	386.37	386.92	31937.60	0.0213	
4	32.49	59.21	105.90	382.60	383.86	382.22	439.15	439.64	31912.51	0.0213	
5	37.49	59.21	105.90	382.60	383.86	382.22	439.15	439.64	31868.00	0.0213	
6	47.0	59.21	105.90	382.60	383.86	382.22	439.15	439.64	31857.10	0.0213	
7	57.0	59.21	105.90	382.60	383.86	382.22	439.15	439.64	31809.16	0.0212	
8	67.0	59.21	105.90	382.60	383.86	382.22	439.15	439.64	31813.64	0.0211	
9	77.0	59.21	105.90	382.60	383.86	382.22	439.15	439.64	31831.05	0.0211	
10	87.0	59.21	105.90	382.60	383.86	382.22	439.15	439.64	31441.91	0.0210	
11	97.0	59.21	105.90	382.60	383.86	382.22	439.15	439.64	31330.02	0.0210	
12	107.0	59.21	105.90	382.60	383.86	382.22	439.15	439.64	31194.35	0.0209	
13	117.0	59.21	105.90	382.60	383.86	382.22	439.15	439.64	31154.41	0.0209	
14	127.0	59.21	105.90	382.60	383.86	382.22	439.15	439.64	31003.02	0.0208	
15	137.0	59.21	105.90	382.60	383.86	382.22	439.15	439.64	30950.99	0.0207	
16	147.0	59.21	105.90	382.60	383.86	382.22	439.15	439.64	30921.10	0.0206	
17	157.0	59.21	105.90	382.60	383.86	382.22	439.15	439.64	30891.46	0.0205	
18	167.0	59.21	105.90	382.60	383.86	382.22	439.15	439.64	30891.61	0.0204	
19	177.0	59.21	105.90	382.60	383.86	382.22	439.15	439.64	30843.39	0.0204	
20	187.0	59.21	105.90	382.60	383.86	382.22	439.15	439.64	30800.49	0.0203	
21	197.0	59.21	105.90	382.60	383.86	382.22	439.15	439.64	29864.48	0.0202	
22	207.0	59.21	105.90	382.60	383.86	382.22	439.15	439.64	29736.82	0.0202	
23	217.0	59.21	105.90	382.60	383.86	382.22	439.15	439.64	29636.56	0.0201	
24	227.0	59.21	105.90	382.60	383.86	382.22	439.15	439.64	29550.22	0.0201	
25	237.0	59.21	105.90	382.60	383.86	382.22	439.15	439.64	29474.43	0.0201	
26	247.0	59.21	105.90	382.60	383.86	382.22	439.15	439.64	29405.55	0.0200	
27	257.0	59.21	105.90	382.60	383.86	382.22	439.15	439.64	29343.93	0.0200	
28	267.0	59.21	105.90	382.60	383.86	382.22	439.15	439.64	29289.84	0.0200	
29	277.0	59.21	105.90	382.60	383.86	382.22	439.15	439.64	29241.35	0.0200	
30	287.0	59.21	105.90	382.60	383.86	382.22	439.15	439.64	29198.32	0.0200	
31	297.0	59.21	105.90	382.60	383.86	382.22	439.15	439.64	29160.37	0.0200	
32	307.0	59.21	105.90	382.60	383.86	382.22	439.15	439.64	29127.14	0.0200	
33	317.0	59.21	105.90	382.60	383.86	382.22	439.15	439.64	29098.14	0.0200	
34	327.0	59.21	105.90	382.60	383.86	382.22	439.15	439.64	29072.74	0.0200	
CURE TOP ASSEMBLY OUTLET		21.30		556.19	556.19	556.19	559.64	559.64	29161.70	0.0200	
UPPER PLENUM		10.94		556.48	556.48	556.48	559.64	559.64	29161.70	0.0200	
ORIFICE									4.97		
LOSS COEFFICIENT											

TABLE 4.3  
 Thermal-Hydraulic Results for the Hot Pin in Zone 1 of (EC)FMSR

S A T U R N

PEAK P.O.H. PIN WITH HOT CHANNEL EFFECT

LINEP POWER = 4.97 MW/FT      MASS FLOW RATE = 4500F±03 GM/CM<sup>2</sup>S

ZONE = 1      PEAKING FACTOR = 1.044

AXIAL NODE	HEIGHT (CM)	PRESSURE (PSI)	SATURATION	COOLANT	TEMPERATURE (C)	CLAD	INNER	OUTER	FUEL PELLETS SURFACE	FUEL INNER SURFACE	FUEL CENTERLINE	HTR (BTU/HR /FT <sup>2</sup> /F)	REYNOLDS NUMBER	FRICTION FACTOR
LOWER PLENUM														
CORRE PLENUM														
CORE SUPPORT ROD														
INLET NOZZLE														
SMILED/ORIFICE														
1	4.17	100.00	173.48	380.53	321.67	361.10	385.30	385.08	385.08	385.08	385.08	27567.23	6308.49	0.213
2	12.50	99.02	169.34	381.02	321.80	361.18	387.32	384.75	384.75	384.75	384.75	27551.45	6285.93	0.213
3	20.83	92.64	165.10	381.84	321.95	362.23	393.28	394.66	394.66	394.66	394.66	27551.45	6285.93	0.213
4	27.49	80.74	156.74	386.07	324.42	364.42	425.33	425.33	425.33	425.33	425.33	27522.53	6118.94	0.213
5	32.49	60.25	145.99	396.08	400.08	400.08	471.32	471.32	471.32	471.32	471.32	27413.98	5806.30	0.213
6	37.49	58.13	135.31	391.15	405.54	407.26	488.83	488.83	488.83	488.83	488.83	27412.18	5811.07	0.212
7	42.49	57.05	125.58	395.86	413.68	414.47	506.38	506.38	506.38	506.38	506.38	27342.94	5693.68	0.212
8	47.49	55.97	115.81	411.52	421.32	422.28	523.78	523.78	523.78	523.78	523.78	27264.54	5534.16	0.211
9	52.49	54.89	105.01	417.44	430.58	430.58	539.38	539.38	539.38	539.38	539.38	27177.46	5389.18	0.211
10	57.49	53.81	94.25	417.10	439.84	439.84	555.98	555.98	555.98	555.98	555.98	27082.34	5244.20	0.210
11	62.49	52.73	83.49	421.54	447.34	448.54	573.26	573.26	573.26	573.26	573.26	26979.84	5108.85	0.210
12	67.49	51.65	72.73	428.82	454.45	454.45	591.52	591.52	591.52	591.52	591.52	26851.24	4984.44	0.209
13	72.49	50.57	62.07	436.08	461.55	461.55	610.56	610.56	610.56	610.56	610.56	26695.63	4871.63	0.209
14	77.49	49.49	51.31	443.32	468.65	468.65	628.46	628.46	628.46	628.46	628.46	26532.02	4765.19	0.207
15	82.49	48.41	40.55	450.56	475.75	475.75	646.37	646.37	646.37	646.37	646.37	26368.41	4664.49	0.205
16	87.49	47.33	29.79	457.80	482.85	482.85	664.28	664.28	664.28	664.28	664.28	26204.80	4569.41	0.205
17	92.49	46.25	19.03	465.04	490.00	490.00	682.19	682.19	682.19	682.19	682.19	26041.19	4474.42	0.204
18	97.49	45.17	8.27	472.28	497.10	497.10	700.10	700.10	700.10	700.10	700.10	25877.58	4389.42	0.203
19	102.49	44.09	-2.49	479.52	504.20	504.20	718.01	718.01	718.01	718.01	718.01	25713.97	4304.42	0.202
20	107.49	43.01	-11.73	486.76	511.30	511.30	735.92	735.92	735.92	735.92	735.92	25550.36	4219.42	0.201
21	112.49	41.93	-20.97	494.00	518.40	518.40	753.83	753.83	753.83	753.83	753.83	25386.75	4134.42	0.200
22	117.49	40.85	-30.21	501.24	525.50	525.50	771.74	771.74	771.74	771.74	771.74	25223.14	4049.42	0.199
23	122.49	39.77	-39.45	508.48	532.60	532.60	789.65	789.65	789.65	789.65	789.65	25059.53	3964.42	0.198
24	127.49	38.69	-48.69	515.72	539.70	539.70	807.56	807.56	807.56	807.56	807.56	24895.92	3879.42	0.197
25	132.49	37.61	-57.93	522.96	546.80	546.80	825.47	825.47	825.47	825.47	825.47	24732.31	3794.42	0.196
26	137.49	36.53	-67.17	530.20	553.90	553.90	843.38	843.38	843.38	843.38	843.38	24568.70	3709.42	0.195
27	142.49	35.45	-76.41	537.44	561.00	561.00	861.29	861.29	861.29	861.29	861.29	24405.09	3624.42	0.194
28	147.49	34.37	-85.65	544.68	568.10	568.10	879.20	879.20	879.20	879.20	879.20	24241.48	3539.42	0.193
29	152.49	33.29	-94.89	551.92	575.20	575.20	897.11	897.11	897.11	897.11	897.11	24077.87	3454.42	0.192
30	157.49	32.21	-104.13	559.16	582.30	582.30	915.02	915.02	915.02	915.02	915.02	23914.26	3369.42	0.191
31	162.49	31.13	-113.37	566.40	589.40	589.40	932.93	932.93	932.93	932.93	932.93	23750.65	3284.42	0.190
32	167.49	30.05	-122.61	573.64	596.50	596.50	950.84	950.84	950.84	950.84	950.84	23587.04	3199.42	0.189
33	172.49	28.97	-131.85	580.88	603.60	603.60	968.75	968.75	968.75	968.75	968.75	23423.43	3114.42	0.188
34	177.49	27.89	-141.09	588.12	610.70	610.70	986.66	986.66	986.66	986.66	986.66	23259.82	3029.42	0.187
UPPER PLENUM														
OUTLET ASSEMBLY														
ORIFICE														4.97

## 5. (EC)FMSR FUEL CYCLE COST ANALYSIS

### 5.1 INTRODUCTION

A preliminary study has been made of the economic performance of the (EC)FMSR fuel cycle. The initial results indicate that the (EC)FMSR fuel cycle costs are smaller than those calculated for the conventional fast breeder reactors. This is mainly due to the long residence times for the fuel and blanket assemblies. Although these results are preliminary and more detailed economics calculations are necessary, the potential for low (EC)FMSR fuel cycle costs is an attractive advantage of this fast breeder reactor concept. In this section the basis for the fuel cycle cost calculations, including the fuel cycle cost model and the assumed economic environment, will be discussed. This will be followed by a presentation of results, followed by some conclusions.

### 5.2 FUEL CYCLE COST MODEL AND THE ECONOMIC ENVIRONMENT

The fuel cycle cost calculations were performed using the simple model developed by Abbaspour<sup>(17)</sup> which was a follow-on to earlier work by Brewer.<sup>(18)</sup>

In this model the levelized fuel cycle cost  $e$  (mills/kwhe) is represented by the relation:

$$e = \frac{1}{E} \sum_i M_i C_i F_i G_i$$

where

$E$  = total electricity generated by a batch of fuel (or blanket) during its residence in the reactor, (MWhe),

$M_i$  = the mass flow in stream  $i$ , (kg),

$C_i$  = the unit cost of the material in step  $i$ , (\$/kg),

$F_i$  = a "financial weighting factor," and

$G_i$  = the escalation factor.

The combined financial weighting and escalation factor is calculated from the relation

$$(FG)_i = \frac{\left[ \left( \frac{1}{1-\tau} \right) e^{-(x-y_i)t_i} - \left( \frac{\tau}{1-\tau} \right) e^{y_i t_i} \left( \frac{1-e^{-xT}}{xT} \right) \right]}{\left[ \frac{1-e^{-(x-y)T}}{(x-y)T} \right]}$$

where

$\tau$  = the tax rate,  $0 \leq \tau \leq 1$ ,

$x$  = the discount rate, and is given by  $x = (1-\tau)r_b f_b + r_s f_s$ ,

$r_b$  = the rate of return to the bondholders,

$f_b$  = the fraction of the total investment from bonds,

$r_s$  = the rate of return to the stockholders,

$f_s$  = the fraction of the total investment from stocks;  $f_b + f_s = 1.0$ ,

$t_i$  = the lag or lead time for transaction  $i$ , measured from the beginning of the batch irradiation, (yr),

$T$  = the total residence time for a batch of fuel (or blanket) in the reactor (yr),

$y_i$  = the escalation rate for transaction  $i$ ,

$y$  = the escalation rate allowed by the rate commission for the price of electricity.

It should be noted that this relationship is derived for the front end of the fuel cycle (plutonium purchase and fabrication) where transactions are depreciated. In the back end of the fuel cycle (spent fuel shipping, reprocessing, waste storage and plutonium credit), the transactions are more customarily expensed rather than depreciated, although some controversy exists about the choice of the method. For the expensed transactions, the tax rate  $\tau$  in the combined financial factor must be set equal to zero. Thus, the factor reduces to

$$(FG)_i = \frac{(x-y)T}{1-e^{-(x-y)T}} e^{-(x-y_i)t_i}$$

This model has been checked against a more sophisticated fuel cycle cost code, MITCOST,<sup>(19)</sup> with the results showing good agreement.<sup>(17)</sup>

For the reference economic and financial environment a set of values employed in the recent NASAP study<sup>(20)</sup> was adopted. These are given in Table 5.1. It should be noted that these values are for oxide fuel. No values for metal have been provided in the NASAP report.

The only unit cost not shown in Table 5.1 is the unit price of plutonium. Currently there is a considerable uncertainty on the correct method of calculating the unit price of plutonium. There are several methods that can be used to calculate a unit price for plutonium in a nuclear economy that includes a mixture of light water and breeder reactors. In one method the cost of plutonium is assumed to be equal to the cost of the recovery of fissile plutonium from light water spent fuel with no additional value attached to the plutonium. Table 5.2 shows the price of plutonium based on the recovery costs from typical PWR discharge fuel as a function of reprocessing cost. Note that based on this approach, once the breeder reactors constitute a sizable fraction of the total nuclear power installed, the unit cost of plutonium might logically

TABLE 5.1  
Unit Cost and Financial Parameters Used in the  
Fuel Cycle Cost Calculations

Transaction	Unit Cost (\$/kg HM)	
Fuel Assembly Fabrication	650	
Radial Blanket Assembly Fabrication	140	
Spent Fuel Shipping	90	
Fuel Assembly Reprocessing	450	
Blanket Assembly Reprocessing	390	
Waste Shipping and Storage	125	
<u>Financial Parameters</u>	<u>Uninflated</u>	<u>Actual*</u>
Bond Rate of Return	2.5 %/yr	8.1 %/yr
Bond Fraction	0.55	
Stock Rate of Return	7.0 %/yr	12.9 %/yr
Stock Fraction	0.45	
Income Tax Fraction, $\tau$	0.5	
Discount Rate, $x^{**}$	3.83 %/yr	8.03 %/yr

\*Based on an inflation rate of 5.5% per year  
 $x^{**} = (1-\tau)f_B r_B + f_S r_S$

TABLE 5.2  
Unit Cost of Fissile Plutonium Based on the  
Recovery Costs from PWR Spent Fuel

Unit Cost of Reprocessing (\$/kg HM)	Source	Unit Price of Fissile Plutonium* (\$/gr)
150	Ref. 21	23.11
250	Semi-Remote "AGNS" Type Facility Ref. 20	38.51
370	Fully Remote "Canyon" Type Facility Ref. 20	57.00

\*Based on a fissile plutonium concentration of 0.6556% in the LWR discharged fuel and 1% reprocessing losses.(20)

be based on recovery charges from breeder reactor irradiated fuel; this would reduce the cost of plutonium to 5-10 \$/gr due to the high fissile plutonium concentration (on the order of 7-10%, including the axial blanket) in the breeder's spent fuel.

A second method of calculating the unit price of plutonium is based on the indifference value of plutonium in light water reactors. The indifference value of plutonium in light water reactors is the value of plutonium that results in equal fuel cycle cost between a plutonium-fueled LWR and a conventional low enrichment U-235-fueled LWR. In other words, at the indifference price of plutonium a utility owning a light water reactor can either use low enrichment U-235 to operate the reactor, or buy plutonium at the indifference value (instead of low enrichment U-235) and end up with the same levelized fuel cycle cost. Based on a U<sub>308</sub> unit price of 40 \$/lb and a separative work unit (swu) unit price of 100 \$/kg, the indifference value of the plutonium is equal to 27 \$/gr.

Finally, in view of the uncertainties in the price of plutonium and lack of an acceptable method of pricing the plutonium, it has been suggested that in the economics analysis no value should be assigned to plutonium. The argument in favor of the exclusion of plutonium price is that in a nuclear economy consisting of a mixture of light water and breeder reactors, the same utilities that own the light water reactors will also own the breeder reactors. Thus, in effect, the plutonium transactions between light water reactors and breeders, or vice versa, will not go beyond the accounting boundary of a utility that owns the mixture of fast and thermal reactors. This argument is valid if one assumes that all utilities own a mixture of thermal and fast reactors and they are individually large enough to be self-sufficient with respect to plutonium needs. If this is not the case, then the price of plutonium would be at least equal to the indifference value of plutonium in light water reactors, since if reprocessing and recycling of plutonium in LWRs is permitted, a utility owning LWRs should be willing to buy plutonium at its indifference value and to run the LWRs on the plutonium cycle. If recycling of plutonium in light water reactors is not permitted by the government due to safeguards or resource-requirement considerations, then the plutonium would be available for breeder use, and the argument favoring a low value of plutonium would be valid. With these uncertainties in the price of plutonium in mind, the levelized fuel cycle cost of the (EC)FMSR was calculated for two plutonium prices. First the indifference value of plutonium (27 \$/gr) representing the lower range of plutonium value and next a plutonium unit price of \$100/gr suggested in a recent study<sup>(7)</sup> and representing the high range of plutonium value. Similar calculations were also performed for a homogeneous<sup>(22)</sup> and a heterogeneous<sup>(7)</sup> LMFBR. The results are discussed in the next section.

### 5.3 RESULTS AND CONCLUSIONS

The detailed cash flow associated with the core and blanket assemblies of the (EC)FMSR is shown in Table 5.3. The cash flow is for a unit plutonium price of \$27/gr. The most interesting point in Table 5.3 worth noting is the importance of the assumed price of plutonium and its large impact on the levelized fuel cycle cost. This point indicates the need for a comprehensive study of the current methods of calculation of the price of plutonium which



TABLE 5.3

Cash Flow Associated with Core and Blanket  
Fuel Assemblies of (EC)FMSR

Transaction	$t_i$ Time (years)	$C_i$ Unit Cost (\$/kg)	$M_i$ Mass Flow (kg)	$(FG)_i$ Financial Factor	$C_i M_i (FG)_i * 10^6$ (\\$)
1. Fissile Pu Purchase					
Inner Core	-1.0	27,000	3,150	1.5852	134.821
Outer Core	-1.0	27,000	4,110	1.5852	175.909
2. Fuel Fabrication					
Inner Core	-0.5	650	42,360	1.5355	42.278
Outer Core	-0.5	650	51,110	1.5355	51.011
Radial Blanket	-0.5	150	10,591	1.5355	2.439
Axial Blanket	-0.5	140	35,948	1.5355	7.727
3. Spent Fuel Shipping	11.0	90	140,009	0.8569	10.798
4. Reprocessing					
Inner Core	11.5	450	42,360	0.8461	16.128
Outer Core	11.5	450	51,110	0.8461	19.460
Blankets	11.5	450	46,539	0.8461	17.339
5. Waste Shipping and Storage	13.0	125	140,009	0.8146	14.256
6. Pu Credit					
Inner Core	11.5	27,000	3,672	0.8461	- 83.885
Outer Core	11.5	27,000	4,390	0.8461	-100.029
Blankets	11.5	27,000	1,200	0.8461	- 27.414
<b>TOTAL</b>					<b>280.890</b>

$$E = 6.57 \times 10^{10} \text{ kwhe}$$

would result in a unified method of plutonium pricing. As was mentioned earlier, similar calculations were also performed for homogeneous and heterogeneous LMFBRs. The cash flows for these cores are shown in Tables 5.4 and 5.5. Note that the masses given for the homogeneous LMFBR (Table 5.4) are for a 1200-MW(e) core, whereas the masses for the (EC)FMSR and the heterogeneous core are for 1000-MW(e) cores.

The levelized fuel cycle cost for the (EC)FMSR and the homogeneous and heterogeneous LMFBRs is given in Table 5.6. The fuel cycles shown are based on a capacity factor of 0.75. A higher capacity factor might be expected for the (EC)FMSR due to its long fuel cycle length. This would result in a lower fuel cycle cost for the (EC)FMSR compared to the values shown in Table 5.6.

It can be seen that at low plutonium values the levelized fuel cycle cost of the (EC)FMSR is lower than those of both the homogeneous and heterogeneous LMFBRs. At high plutonium prices the levelized fuel cycle cost of the (EC)FMSR is comparable to that of the homogeneous LMFBR but is still lower than that of the heterogeneous LMFBR. It is also interesting to note that the lower the price of plutonium the more favorable the (EC)FMSR looks compared with conventional LMFBRs. As was discussed earlier, once a sizable fraction of nuclear electricity is generated by fast reactors, the cost of plutonium based on recovery from spent fast reactor fuel could be as low as 5-10 \$/gr. In this situation the (EC)FMSR fuel cycle costs would look very attractive economically compared to conventional LMFBRs.

The basic conclusions of the economic analysis can be summarized as follows:

- a) The FMSR fuel cycle cost is competitive with that of the conventional homogeneous LMFBR and lower than that of the more probable heterogeneous LMFBR.
- b) Longer cycle cores are economically attractive. If the price of plutonium falls below the LWR-based value of \$27/gm in a breeder economy, the FMSR would be even more attractive.
- c) There are large uncertainties in fuel cycle cost calculations, primarily due to uncertainties in the unit price of plutonium and the lack of cost data for metal fuel when that fuel is of 1000 MW(e) dimensions. Significant improvements can be made with modest further studies.

TABLE 5.4

Cash Flow Associated with Core and Blanket Fuel Assemblies  
of a Homogeneous LMFBR (1200 MW(e))

Transaction	$t_i$ Time (years)	$C_i$ Unit Cost (\$/kg)	$M_i$ Mass Flow (kg)	$(FG)_i$ Financial Factor	$C_i M_i F_i G_i * 10^6$ (\\$)
1. Fissile Pu Purchase	-1.0	27,000	2009.5	1.2066	65.465
2. Fuel Fabrication					
Core	-0.5	650	15760.5	1.1552	11.834
Radial Blanket	-0.5	150	4979.6	1.3031	0.973
Axial Blanket	-0.5	140	11820.0	1.1552	1.911
3. Spent Fuel Shipping					
Core & Axial Blanket	3.0	90	27580.5	0.9505	2.3593
Radial Blanket	6.0	90	4979.6	0.9145	0.4098
4. Reprocessing					
Core	3.5	450	15760.5	0.9386	6.656
Radial Blanket	6.5	450	4979.6	0.9030	2.023
Axial Blankete	3.5	450	11820.0	0.9386	4.992
5. Waste Shipping & Storage					
Core & Axial Blanket	5.0	125	27580.5	0.9036	3.115
Radial Blanket	8.0	125	4979.6	0.8649	0.538
6. Pu Credit					
Core	3.5	22,000	1939.2	0.9386	-49.144
Radial Blanket	6.5	22,000	114.8	0.9030	- 2.798
Axial Blanket	3.5	22,000	174.5	0.9386	- 4.422
<b>TOTAL</b>					<b>43.912</b>

$$E = 7.884 \times 10^9 \text{ kwhe}$$

TABLE 5.5

Cash Flow Associated with Core and Blanket Fuel Assemblies  
of a Heterogeneous LMFBR (1000 MW(e) Core)

Transaction	$t_i$ Time (years)	$C_i$ Unit Cost (\$/kg)	$M_i$ Mass Flow (kg)	$(FG)_i$ Financial Factor	$C_i M_i F_i G_i * 10^6$ (\\$)
1. Fissile Pu Purchase	-1.0	27,000	1852.9	1.2066	60.364
2. Fuel Fabrication					
Core	-0.5	650	10606.5	1.1552	7.964
Axial Blanket	-0.5	140	18290.2	1.1552	2.958
Internal Blanket	-0.5	150	13780.5	1.1552	2.387
Radial Blanket	-0.5	150	5636.3	1.3031	1.101
3. Spent Fuel Shipping					
Core & Axial Blanket	3.0	90	27580.5	0.9505	2.3593
Internal Blanket	3.0	90	13780.5	0.9505	1.178
Radial Blanket	6.0	90	5636.3	0.9145	0.463
4. Reprocessing					
Core & Axial Blanket	3.5	450	28896.7	0.9386	12.205
Internal Blanket	3.5	450	13780.5	0.9386	5.820
Radial Blanket	6.5	450	15636.3	0.9030	2.290
5. Waste Shipping & Storage					
Core & Axial Blanket	5.0	125	28896.7	0.9036	3.263
Internal Blanket	5.0	125	13780.5	0.9036	1.556
Radial Blanket	8.0	125	5636.3	0.8649	0.609
6. Pu Credit					
Core	3.5	22,000	1704.1	0.9386	-43.185
Axial Blanket	3.5	22,000	80.7	0.9386	- 2.045
Internal Blanket	3.5	27,000	275.9	0.9386	- 6.991
Radial Blanket	6.5	27,000	90.7	0.9030	- 2.211
<b>TOTAL</b>					<b>50.197</b>

$$E = 6.57 \times 10^9 \text{ kwhe}$$

TABLE 5.6

Comparison Between the Levelized Fuel Cycle Cost of the (EC)FMSR  
and a Homogeneous and Heterogeneous LMFBR

Core	Fuel Cycle Cost (Mills/kwhe)	
	Pu (27\$/gr)	Pu (100\$/gr)
(EC)FMSR (10 yr core)	4.27	8.36
Homogeneous LMFBR <sup>(22)</sup>	5.56	8.69
Heterogeneous LMFBR <sup>(7)</sup>	7.64	10.08

## 6. THE 30-YEAR (EC)FMSR

### 6.1 PRELIMINARY RESULTS OF THE 30-YEAR (EC)FMSR

As an extension of the 10-year (EC)FMSR, a preliminary study was done on the design and performance of a 30-year (EC)FMSR. The most noticeable advantages of such a core would be its long fuel cycle length, which results in a core that would be loaded only once during the life of the reactor.

To be able to design such a core with acceptable burnup and fluence, it was necessary to lower the power density compared to that of the 10-year FMSR core by increasing the volume of the core. After several design changes, it was decided that the design should start with a 70% increase in the core volume. This 70% increase in volume was accomplished by adding three rows of fuel assemblies to the outer core boundary of the 10-year FMSR and increasing the core height from 160 cm to 180 cm. The core was divided into two sections of inner and outer core with equal volumes but different enrichments and BeO concentrations to keep the power peaking to a minimum. To be able to keep the power shape relatively flat throughout the 30-year life of the core, it was found that the conversion ratio in the outer core should be comparable to the conversion ratio in the inner core. This was accomplished by a decrease in BeO concentration and a slight increase in the enrichment in the outer core compared to the inner core. These are gross preliminary changes. Further refinement of the design will occur in the future.

Table 6.1 compares the general characteristics of the 10-year and 30-year (EC)FMSR. As can be seen in the table, the inner core fissile plutonium enrichment is 7.0%. The BeO in the inner core assemblies which takes 25% of the volume of the assembly has a density equal to 70% of the theoretical density of the BeO.

The outer core's fissile enrichment is 7.3%. To increase the power production from the outer core and also boost the conversion ratio in this region, the fraction of the assemblies occupied by fuel was increased from 0.75 with characteristics of the inner core to 0.85. The BeO density in these assemblies is 50% of the theoretical BeO density. Also BeO was removed from the last row of the outer core.

The radial blanket consists of one row of 3% enriched assemblies. There is no BeO in the radial blanket assemblies. The inclusion of 3% fissile plutonium in the radial blanket helped to decrease the power buildup from beginning of life to the end of life in the radial blanket. It also has reduced the neutron leakage from the outer core to the radial blanket, thereby increasing the power production in the outer core. The new fission product treatment developed at BNL was used in these calculations.

Figure 6.1 shows variation of the power profile over the life of the core. As can be seen, the power peaks in the boundary of the inner and outer core. The increase in the conversion ratio in the outer core region has reduced the power shift from the outer core region to the center of the core, consequently reducing the peak burnup and fluence.

TABLE 6.1

Comparison Between 10- and 30-Year (EC)FMSR Cores

	<u>10-Year FMSR</u>	<u>30-Year FMSR</u>
Core Height, cm	160	180
Core Radius + Radial Blanket, cm	243	270
Enrichment (% Fissile Pu)		
- Inner Core	7.1	7.0
- Outer Core	7.6	7.3
Fissile Mass (239 + 241) kg	7800	12964/13844*
Number of Fuel Subassemblies	469	721
Number of Blanket Subassemblies	78	96
Fissile Inventory Gain	1.31	1.30
Doppler Coefficient	0.027	0.0216

---

\* Fissile inventory of the core plus radial blanket.

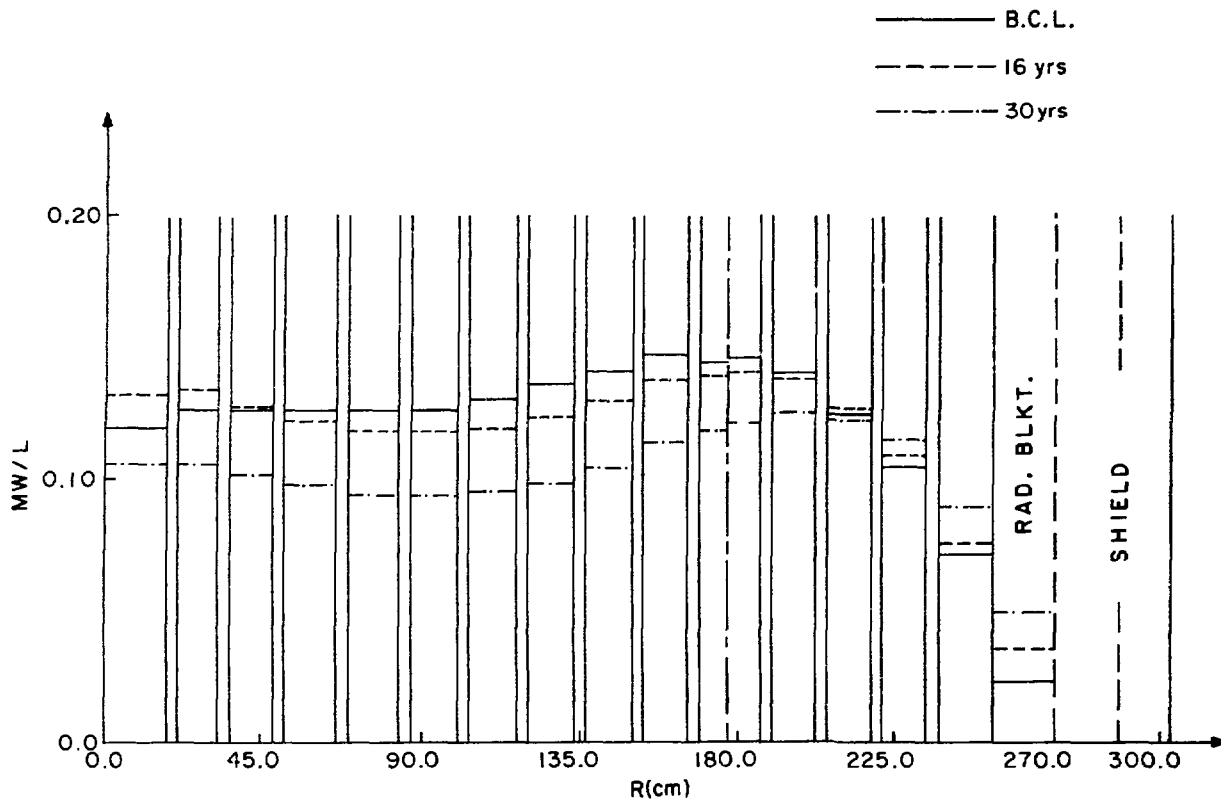


Figure 6.1 30-Year FMSR Radial Power Distribution  
(Zone Average, R-Z)



Table 6.2 shows the variation in  $K_{eff}$ , conversion ratio, peak burnup and peak fluence as a function of time. The peak burnup and fluence ( $E > 0.1$  MeV) are 18.49% and  $5.2 \times 10^{23}$  n/cm<sup>2</sup> respectively. Both of these values can be considered acceptable from the point of view of metal fuel and advanced alloy capability, although both are larger than might be desired. Although no actual sodium void calculation has been performed at this stage of the design, since the basic neutronic characteristics of this core, including burnup, are not much different from those of the 10-year FMSR, the sodium void is not expected to be very different from the values reported for the 10-year FMSR.

To see the effect of the larger core used for the 30-year FMSR on the economics of this core, the levelized fuel cycle cost was calculated for this core, using the same cost assumptions. Table 6.3 shows the cash flow for the 30-year FMSR based on a plutonium unit price of 27 \$/gr. Table 6.4 compares the levelized fuel cycle cost of the 30-year FMSR to that of the 10-year FMSR and a heterogeneous LMFBR. The levelized fuel cycle cost was calculated for two plutonium prices of 27 \$/gr and 100 \$/gr. The \$27/gm represents a price which a LWR would be willing to pay for the plutonium if it were on a Pu recycle and U-235 were available at 35 \$/gm. \$100/gm is an arbitrary very large price which has no relation to any presently conceived market situation. The levelized fuel cycle cost of the 30-year FMSR, at a plutonium price of 27 \$/gr representative of the low range of plutonium price, is 5.17 mills/kwhe. This is higher than the 10-year FMSR but lower than the heterogeneous LMFBR. At a plutonium price of 100 \$/gr the levelized fuel cycle cost of the 30-year FMSR is higher than both the 10-year FMSR and the heterogeneous core. This is mainly due to the large fissile inventory of this core.

The major advantages and disadvantages of the 30-year FMSR are listed in Table 6.5. The advantages of this core include a strong nonproliferation characteristic due to the need for transportation and reprocessing of only one batch of fuel for the full 30-year life of the reactor. In a conventional heterogeneous LMFBR with a fissile inventory of 3000 kg of fissile plutonium and with annual refueling of one half of the core, the total fissile plutonium transportation and reprocessing is four times higher than fissile plutonium transportation and reprocessing requirements of the 30-year FMSR. Also, the need for only one batch of fuel is very attractive to utilities since there would be a saving in the refueling downtime (hence higher capacity factor) and lack of need for an annual refueling license. With respect to safety, the large Doppler coefficient of this core, which is similar to that of the 10-year core, is very attractive.

The fuel cycle cost of the 30-year FMSR is fairly low at low prices of plutonium, but due to its high fissile inventory the fuel cycle cost increases rapidly with higher plutonium prices. The disadvantages of the 30-year FMSR include a large sodium void at the EOL. It is possible with further design changes to reduce the sodium void in the 30-year FMSR, but overall, the value will remain higher than that of the 10-year FMSR. The peak burnup and fluence damage of the 30-year FMSR are high. There have been many irradiations of MARK-II metal fuel to at least 16% heavy metal burnup; about 1000 pins have reached this state without failure. While there have been no irradiations of advanced alloys to beyond approximately  $2 \times 10^{23}$  nvt, the performance to that point of several alloys gives good reason to believe that a fluence

TABLE 6.2

30-Year FMSR Performance

Year (0.75 CF)	K <sub>eff</sub>	Conversion Ratio		Peak Burnup % HM	Peak Fluence x 10 <sup>23</sup> (>0.1 MeV)
		Inner Core	Outer Core		
0	1.005	1.374	1.369	0	0
4	1.009	1.287	1.295	2.69	0.71
8	1.016	1.216	1.231	5.38	1.43
12	1.021	1.160	1.179	8.02	2.16
16	1.024	1.118	1.136	10.58	2.89
20	1.025	1.086	1.101	13.04	3.60
24	1.024	1.061	1.071	15.38	4.27
28	1.021	1.042	1.047	17.43	4.90
30	1.020	1.034	1.036	18.49	5.20

TABLE 6.3

Cash Flow Associated with Core and Blanket Fuel Assemblies of the 30-Year FMSR

Transaction	$t_i$ Time (Years)	$C_i$ Unit Cost (\$/Kg)	$M_i$ Mass Flow (Kg)	$(FG)_i$ Financial Factor	$C_i M_i F_i G_i^* 10^6$ (\$)
1. Fissile Pu Purchase					
Inner Core	-1	27000	5799	2.4169	378.421
Outer Core	-1	27000	7165	2.4169	467.561
Radial Blanket	-1	27000	880	2.4169	57.425
2. Fuel Fabrication					
Inner Core	-0.5	650	82234	2.3659	126.462
Outer Core	-0.5	650	97144	2.3659	149.391
Radial Blanket	-0.5	150	56290	2.3659	19.976
Axial Blanket	-0.5	140	78331	2.3659	25.945
3. Spent Fuel Shipping	31	90	313999	0.6513	18.405
4. Reprocessing	31.5	450	313999	0.6431	90.869
5. Waste Shipping and Storage	32	125	313999	0.6350	24.923
6. Pu Credit					
Inner Core	31.5	27000	6989	0.6431	-121.354
Outer Core	31.5	27000	8228	0.6431	-142.868
Blankets	31.5	27000	4367	0.6431	-75.827
<b>Total</b>					<b>1019.330</b>

$$E = 1.971 \times 10^{11} \text{ kwhe}$$

TABLE 6.4

Comparison Between the Levelized Fuel Cycle Cost of the  
10- and 30-Year FMSR and a Heterogeneous LMFBR\*

CORE	Fuel Cycle Cost (Mills/kwhe)	
	Pu (27 \$/gr)	Pu (100 \$/gr)
10-Year FMSR	4.27	8.36
30-Year FMSR	5.17	12.89
Heterogeneous LMFBR <sup>(22)</sup>	7.64	10.08

\* All fuel cycle costs based on a 0.75 capacity factor.

TABLE 6.5

Advantages and Disadvantages of the 30-Year FMSR Design

Advantages

1. One batch of fuel over plant lifetime.
  - A. Strong nonproliferation characteristic.
  - B. Very attractive to utilities.
2. High plant capacity factor.
3. Large Doppler Coefficient.
4. Low fuel cycle cost.
5. Refueling equipment design can be simplified, reducing plant capital costs.

Disadvantages

1. EOL sodium void coefficient relatively large.
2. High burnup and fluence.
3. High fissile plutonium inventory.
4. Long doubling time.

damage level of the order of  $5 \times 10^{23}$  can be sustained, with tolerable swelling and creep. Other disadvantages of this core include a high fissile inventory due to the low power density and large core volume and long doubling time. This might lead to an undesirably long doubling time for some projected power need scenarios.

Overall it seems that there are enough interesting characteristics and advantages in this concept to encourage further work on the core design and optimization of this reactor concept. Most importantly, because of the particularly small design effort which this concept has received, to the present, there is a very large potential for design improvement.

## 7. CONCLUSIONS AND RECOMMENDATIONS

### 7.1 CONCLUSIONS

The FMSR design has changed greatly in one year. There remains a considerable potential for further design improvement in the future. The major conclusions of this study are as follows:

For the Centrally-Moderated FMSR (CM)FMSR:

1. The actual operation of the (CM)FMSR, from the specification of the first core through the management of all subsequent fuel cycles, for the full plant lifetime, has been calculated and shown to be fully acceptable. Equal fuel cycles of more than two calendar years per cycle are used throughout. The resource utilization advantage of this reactor relative to the LWR is approximately a factor of three.
2. While many performance parameters such as reactivity change or local power density variation over the fuel cycle are acceptable, the peak fluence damage to the steel of the clad and duct remains high, as previously. The peak fuel burnup also remains higher than might be desired. Both results can be reduced through changes in the fuel management strategy, but at a cost in reduced resource advantage. Thus a design compromise is available, and can be applied as needed, according to the degree of success of advanced material irradiation programs.
3. While the operating performance of the Extended Cycle FMSR (EC)FMSR is particularly attractive and superior to that of the (CM)FMSR, weighting of the relative proliferation-resistance merits of the two designs may justify further (CM)FMSR design development.
4. The sodium void reactivity gain of the (CM)FMSR, on the basis of preliminary calculations, appears to be better than that of a homogeneous oxide-fueled LMFBR and worse than that of a well-designed heterogeneous LMFBR. Possible intrinsic safety advantages of the metal fuel proposed for the (CM)FMSR may offer valuable compensation in this area. Thus, safety studies for the (CM)FMSR could significantly affect conclusions in this area.

For the Extended Cycle FMSR (EC)FMSR:

1. The performance of the (EC)FMSR, from the point of view of a potential operating utility, is exceptionally attractive. In particular, a ten-year fuel cycle seems to be readily feasible and possesses only small variations in local or regional power, has only modest reactivity changes over the entire fuel cycle, and has greatly improved and acceptable peak fuel burnup and steel fluence damage. The fuel cycle cost appears to be attractive, while the sodium void reactivity gain is in the range of that of the heterogeneous LMFBR. The Doppler effect feedback coefficient is particularly strong.

2. Except for the proposed use of metal fuel, in a mode analogous to that of the Mark-II fuel extensively irradiated in EBR-II, and a BeO moderator, all of the technology on which the (EC)FMSR would depend is a straightforward application of base LMFBR technology. Thus, the technological needs for the (EC)FMSR would be very close to base LMFBR development needs and not in conflict with them.
3. An adaption of the (EC)FMSR design to employ a carbide (or oxide) fuel would put research requirements for the FMSR development strategy into even greater coincidence with current LMFBR research requirements. The possible performance penalty which may occur will be evaluated with care.

## 7.2 RECOMMENDATIONS

For the (CM)FMSR:

1. Further design studies on the (CM)FMSR should depend on a decision on the desirability of the proliferation-resistance advantages of the (CM)FMSR relative to those of the (EC)FMSR. If it is judged that the (EC)FMSR can adequately serve this objective, then further FMSR design efforts should strongly concentrate on that design. Low level work on the (CM)FMSR might continue to provide a backup strategy.
2. If continued, the (CM)FMSR design could be improved with a new design iteration. Such changes as use of improved fission product cross sections, redesign of duct spacing and new choices for fuel volume fractions would result in significant improvements.

For the Extended Cycle FMSR (EC)FMSR:

1. A major effort should be made to evaluate the potential of a carbide (or oxide) fueled (EC)FMSR. The metal-fueled (EC)FMSR should be evaluated in parallel to the extent that the same performance design criteria should be applied to both designs.
2. Because the apparent licensing safety of an LMFBR is an important aspect of its particular design, carefully executed sodium void calculations should be performed for the (EC)FMSR. Because of the sensitivity and uncertainties of these calculations, particularly for this LMFBR with an unusually soft neutron energy spectrum, zero power reactor type critical experiments should be planned for the future.
3. Design optimization, design sensitivity, and cost studies should be pursued as aids in rapid and economical design improvement.
4. Safety studies, at least analytical studies, should be started as soon as funding permits. These should concentrate on the carbide-fueled (EC)FMSR design if that design variation appears to be feasible. Otherwise basic understanding of metal fuel performance

in severe transient conditions should be sought in close collaboration with metal fuel safety studies for the EBR-II safety program.

5. The engineering specification of the metal fuel for the FMSR reactor represents an important area of design uncertainty, largely because of the change from EBR-II fuel dimensions to those more prototypical of a 1000-MW(e) LMFBR. If metal fuel were to remain the preferred fuel for the FMSR, then a design effort to specify this fuel and its irradiation response history would be important. This study would lead to specification of proposed fabrication and in-pile and out-of-pile testing programs for the future.

If a carbide (or oxide) fuel could be shown to be acceptable for the FMSR, then a much reduced fuel design effort would only examine differences between conventional carbide fuel operating conditions and those proposed for the FMSR. The compatibility of the fuel, clad, duct, and grid spacers or wire wrap over the long irradiation times should be assured.



## REFERENCES

1. G. J. Fischer and R. J. Cerbone, "The Fast-Mixed Spectrum Reactor Progress Report for 1979," Brookhaven National Laboratory, BNL-51225 (May 1980); Chapter 2, this report.
2. R. B. Kidman et al., "LIB-IV, A Library of Group Constants for Nuclear Reactor Calculations, Los Alamos Scientific Laboratory, LA-6260-MS (1976).
3. R. W. Hardie et al., "1-DX, A One-Dimensional Diffusion Code for Generating Effective Nuclear Cross-Sections," Battelle Northwest Laboratory, BNWL-954 (1969).
4. W. W. Little et al., "2DB User's Manual," Battelle Northwest Laboratory, BNWL-831 (1969).
5. C. L. Wheeler et al., "COBRA-IV-I: An Interim Version of COBRA for Thermal-Hydraulic Analysis of Rod Bundle Nuclear Fuel Elements and Cores," BNWL-1962, March 1946.
6. G. J. Fischer and R. J. Cerbone, "The Fast-Mixed Spectrum Reactor Interim Report, Initial Feasibility Study," Brookhaven National Laboratory, BNL-50976 (January 1979).
7. W. P. Barthold et al., "Optimization of Radially Heterogeneous 1000-MW(e) LMFBR Core Configurations," Electric Power Research Institute, EPRI-NP-1000 (November 1979).
8. M. T. Simnad, "Shielding and Control Materials for the Gas-Cooled Fast Breeder Reactor," General Atomic Company, GA-A14478 (December 1977).
9. M. Segev, "An Equivalence Relation for a Lattice of Annular Absorbers," (to be published in Nuclear Science and Engineering).
10. R. W. Hardie and W. W. Little, Jr., "PERT-V, A Two-Dimensional Perturbation Code for Fast Reactor Analysis," Battelle Northwest Laboratory, BNWL-1162 (1969).
11. G. Gambler, "Plutonium Recycling in LWRs," Trans. Am. Nucl. Soc., 33, 407(1979).
12. W. Engle, Jr., "A User Manual for ANISN," K-1693 (1967).
13. G. M. Golden and J. V. Tokar, "Thermophysical Properties of Sodium," Argonne National Laboratory, ANL-7323 (1973).
14. S. T. Zegler and M. V. Nevitt, "Structure and Properties of Uranium-Fissium Alloys," Argonne National Laboratory, ANL-6116 (1961).
15. E. H. Novendstern, "Turbulent Flow Pressure Model for Fuel Rod Assemblies Utilizing a Helical Wire-Wrap Space System," Nucl. Eng. & Design 22, 19(1972).

REFERENCES (cont'd.)

16. M. D. Carelli, "CRBR Assemblies Hot Channel Factors Preliminary Analysis," Westinghouse Electric Corp., Advanced Reactors Division, WARD-D-0050 (1974).
17. A. T. Abbaspour and M. J. Driscoll, "The Fuel Cycle Economics of Improved Uranium Utilization in Light Water Reactors," Massachusetts Institute of Technology, COO-4570-9, MITNE-224 MIT-EL-79-001 (January 1979).
18. S. T. Brewer, E. A. Mason and M. J. Driscoll, "The Economics of Fuel Depletion in Fast Breeder Reactor Blankets," Massachusetts Institute of Technology, COO-3060-4, MITNE-123 (November 1972).
19. A. G. Croft, "MITCOST-II - A Computer Code for Nuclear Fuel Cycle Costs," N.E. Thesis, Department of Nuclear Engineering, Massachusetts Institute of Technology (1974).
20. Nonproliferation Alternative System Assessment Program (NASAP), Vol. V, Economics and Systems Analysis, Preliminary Draft (July 1979).
21. R. A. Matzie et al., "Assessment of Thorium Fuel Cycles in Pressurized Water Reactors," TIS-5114 (November 1976).
22. W. P. Barthold and J. C. Beitel, "Performance Characteristics of Homogeneous Versus Heterogeneous Liquid-Metal Fast Breeder Reactors," Nuclear Technology 44, 1(1979).

U.S. GOVERNMENT PRINTING OFFICE: 714-037#5